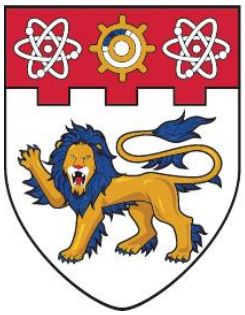

NANYANG TECHNOLOGICAL UNIVERSITY
SINGAPORE

METABOLOMICS STUDY OF DOSE-RESPONSE AND TIME-RESOLVED EFFECT OF BISPHENOL A EXPOSURE *IN VITRO*

Zhao Haoduo
SCHOOL OF CIVIL AND ENVIRONMENTAL ENGINEERING
2022

METABOLOMICS STUDY OF DOSE-RESPONSE AND TIME-RESOLVED EFFECT OF BISPHENOL A EXPOSURE *IN VITRO*

Zhao Haoduo

SCHOOL OF CIVIL AND ENVIRONMENTAL ENGINEERING

A thesis submitted to the Nanyang Technological University in partial fulfilment of the requirement for the degree of
Master of Engineering

2022

Statement of Originality

I hereby certify that the work embodied in this thesis is the result of original research, is free of plagiarised materials, and has not been submitted for a higher degree to any other University or Institution.

2022.7.15 Zhao Haoduo

. . . .

Date

Supervisor Declaration Statement

I have reviewed the content and presentation style of this thesis and declare it is free of plagiarism and of sufficient grammatical clarity to be examined. To the best of my knowledge, the research and writing are those of the candidate except as acknowledged in the Author Attribution Statement. I confirm that the investigations were conducted in accord with the ethics policies and integrity standards of Nanyang Technological University and that the research data are presented honestly and without prejudice.

2022.7.15 Fei Xunchang

. . . . . .

Date

Authorship Attribution Statement

This thesis contains material from **TWO** papers published in the following peer-reviewed journal: **Environment International**; **Frontiers in Environmental Science and Engineering**.

Chapter 3 is published as

Zhao, Haoduo, Liu, Min, Lv, Yunbo, Fang, Mingliang. (2022). "Dose-response metabolomics and pathway sensitivity to map molecular cartography of bisphenol A exposure". Environment International. 158. 106893. 10.1016/j.envint.2021.106893.

The contributions of the co-authors are as follows:

- A/Prof Fang Mingliang provided the initial project direction and edited the manuscript drafts.
- I prepared the manuscript drafts, performed experiments and data analysis.
- Dr. Liu Min co-performed the lab experiment and data analysis.
- Dr. Lv Yunbo co-revised the manuscript.

Chapter 4 is published as

Zhao, Haoduo, Liu, Min, Yang, Junjie, Chen, Yuyang, Fang, Mingliang. (2022). "Time-dependent metabolomics uncover dynamic metabolic adaptions in MCF-7 cells exposed to bisphenol A". Frontiers in Environmental Science and Engineering. https://doi.org/10.1007/s11783-023-1604-5

The contributions of the co-authors are as follows:

- A/Prof Fang Mingliang provided the initial project direction and edited the manuscript drafts.

- I prepared the manuscript drafts, performed experiments and data analysis.
- Dr. Liu Min co-performed the lab experiment and data analysis.
- Dr. Yang Junjie and Mr. Chen Yuyang co-revised the manuscript.

2022.7.15	Zhao Haoduo
. . . .	. . . .
Date	

ACKNOWLEDGEMENTS

The author wishes to express his thankfulness to his supervisor, Prof. Fang Mingliang, as well as Prof. Fei Xunchang, for his invaluable and patient guidance. His helpful advice and enlightenment have led the author to go forward and complete his report.

The author also wishes to express his sincere appreciation to his seniors, Dr. Liu Min, Dr. Zhao Fanrong, Dr. Lv Yunbo, Dr. Xu Tengfei, Dr. Yang Junjie, Dr. Peng Bo and Mr. Chen Yuyang, for their patience and help in the research works.

TABLE OF CONTENTS

PAGE

ABSTRACT

The biochemical consequences induced by xenobiotics exposure are featured with dose-response and time-resolved landscapes. Metabolomics, a systematic study of intercellular chemical fingerprints, exhibits its advantages in toxicological mechanisms identification and dynamic physiology characterization. Yet, most metabolome studies were adopted in single dosing point with static snapshot, while little is known about the continuous dysregulation behavior under environmental stress, regardless of the metabolite/ pathway sensitivity extrapolation.

In this thesis, bisphenol A (BPA), a well acknowledged endocrine disrupting chemical with multiple toxicological endpoints, was chosen as the model compound to systematically investigate the biological dysfunctions in terms of dynamic dose-response and time-resolved change. For the former part, metabolites' dose-response relationships were established based on the dysregulation manner at four consecutive doses, which were further extrapolated into full range cartography prediction and sensitive biomarkers discovery. For the latter part, time-resolved metabolic adaptions were observed from eleven time points to characterize temporal cellular change at different stages. Pathway enrichments suggested the enhancing metabolic requirements for elevated energy homeostasis, oxidative stress response and ER-α mediated cell proliferation. In sum, the dose-response and time-resolved metabolomics studies provided an insightful characterization into xenobiotics' metabolic disruption effect with significant dosage and temporal patterns, which may play essential roles in dynamic hazard identification and chemical risk assessment.

LIST OF TABLES

LIST OF FIGURES

LIST OF PUBLICATIONS

Zhao H, Liu M, Lv Y, Fang M. Dose-response metabolomics and pathway sensitivity to map molecular cartography of bisphenol A exposure. *Environ Int*. 2022 Jan;158:106893. doi: 10.1016/j.envint.2021.106893. Epub 2021 Sep 27. PMID: 34592654. (Zhao, Liu et al. 2021)

Zhao, H., Liu, M., Yang, J. et al. Time-dependent metabolomics uncover dynamic metabolic adaptions in MCF-7 cells exposed to bisphenol A. Front. Environ. Sci. Eng. 17, 4 (2023). https://doi.org/10.1007/s11783-023-1604-5. (Zhao, Liu et al. 2022)

Peng B, **Zhao H**, Keerthisinghe TP, Yu Y, Chen D, Huang Y, Fang M. Gut microbial metabolite p-cresol alters biotransformation of bisphenol A: Enzyme competition or gene induction? *J Hazard Mater.* 2022 Mar 15;426:128093. doi: 10.1016/j.jhazmat.2021.128093. Epub 2021 Dec 16. PMID: 34952505. (Peng, Zhao et al. 2022)

Wang, D.; **Zhao, H**.; Fei, X.; Synder, S. A.; Fang, M.; Liu, M., A comprehensive review on the analytical method, occurrence, transformation and toxicity of a reactive pollutant: BADGE. *Environ Int* 2021, *155*, 106701.(Wang, Zhao et al. 2021)

Xu, T.; **Zhao, H.**; Wang, M.; Chow, A.; Fang, M., Metabolomics and In Silico Docking-Directed Discovery of Small-Molecule Enzyme Targets. *Anal Chem* 2021, *93* (6), 3072-3081.(Xu, Zhao et al. 2021)

Xu, T.; Chen, L.; Lim, Y. T.; **Zhao, H**.; Chen, H.; Chen, M. W.; Huan, T.; Huang, Y.; Sobota, R. M.; Fang, M., System Biology-Guided Chemical Proteomics to Discover Protein Targets of Monoethylhexyl Phthalate in Regulating Cell Cycle. *Environ Sci Technol* 2021, *55* (3), 1842-1851.(Xu, Chen et al. 2021)

Xu, T.; Lim, Y. T.; Chen, L.; **Zhao, H**.; Low, J. H.; Xia, Y.; Sobota, R. M.; Fang, M., A Novel Mechanism of Monoethylhexyl Phthalate in Lipid Accumulation via Inhibiting Fatty Acid Beta-Oxidation on Hepatic Cells. *Environ Sci Technol* 2020, 54 (24), 15925-15934.(Xu, Lim et al. 2020)

CHAPTER 1. INTRODUCTION

1.1 Background

Bisphenol A (BPA), a typical bisphenols (BPs) material, is widely used in the synthesis of polycarbonate plastics and epoxy resins **(Fig. 1.1).** BPA's presence in environment is ubiquitous. Its occurrences have been proved to be present in varieties of environmental matrices, including atmosphere (Fu and Kawamura 2010), indoor dust (Liao, Liu et al. 2012), primary influent of wastewater treatment plant (WWTP) (Hu, Zhu et al. 2019), sludge and soil in dense industrial area (Lin, Wang et al. 2017). As a coating material for canned food and beverages, it is also able to migrate to foods when heated and further consumed by human beings. Plenty of studies have validated its presence in in human placenta, fetal serum and milk in pregnant women, through dermal exposure and ingestion uptake.

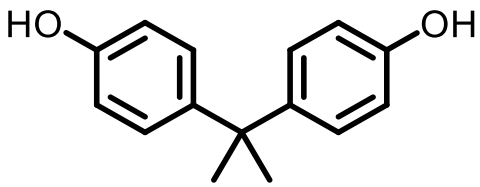

Fig. 1.1 Chemical structure of Bisphenol A

This huge amount of BPA usage and exposure undoubtedly raised tremendous public safety concerns. BPA is suspected to be related with endocrine-disrupting effects on birds and aquatic species with sufficient ecotoxicological evidences. According to epidemic survey and molecular toxicology results, exposure to BPA is linked with pleiotropic toxic effects such as affecting estrogenic, androgenic, thyroid, retinoid and prostaglandin signaling pathways as well as cholesterol and lipid homeostasis.

Metabolomics is the systematic study of the dysregulate chemical fingerprints induced by specific cellular processes, also the study of the small molecule metabolite as a whole scale. It is widely applied in plenty of research fields such as disease

diagnosis, pharmaceutical development, nutrition science, toxicology, environmental science and other areas closely related to human health care. Omics Studies regarded BPA exposure have confirmed its perturbation effects to induce metabolome disorders.

Dose-response relationship describes the magnitude of the response of an organism, as a function of exposure doses to a stimulus or stressor after a certain exposure time. It is commonly visualized as dose-response curves, with stimulus quantity level versus response intensity. Although various toxicology endpoints upon BPA exposure like Median Lethal Dose (LD50) and No Observed Effect Concentration (NOEC) have been systematically well studied, little research is regarding in the adverse effect induced by BPA with omics-scale dose-response dysregulation behavior.

Time-resolved omics strategies have been heavily utilized to dynamically monitor and characterize biological dysfunctions in a continuously-changing micro-environment. Unlike the "snapshot" present in single point omics study, time-resolved research provides an insightful tool to investigate xenobiotics toxicological mechanisms and sequential metabolic transitions, as for intracellular metabolome is ever-changing and real-time metabolic balance state is vulnerable. Up to date, the time-resolved omics disturbing effect of BPA exposure is still unexplored.

1.2 Purpose and scope

This report is a write-up on the research progress of the candidate over the two years' M.Eng study, including literature review, two original studies, and outlook for future recommendations. The main M.Eng research topic aims to explore the endocrine-disrupting chemical BPA's adverse effect on metabolome dysregulation behavior in a dose-response and time-resolved manner. On one hand, global metabolomics and TOXcms (an R-package based dose-response metabolomics methodology) strategies

were employed to determine the significant dysregulated metabolites. Dose-response curves were set up based on the metabolic toxicity data, with prediction models established within the applicable domain. Specifically, the effect concentration of certain response pinpoints were investigated to report metabolites' toxic sensitivity. On the other hand, time-resolved metabolomics study was carried out at 11 time points, to characterize the dynamic metabolome dysregulation under BPA exposure within 8 hours. Metabolites of significant time-induced effect were identified, and time-series pathway analysis was conducted to investigate temporal metabolic adaptions resulted from transitions in cellular biological function requirements.

The detailed tasks involve:

1) Literature review on (i) the properties, application and occurrences of BPA in environmental metrics and biological specimen, (ii) the *in vivo* and *in vitro* toxicology studies on BPA, (iii) the history, methodology and application of metabolomics and (iv) the research progress on dose-response and time-resolved study;
2) The study of "Dose-dependent Metabolomics and Pathway Sensitivity to Map Molecular Cartography of Bisphenol A exposure *in vitro*";
3) The study of "Time-resolved Metabolomics Uncover Dynamic Metabolic Adaptions of Bisphenol A exposure *in vitro*";
4) Summary of research findings and discussion on future topics.

1.3 Organization of the report

This report consists of five chapters. Chapter 1 is an introduction to the background and objective of the MEng study. Chapter 2 mainly reviewed relevant research works carried out in relation to BPA, dose-response and time-resolved studies. Chapter 3 introduced the dose-response metabolomics study of bisphenol A exposure. Chapter 4 presented the time-resolved metabolomics after bisphenol A exposure. Chapter 5

gave a summary of the report and presents the potential future topics.

CHAPTER 2. LITERATURE REVIEW

2.1 Literature Review on Bisphenol A (BPA)

2.1.1 Review on the properties and applications of BPA

2.1.1.1 The physical and chemical properties of BPA

Bisphenol A (BPA), 2,2-bis(4-hydroxyphenyl) propane (CAS: 80-05-7), is a common industrial product and the reaction chemical of acetone with phenol **(Fig. 2.1)**. BPA is an organic synthetic compound with chemical formula to be $(CH_3)_2C(C_6H_4OH)_2$. It belongs to the group of diphenylmethane derivatives and bisphenols materials, with two hydroxyphenyl groups. In standard state, BPA is a colorless solid that is soluble in organic solvents, but poorly soluble in water (Chen, Kannan et al. 2016).

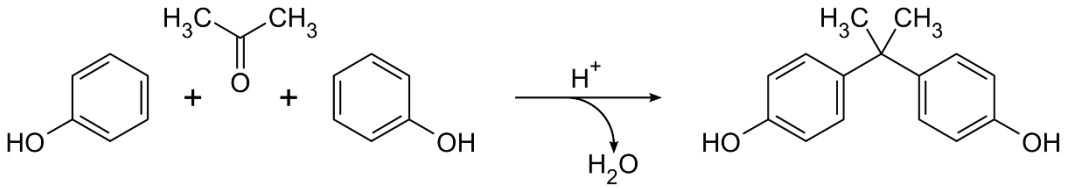

Fig. 2.1 A typical pathway of industrial synthesis of bisphenol A

BPA's physical and chemical properties are as follows: BPA is white to light brown solid flakes or powder in room temperature. It has mild phenolic or weak medicine odor. The boiling point is 360.5 °C at 760 mm Hg. The melting point is 150-157 °C. The flash point is 227 °C. BPA solubility in water is very low, approximately 120 mg/L at 25 °C, yet it is very soluble in ethanol, ether, benzene and alkali. The density is 1.195 at 25 °C (water = 1). The Octanol/Water Partition Coefficient (log Kow) is 3.32. The vapor pressure is 0.02 mm Hg at 170 °C (Rykowska and Wasiak 2006). And the Henry's Law constant equals to 4.0×10^{-11} atm-cu m/mol at 25 °C. The heat

of combustion is -7.465 J/kmol. The acid dissociation constant (pKa) equals to 9.6 (Kim, Chen et al. 2021).

2.1.1.2 The applications of BPA

BPA is firstly reported by chemist Aleksandr Dianin in 1891, and has been widely applied in the production of polycarbonate plastics in 1950s. As for BPA acts as a monomer in polycarbonate plastics, its polymerization reaction with phosgene is conducted under biphasic conditions; while the hydrochloric acid is scavenged with aqueous base **(Fig. 2.2)**. In production of major classes of resins, specifically the vinyl ester resins, the production process usually begins with alkylation of BPA with epichlorohydrin.

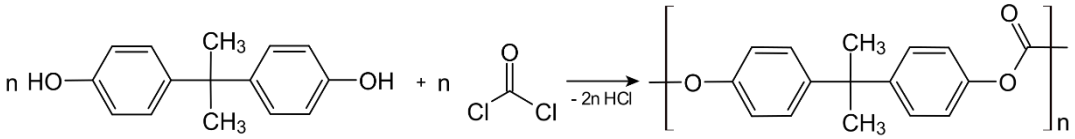

Fig. 2.2 Polymerization process of bisphenol A

Nowadays, BPA is greatly consumed as bisphenol plasticizer in epoxy resins and polycarbonate plastics manufacturing industries, as well as daily products, food packages, plastic bottles, paper products and medical equipment(Fernandez, Arrebola et al. 2007). For a specialized BPA derivative tetrabromobisphenol A (TBBPA) which is brominated dinitrobisphenol A, is capable with brominated flame retardants (BFR) properties. Due to the world's increasing demand for plastic, the production of BPA has grown consistently over the past few years. It is reported that the global demand of BPA has increased from 3.2 million tons in 2003 to 5.5 million tons in

2011 (Flint, Markle et al. 2012), and the global product volume of BPA reached approximately 10.3 million metric tons in 2019 (Garside 2020). Considering the byproducts of BPA analogues in the production process, this huge amount of BPs materials has arisen public's alerting concerns about their environmental impacts and health issues.

2.1.2 Review on the occurrences of BPA in environmental matrices

BPA is ubiquitous in environment compartments **(Fig. 2.3)**. In this study, BPA occurrences in indoor dust, water, sediments, sludge and aquatic species were reviewed.

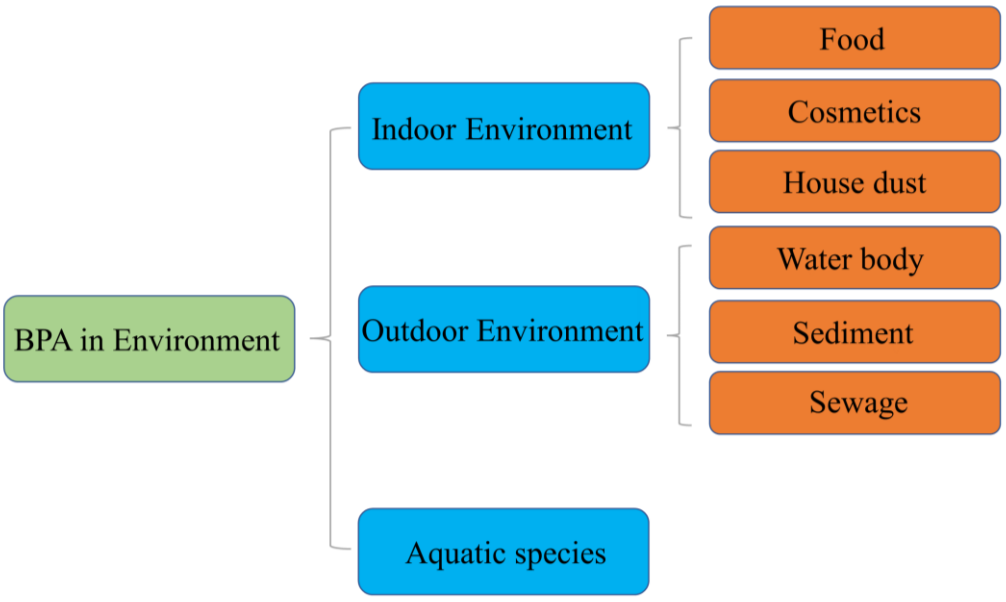

Fig. 2.3 Environment occurrences of bisphenol A

2.1.2.1 Review on BPA occurrences in indoor dust samples

BPA contaminates the indoor environment as it is widely used in furniture coating, floor varnishes, food packaging. Its occurrences in indoor house dust have been found in multiple countries all over the world, with great variations between different regions. According to a survey conducted in 2015 (Wang, Abualnaja et al. 2015), BPA was identified in indoor dust samples collected from 12 countries, including China, Colombia, Greece, India, Japan, Kuwait, Pakistan, Romania, Saudi Arabia, South Korea, U.S., and Vietnam. Among them, samples from Japan showed the highest BPA concentration with 1700 ng/g, while its minimum detection is about 66 ng/g in Pakistan indoor dust. The samples collected from western countries showed higher BPA concentrations in comparison with the Asian ones (USA 1500 ng/g > Vietnam 230 ng/g, Greece 1500 ng/g > India 130 ng/g). Samples in China illustrated a moderate BPA occurrence, with the concentration of about 330 ng/g. The median estimated daily intake (EDI) of BPA through dust ingestion was the highest in Greece (1.6-17 ng/kg bw/day), Japan (1.3-16) and the U.S. (0.89 – 9.6) for various age groups. Eight BPs analogues like BPS, BPAF and tetrabromobisphenol A (TBBPA) are also analyzed, while BPA was the predominant compound in dust from all countries. The results are also consistent with an early study published in 2012 (Liao, Liu et al. 2012), in which they analyzed BPs in 156 indoor dust samples collected from the United States, China, Japan, and Korea. The bisphenol materials total concentration in indoor dust samples were in the range of 26 – 1.1×10^5 ng/g, with GM equals to 2.29×10^3 ng/g. BPA, BPS, and BPF were the three major bisphenols, accounting for more than 98% of the total BPs concentrations. The samples from Korea contained the highest concentrations of both individual BPA and total bisphenols. BPA concentrations in dust were additionally compared among three microenvironments (house, office, and laboratory), with the highest concentration in

office, followed by laboratory samples, slightly higher than house ones. The details are included in **Table 2.1.**

2.1.2.2 Review on BPA occurrences in Water Samples

Sufficient studies have proved BPA along with other BPs presence in water body ranging from river, lake, seawater and sewage. According to a survey conducted in 2015 (Yamazaki, Yamashita et al. 2015), BPA concentrations are determined in river water, surface and subsurface seawater from river and bays collected in Japan, Korea, China, and India. For the river water samples, BPA was detected with the highest concentrations in India with GM equals to 380 ng/L, while lowest in Japan with 12 ng/L. High concentrations of BPA (45–213 ng/L) were also found in river water samples collected from Korea. Chinese samples showed comparably low BPA existence, with GM equals to 22.2 ng/L. For the subsurface seawater sample, BPA was found at a concentration range of 219–431 ng/L at Tokyo Bay. This is mainly contributed to a nearby hazardous waste disposal facility (Hashimoto, Horiuchi et al. 2005). BPA's occurrences in water have also been validated with range from 0.05 to 4.35ng/L in river water and sewage (Wang, Li et al. 2021). In total, BPA in water shows a higher concentration than indoor dust samples. Yet, due to the exposure mode, BPA in air particulates undoubtedly poses greater threat to human health. The details are summarized in **Table 2.1**.

2.1.2.3 Review on BPA occurrences in Sediment Samples

BPA's concentration in the sediments is very important. As an industrial raw material, BPA frequently exchanges with water and vapor media along its production and emission process. Studies have been made to investigate BPs concentrations in the sediments collected from USA, Korea and Japan (Liao, Liu et al. 2012). Among the 172 samples, sediments from Korea demonstrated the highest BPA presences of 567

ng/g dw, followed by Japan of 8.17 ng/g. USA sediments proved to be with the least volume of total BPA of 5.14 ng/g. This is in line with the total BPs concentration rankings (Korea 977 ng/g > Japan 12.5 ng/g > USA 8.58 ng/g). China has reported BPA occurrences in solid samples collected near bay with concentration of 9.1 ng/g dw (Yang, Lu et al. 2014). Several other studies have also proved BPA ubiquitous occurrences in sediment samples globally, including Germany, Netherlands, Italy and United Kingdom (Liao, Liu et al. 2012). The details are included in **Table 2.1.**

2.1.2.4 Review on BPA occurrences in Sludge Samples

BPA in sludge samples have been surveyed systematically, as for it is a vital indicator about WWTP's treatment capacity for BPs matters. Also, as for the microbiome bioaccumulation effect, BPA concentrations in sludge were observed with 2-3 orders higher than influent water. BPA has been detected in sludge samples collected from 52 WWTPs in 30 cities in China, with mean concentration to be 9.4 ng/g (Song, Song et al. 2014). In another study, BPA was found to be over 220 ng/g in sludge collected from 74 WWTPs in USA (Yu, Xue et al. 2015). Researchers have also reported BPA occurrence in Korea WWTPs, with high concentration of 275 ng/g (Lee, Liao et al. 2015). Interestingly, the BPA concentration in sludge is in positive correlation with concentration in water, which may due to the relative approximate treatment efficiency of BPs analogues in WWTP all over the world. The details are included in **Table 2.1.**

2.1.2.5 Review on BPA occurrences in Aquatic species

BPA has been reported to be extensively detected in aquatic organisms, as for their living conditions were heavily affected. The influenced species included angiosperms, invertebrates, molluscs, crustaceans, insects, amphibians, fish, etc. In a global biology research of BPA occurrence (Wu and Seebacher 2020), BPA concentration

in fish was reported to be highest (2500-10000 ng/g), followed by plankton (~1300 ng/g), invertebrates (~1100 ng/g) and other organisms. Also, BPA concentrations in aquatic species were characteristically distinct with taxa, sex, region and developmental period features. The eco-toxicological effects of BPA were furtherly discussed in Chapter 2.1.4.

Table 2.1. Concentrations of bisphenol analogues in environmental matrices (Chen, Kannan et al. 2016). [a]

Matrix	Region	Year	N	Unit	BPA	BPAF	BPAP	BPB	BPE	BPF	BPP	BPS	BPZ	Total
Sediment														
	USA	1998-2012	82	ng/g	1.49	nd	nd	nd	nd	1.44	nd	nd	nd	3.24
	Japan	2012	56	ng/g	8.30	nd	nd	nd	nd	3.57	nd	nd	nd	12.6
	Korea	2008	34	ng/g	6.02	nd	nd	nd	nd	nd	nd	nd	nd	8.84
Sediment	China	2012	5	ng/g	9.10	489		nd		0.6		0.07		498
Sediment	China		13	ng/g		169								
Water	Japan	2013-2014	18	ng/L	12					215		3.4		
	China		6	ng/L	22.2					277		nd		
	Korea		10	ng/L	63					nd		nd		
	India		14	ng/L	380					nd		26.5		
Water	China		16	ng/L		3080								
Water	China	2012	5	ng/L	11.40	2.2		nd		nd		0.51		14.1
Soil	China		68	ng/g		0.35								
Sludge	Korea	2011	40	ng/g	275	nd	nd	nd		249	nd	3.8	nd	769
Sludge	China	2010-2011	52	ng/g	9.40	0.4			0.06	1.9		4.3		101
Sludge	USA	2006-2007	76	ng/g	222	<1.8	<1.8	<1.8		8.2	<1.8	5.8	<1.8	265
Indoor dust	China		17	ng/g		124								
Indoor dust	China	2012-2014	34	ng/g	330	1.9	<0.5	<1		<1	<2	<2	<0.5	350
	Colombia		42	ng/g	120	2.2	<0.5	<1		33	<2	2.4	<0.5	180
	Greece		28	ng/g	1500	2.5	<0.5	<1		780	<2	860	<0.5	3900
	India		35	ng/g	130	1.5	<0.5	<1		6.7	<2	4.2	<0.5	180
	Japan		14	ng/g	1700	4.1	<0.5	<1		230	<2	160	<0.5	2600
	South Korea		16	ng/g	720	3.0	<0.5	<1		1000	<2	3.6	<0.5	1600
	Kuwait		17	ng/g	250	2.5	<0.5	<1		22	<2	20	<0.5	380
	Pakistan		22	ng/g	66	1.3	<0.5	<1		50	<2	1.8	<0.5	150
	Romania		23	ng/g	600	0.39	<0.5	<1		2.0	<2	82	<0.5	870
	Saudi Arabia		19	ng/g	650	2.2	<0.5	<1		73	<2	28	<0.5	1200
	US		22	ng/g	1500	1.4	<0.5	<1		200	<2	<2	<0.5	220
	Vietnam		12	ng/g	230	1.1	<0.5	<1		57	<2	<2	<0.5	400
	All		284	ng/g	440	1.8	<0.5	<1		36	<2	3.2	<0.5	610
Indoor dust	US	2006, 2010	38	µg/g	1.60	<0.001	<0.001	<0.001		0.05	<0.001	0.63	0.001	2.54
	China	2010	55	µg/g	0.63	<0.001	<0.001	<0.001		0.04	<0.001	0.13	0.001	1.11
	Japan	2012	22	µg/g	2.70	<0.001	<0.001	<0.001		0.06	<0.001	0.82	0.001	3.79

[a] Median, geometric mean, or mean values, whichever available, were summarized in this table. A range of concentrations was given if no mean or median data were reported. Blank cells indicate that the compound was not examined or the information was missing from original references. nd = non-detectable.

2.1.3 Review on the occurrences of BPA in Human Specimen

In addition to environmental samples, BPA is proved to be present in multiple human specimens **(Fig. 2.4)**. According to a risk assessment study in 2010 (Goetz, Wormuth et al. 2010), the most dominant contribution for BPA human exposure is canned food for adults, and polycarbonate products for infants. Comprehensive understanding regarding BPA exposure, fate and distribution in human is well studied. In this study, BPA occurrences in human urine and blood serum were reviewed.

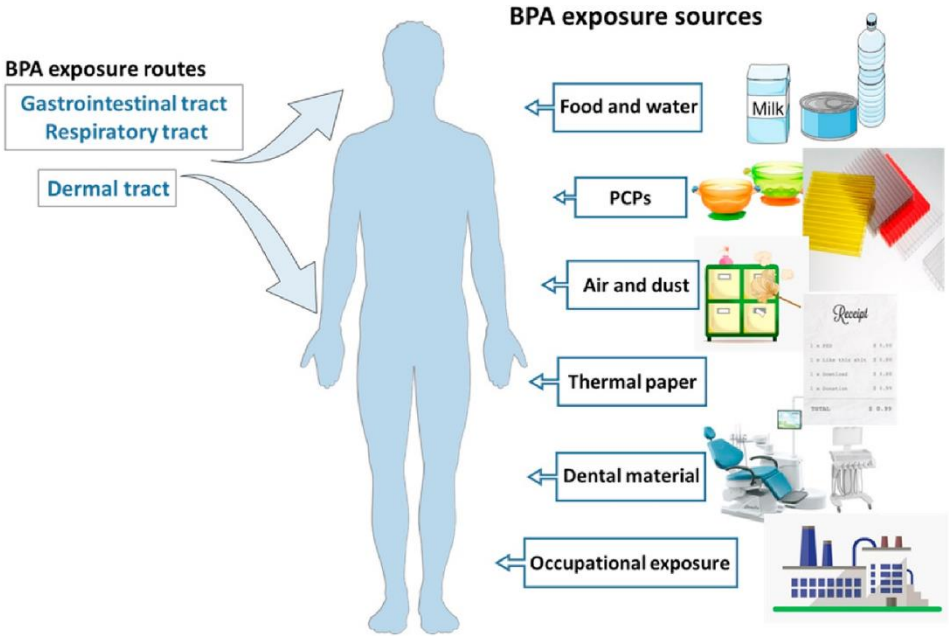

Fig. 2.4 Exposure sources and routes of bisphenol A (modified from (Ma, Liu et al. 2019))

2.1.3.1 Review on BPA occurrences in Human Urine

As for BPA seldom involves in metabolism and biotransformation in human interior milieu, it is commonly excreted as BPA-conjugates outside human body. Thus, urine plays an important role in BPs exposure level monitoring and assessment. The urinary

concentrations of BPA have been well studied and widely utilized to evaluate BPs exposure level (Vandenberg, Hauser et al. 2007). Yang et al. reported BPA existence in human urine samples collected in China, with concentration mean about 0.886 ng/mL (Yang, Guan et al. 2014). Xue et al. observed 26 EDCs presence, including BPA with concentration of 5.08 ng/mL, in the urine samples collected from Indian children (Xue, Wu et al. 2015). Also, the results showed a higher BPA occurrence in obese people than non-obese ones. Asimakopoulos et al. investigated several xenobiotics exposure level in Saudi Arabia population urine samples, with BPA concentration as 4.92 ng/mL (Asimakopoulos, Xue et al. 2017). In another comprehensive study about the urinary BPA level and in-time BPs monitoring in Asian countries population, researchers tested 296 urine samples from seven Asian countries including China, India, Japan, Korea, Kuwait, Malaysia, and Vietnam (Zhang, Alomirah et al. 2011). The result suggested the highest BPA level (2 ng/mL) in the samples from Korea, followed by India (1.59 ng/mL) and Vietnam (1.42 ng/mL). Samples from China shows comparably moderate BPA occurrence (1.1 ng/mL). The Japan samples contain the minimum BPA quantity (0.84 ng/mL). This is in contrast with previous experimental compartment study, which indicates indoor dust and water samples contains relatively high BPA. This may imply that lifestyle is a co-factor in determining the exposure condition. The details are included in **Table 2.2.**

2.1.3.2 Review on BPA occurrences in Human Serum

BPA occurrence in human inner-environmental is essential for *in vivo* exposure condition assessment and toxicology effect identification. Up to date, limited research has regarded BPA occurrences in human serum, as well as breast milk in pregnant women. BPA concentration is determined (5.08 ng/mL) for samples collected from patients (N=58) with endometriosis in Italy (Cobellis, Colacurci et al. 2009), which

is 60% higher than the control group. They also demonstrated BPA can increase the sensitivity of the endometriotic cells to estradiol. These studies further suggested that the study of BPA exposure levels and toxicity mechanisms in populations is of great significance to public health issues. The details are included in **Table 2.2.**

Table 2.2. Concentrations of bisphenol analogues in human specimens(Chen, Kannan et al. 2016). [a]

Matrix	Region	Year	N	Unit	BPA	BPAF	BPAP	BPB	BPE	BPF	BPP	BPS	BPZ	Total
Human														
Urine [b]	USA	2010-2011	31	ng/mL								0.299		
	China		89	ng/mL	1.1							0.226		
	India		38	ng/mL	1.59							0.072		
	Japan		36	ng/mL	0.84							1.18		
	Korea		33	ng/mL	2							0.030		
	Kuwait		30	ng/mL	1.24							0.172		
	Malaysia		29	ng/mL	1							0.071		
	Vietnam		29	ng/mL	1.42							0.160		
	All		315	ng/mL	1.2							0.168		
Urine	China	2013	94	ng/mL	0.886	0.018				0.228		0.029		
Urine	Saudi Arabia	2014	130	ng/ml	4.92	0.05	0.3	0.05		0.19	0.093	13.3	0.06	19.0
Urine	India	2012-2013	76	ng/mL	5.08							0.04		
Serum	Italy		69	ng/mL	2.91			5.15						

[a] Median, geometric mean, or mean values, whichever available, were summarized in this table. A range of concentrations was given if no mean or median data were reported. Blank cells indicate that the compound was not examined or the information was missing from original references. nd = non-detectable.

2.1.4 Review on the toxicity of BPA

The toxicity effects of BPA are multifaceted and multilayered. Epidemiology suggested its endocrine-disrupting potentials, which has been validated by a variety of *in vitro* bioassays, ranging from estrogenic, antiestrogenic, androgenic and antiandrogenic (Chen, Kannan et al. 2016). Furtherly, BPA can pose adverse effects on whole endocrine systems through hormone regulation. It is also capable to reach the intestinal epithelium and could cause structural or functional damages through food intake. Available studies have demonstrated the adverse effects of BPA both in model animals and human specimens, and both *in vivo* and *in vitro* studies have indicated that BPA exhibits mutagenicity, genotoxicity, cytotoxicity, acute oral toxicity as well as developmental reproductive toxicity **(Fig. 2.5, Fig. 2.6) .**

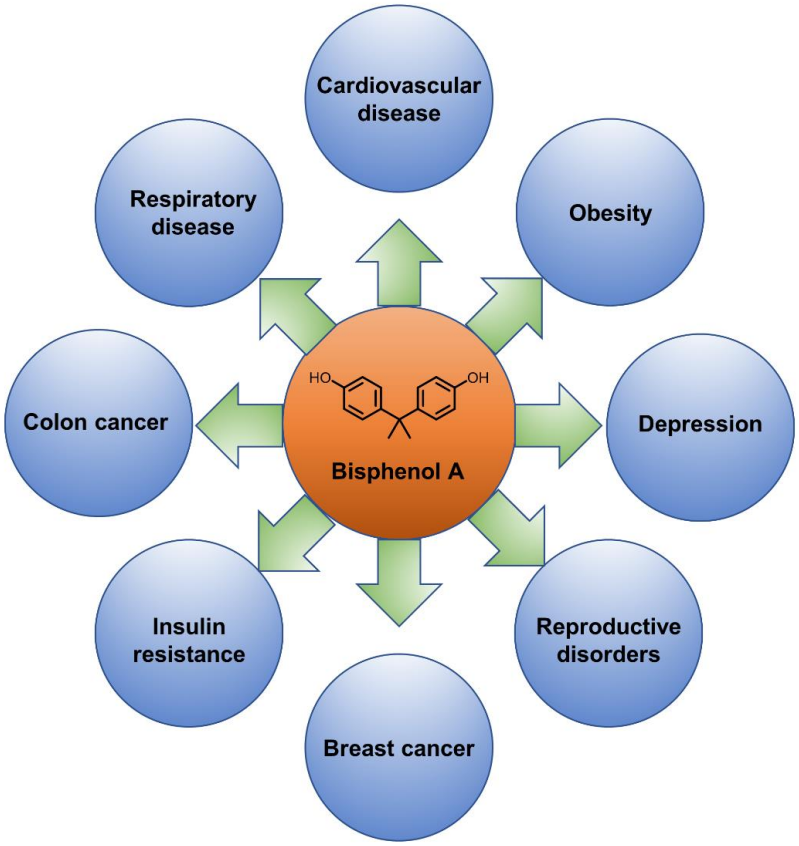

Fig. 2.5 Review on toxicity effects of BPA *in vivo* and *in vitro*

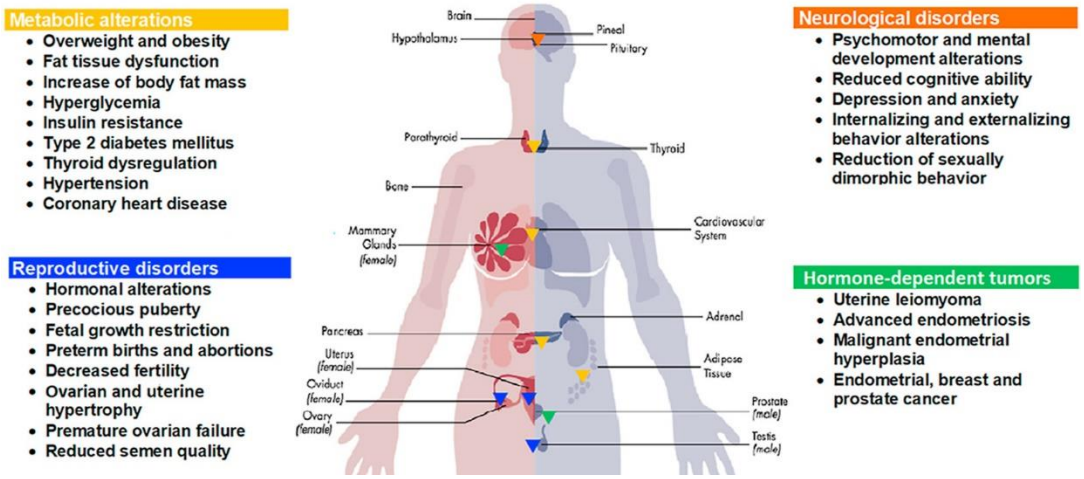

Fig. 2.6 Toxicity effect of BPA in population (Martinez-Ibarra, Martinez-Razo et al. 2021)

2.1.4.1 Review on the *in vivo* toxicity of BPA

2.1.4.1.1 Acute toxicity

Several studies have been conducted to investigate the acute toxicity of BPA for both single-dose and full-dose tests. The test exposure routes included oral, dermal, inhalation and intraperitoneal. In full-dose oral tests, the oral LD_{50} for BPA was reported to be 4 mg/kg in guinea pig, 3250 mg/kg in rat, 2400 mg/kg in mice, and 2230 mg/kg in rabbits (Michalowicz 2014). Thus, the early-stage investigations illustrated comparably low acute toxicity of BPA. Its rapid metabolism as well as inconsiderable contamination of food makes it safe to be added in food packages and receipt paper (Pant and Deshpande 2012).

2.1.4.1.2 Developmental toxicity

Sufficient work in lab has evaluated BPA's developmental toxicity effect for survival and growth in rodents. It has been proved to interfere with embryonic programs of development, morphological sex differentiation, perturbation of the brain and recognition behavior and immune responsiveness (Golub, Wu et al. 2010). A 1250 mg/kg dosage of BPA oral exposure caused 18% mortality in the rodent models, with the symptoms of increased gestation length and body weight loss. Extensive research has been paying much attention to BPA developmental toxicity in aquatic animals on ecotoxicology level. An embryo-larval development study was carried out to test the adverse effects of BPA on *Rhinella arenarum* by means of standardized bioassays (Hutler Wolkowicz, Svartz et al. 2016). Their study suggested that BPA was more toxic to embryos than to larvae at all exposure times. At acute exposure, the lethality rates of embryos exposed to concentrations of 0.0005 mg/L BPA and greater were significantly higher than rates in the vehicle control, whereas lethality rates of larvae were significantly higher in concentrations of 10 mg/L BPA and greater. A significant increase in toxicity was observed with 96-median lethal concentrations were 0.04 mg/L and 2.2 ml/L BPA for embryos and larvae respectively. In another study regarding *Danio rerio* embryos, the LC_{50} was determined for as 70 μM after 24 hours, 72 μM after 48 hours, 47 μM after 72 hours and 31 μM after 96 hours exposure. It is also worth noted that low dose BPA had induced morphological and physiological alterations, such as yolk sac and pericardial edema, hatching delay or inhibition, spine deformation, decreasing in heartbeat rate and mortality (Scopel, Sousa et al. 2021). These *in vivo* studies have suggested BPA's relatively low acute toxicity to extinguished organisms. Yet, the chronic *in vitro* toxicology study is still promising to clarify the mode of action and biological mechanisms of BPA induced adverse effect.

2.1.4.2 Review on the *in vitro* toxicity of BPA

2.1.4.2.1 Cytotoxicity

Cytotoxicity is defined as the toxicity resulted from the action of chemotherapeutic agents on living cells. Studies have reported the cytotoxicity of BPA in multiple cell line assays. BPA mainly induces cytotoxicity with the formation of reactive oxygen species (ROS), which impairs intracellular lipids and proteins. The cell viability of Human immortalized keratinocytes (HaCaT) cells is reported to be 60% and 12% after exposure to 50 μg/mL and 100 μg/mL BPA by MTT assay (Son, Nam et al. 2018). Another study conducted by MTT assay certified that the half maximal inhibitory concentration (IC_{50}) for Michigan Cancer Foundation-7 (MCF-7) cell, male and female amniocytes were 100, 40 and 4 μg/ml, respectively (Aghajanpour-Mir, Zabihi et al. 2016). Neri et al. reported that BPA posed cytotoxicity to human monocytes cell, with effect concentrations of BPA corresponding to 50% of the cell viability and necrosis as 1.39 and 1.48 ng/ml, respectively (Neri, Virzi et al. 2015). McGlinchey et al. tested BPA's inhibition effect on Chinese hamster ovary (CHO-K1) cells by Neutral Red Assay, and implied the existence of a cytotoxicity threshold between $1x10^{-7}$M to $1x10^{-6}$M BPA, over which a proportionately large increase in cytotoxicity is observed (McGlinchey 2009). Fujiwara et al. reported that BPA exposure didn't induce ReNcell VM cell death within the concentration range between 10^{-16} and 10^{-10} M (Fujiwara, Miyazaki et al. 2018). Padberg et al. observed a EC_{50} value of BPA is 261 ± 27 μM in HepG2 culturing (Padberg, Tarnow et al. 2019). The cytotoxicity data helps researchers to better understand the cell tolerance level to BPA exposure stress, and provide instructions on the proposed biomedical use in the outreached *in vitro* test. In general, the cytotoxicity of BPA is not as severe as other highly toxic

chemicals, like polycyclic aromatic hydrocarbons (PAHs) and dioxin.

2.1.4.2.2 Endocrine disruption effect

Endocrine disrupting chemicals (EDCs) are exogenous chemical substances with endocrine disruption effect. They can interfere with the endocrine and nervous system and cause abnormal effects in humans and animals, even with trivial amounts. EDCs are to do with disorders of the reproductive organs of animals and humans, abnormal behavior, reduced reproductive capacity and death of embryos (Crisp, Clegg et al. 1998). As for its estrogen-mimic ability, BPA is one of the chemicals which are firstly recognized with EDCs effect. Plenty of research has proved BPA's similar potency to estradiol in stimulating cellular responses, including estrogenic, antiestrogenic, androgenic and antiandrogenic effect (Rubin 2011). However, it is reported that BPA has a lower binding affinity with ER-α and ER-β receptors of 1000 folds in reference to estradiol (Kuiper, Lemmen et al. 1998). Considering the trace and highly-efficient characteristics of endogenous hormone, BPA with relatively low abundance still poses great threat to hormone balances. The competitive binding of BPA is the basic mode of action, which will induce disturbances in hormone signaling and endocrine disorder. Liu et al. characterized BPA's binding pocket with ERRγ *in silico* (Liu, Matsushima et al. 2014). Eckstrum et al. reported BPA's alteration effect in the ER-mediated transcription of sex-difference-gene with multiple targets affected (Eckstrum, Weis et al. 2016).

2.1.4.2.3 Reproductive toxicity

Reproductive toxicity refers to the effects and damage of chemicals on the reproductive systems, including adverse effects on adult sexual function or fertility, and developmental toxicity to offspring. BPA's endocrine disruption effect is linked with reproductive toxicity, which also depends on sex differentiation. According to

epidemiology data, on one hand in males, exposure to high serum concentration of BPA (1.53–2.22 μg/L) especially during developmental stage can result in alteration of sperm parameters, testicular and epididymal atrophy, and reduction of testosterone levels (Karnam, Ghosh et al. 2015). On the other hand in females, high serum concentration of BPA (1.53–2.22 μg/L) induces changes in estradiol E2, which resulted to hormone system imbalance and metabolic abnormalities such as menstrual irregularities, higher implantation failure, and ineffective gonadotropin fertility treatment (Martinez-Pena, Rivera-Banos et al. 2017). It is also verified that exposure to BPA under developmental stage damages reproduction potential in *Danio rerio* embryos and hormone balance in adult zebrafish (Naderi, Wong et al. 2014). Apart from ER, BPA is also reported with potential of thyroid receptor (TR), thyroid transport receptor (TTR), androgen receptor (AR) perturbation effect, which will induce developmental toxicity for organisms. BPA make effects on the development of the thyroid and hypothalamic pituitary gland, through regulating hormone synthesis and inducing endocrine disorders in the thalamus and spleen (Peyre, Rouimi et al. 2014).

2.1.4.2.4 Genotoxicity

Genotoxicity measures the extent to which a pollutant can directly or indirectly damage cellular DNA, producing mutagenic and carcinogenic effects. BPA can cause chromosomal aberrations through ER-dependent pathways (Aghajanpour-Mir, Zabihi et al. 2016). In addition, BPA is implied to promote tumorgenesis procedure of certain susceptible cells by increasing the level of chromosomal instability. Dobrzynska et al. demonstrated BPA's specific accumulation and induced DNA impairment in lymphocytes and cells from kidneys, spleen and lung (Dobrzyńska and Radzikowska 2013). Fic et al. tested BPA exposure effect for HepG2 cell, and found significant genome damage with DNA fragmentation (Fic, Zegura et al. 2013).

Mlakar et al. reported BPA induced expression of genes related to fetal development and immune response in cultured estrogen-dependent osteosarcoma cells (Fic, Mlakar et al. 2015). Castro et al. observed a decreasing trend for 5α-R2 and 5α-R3 mRNA and protein levels in in the BPA post-exposure prefrontal cortex cells, which may impose nervous system disorders and recognition deficiencies (Castro, Sanchez et al. 2015). Other studies also demonstrated BPA's potential to induce DNA double-strand breaks, oxidative DNA damage and micronuclei increase (Lee, Liu et al. 2013, Ramos, Ladeira et al. 2019).

2.1.4.2.5 Mutagenicity

Mutagenicity is corresponding to the induction of permanent alterations in the structure or abundance of the genetic material of cells and organisms. The changes may involve a single gene, gene segments or chromosomes (Kazius, McGuire et al. 2005). BPA's mutagenicity is tightly linked with genotoxicity, yet the former pays more emphasis on the mutation induction effect. Kovacic et al. reported BPA can induce DNA base modifications through ROS formation (Kovacic 2010). Atikinson et al. observed the formation of DNA adduct from BPA and its endogenous metabolite bisphenol o-quinone, with concentration 14.25–228 ng/mL (Atkinson and Roy 1995). The cancer-like biomarkers raised great concerns about BPA's carcinogenicity effect, also suggested BPA as a potential mutagen as for its binding affinity with deoxyguanosine. In another epigenetics study regarding BPA's DNA methylation consequences on MCF cell, 70% reduction in the formation of tubules in the collagen under 10^{-6} M BPA stress is reported (Fernandez, Huang et al. 2012). Methylation analysis showed the hypermethylation of BCL2L11, PARD6G, while NUP98 and CtIP are hypomethylated. The researches further demonstrated the upregulation of repair genes (RCA1/2, BARD1, RAD51, etc.), also the downregulation of apoptotic genes (PDCD5 and BCL2L11). The result suggested the toxic effects of BPA on

transcription process, also with negative feedback antioxidant system activation to delay cell apoptosis (Jalal, Surendranath et al. 2018). Besides, the signaling pathway disturbance induced by BPA is considered to contribute to cancer targeting, disease morphology and cellular mutagenicity.

2.1.4.2.6 Carcinogenicity

Carcinogenicity evaluates carcinogen's induction effect of abnormal biomolecules, compensatory cell proliferation, activation of proto-oncogenes, inactivation of oncogenes, defective DNA damage repair and epigenetic changes, etc., which finally leading to tumorigenesis. BPA's carcinogenicity is a result from its genotoxicity and mutagenicity. BPA is commonly recognized with canceration risk in consequence for the binding with ER and AR. The competitive binding undoubtedly leads to disturbances in nuclear receptor signaling and transcription procedure. Soto et al. observed adverse effect posed by BPA on breast gland development and galactophore tumors induction in rodents (Michalowicz 2014). In another study on mice, Huff et al. demonstrated BPA's adverse outcomes on hematopoietic cancer development in testes (Huff 2001). As for BPA's mimic effect for estradiol, the sex hormone, many carcinogenicity consequences are to do with pathway signaling in sex organs. Breast, testes and prostate included. The mode of action covers DNA methylation, chromatin remodeling and neoplastic disease development (Doherty, Bromer et al. 2010). Anna et al. tested BPA's capacity to stimulate proliferation in OVCAR-3 cancer cell line (Doherty, Bromer et al. 2010). Other research report an increase in the level of tumor necrosis factor (TNF-α) and induction of apoptosis and necrosis of the cells after exposure to BPA (Richter, Birnbaum et al. 2007). In summary, BPA is corresponding to carcinogenetic effect in ER and AR-sensitive *in vivo* organs and *in vitro* cell lines.

2.1.4.2.7 Immunotoxicity

Immunotoxicity is defined as the toxicological effect on immune system from toxicant post-exposure. BPA is widely reported to interfere with cell proliferation (T lymphocytes and B lymphocytes for example), and activity inhibition in immune system. Its immunotoxicity mechanisms are suspected from its adverse effects on ER, AR and peroxisome proliferator-activated receptor (PPAR) signaling function in immune response and antioxidant feedback. Lee et al. observed an increase of interleukin 4 (IL-4) and IL-8 in mouse T lymphocytes after exposure to BPA, which plays a key role in regulating humoral immunity and adaptive immunity (Lee and Lim 2010). Sakazaki et al. proved that B lymphocytes is extremely sensitive to mitogenesis inhibition under BPA stress (1μM) mouse spleen (Sakazaki, Ueno et al. 2002). Similarly, in another study, Wetheril et al. noticed the proliferation of B lymphocytes along with the stimulated expression of antibodies and cytokines (Wetherill, Akingbemi et al. 2007). Though limited research has been investigating BPA's immunotoxicity potential to human health, it is suggested that BPA can impair immune function, promote respiratory allergy and airway inflammation, also compromise immunological tolerance to dietary proteins (**Fig. 2.7**) (Kimber 2017).

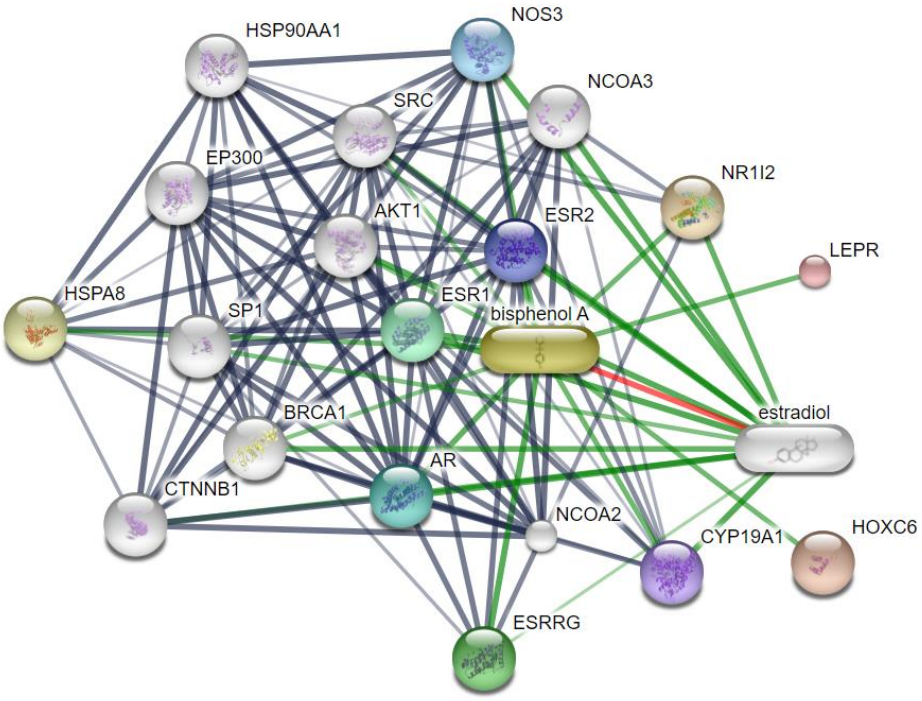

Fig. 2.7 Enzyme and receptor targets of BPA in human, plotted by STRING database (https://string-db.org/)

2.2 Literature Review on Metabolomics Research

2.2.1 Review on the development and application of Metabolomics Study

Metabolomics is the comprehensive study of metabolite fingerprints in cells, tissues, fluid, organs and organisms, or small molecular substrates, intermediates and metabolites generated through cellular processes. The metabolomics study provides a biochemical and phenotype-relevant overview of the biological system, and the physiological effects of diseases, nutrition, medical treatment or genetic modification on the organism (Jordan, Nordenstam et al. 2009). It is a newly emerging omics-study field, acting as an essential contributor to system biology research. One of the challenges of system biology and functional genomics is to integrate proteomic, transcriptomic and metabonomic information to better understand cell biology. When messenger RNA gene expression data and proteomics analysis cannot describe all the physiological activities in the cell, metabolic analysis can obtain a transient snapshot of the cell physiology (Patti, Yanes et al. 2012).

It is commonly acknowledged that modern metabolomics is founded Dr. Jeremy Nicholson in 1998 (Holmes, Nicholson et al. 1998) . In 2005, METLIN, the first metabolomics network database for the characterization of human metabolites was established by Siuzdak laboratory at the Scripps Research Institute. METLIN contains over 450,000 metabolites (in 2019) and other chemical entities, each with experimental tandem mass spectrometry data generated from molecular standards at multiple collision energies, in both positive and negative ionization modes. It provides groundbreaking technical support for spectral alignment, metabolite profiling and data analysis (Guijas and Siuzdak 2018). In 2007, the Human Metabolome Project, researchers led by Dr. David Wishart completed the first draft of the Human Metabolome Database. It included a database of approximately 2500 metabolites, as well as 1200 drugs and 3500 nutritional components, which is still

being updated and providing data support for researchers nowadays (Wishart, Feunang et al. 2018). In 2015, metabolome profiling in real-time was demonstrated for the first time, which revealed changes in metabolite dysregulation and disturbed pathway orders in time series.

Common applications for studying human, microbial or plant metabolomics include: pharmaceutical research to help describe and identify new biomarkers of disease and evaluate toxicity for personalized medicine; integration of functional genomics, or study the interaction of genome, transcriptome, proteome, and metabolome to predict gene function; microorganisms excavation and strain optimization; plant metabolomics for agricultural biotechnology; environmental research, testing the impact of pollutants in aquatic or terrestrial ecosystems, optimizing the production of biofuels; nutrition research, evaluating nutritional levels and conducting food safety testing (Guijas and Siuzdak 2018). As a discipline developed in the new century with the goal of information processing and modeling integration, also an important branch of systems biology, metabolomics assays have been widely used in the medical field and food field with their own advantages. Metabolomic study will continue to develop and innovate, and make great contributions to the progress and development of mankind.

2.2.2 Review on the Analysis Methodology of Metabolomics Study

2.2.2.1 Untargeted Metabolomics

Untargeted metabolomics, also known as global metabolomics, is the process of comparing the metabolome (all metabolites of an organism) of a control group with that of an experimental group to identify differences in their metabolites. Metabolomics research provides a means for researchers to step out of the sea of metabolites and provide a comprehensive overview to identify differentially

regulated metabolites. Then, by working backwards through the known metabolic pathways to identify regulatory enzymes and genes, insights into disease pathogenesis and drug treatment mechanisms can be completed.

The general analysis process of non-targeted metabolomics is: (i) Metabolic profiling (also called differential expression analysis): in a set of experimental and control samples, metabolites of interest with statistically significant changes in abundance are searched for; (ii) Identification: after performing metabolic profiling, the chemical structures and identity of these metabolites are determined; (iii) Interpretation: the final step of the research process, the association between the identified metabolites and biological processes or biological states is interpreted (Schrimpe-Rutledge, Codreanu et al. 2016) **(Fig. 2.8) .**

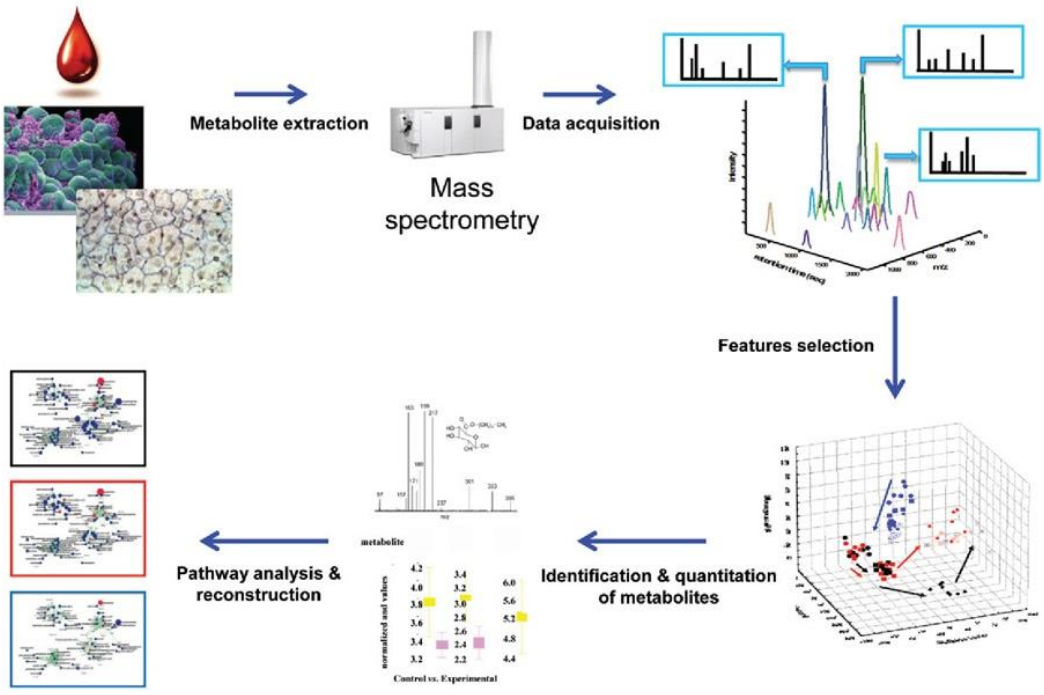

Fig. 2.8 A typical workflow of an untargeted metabolomics research, modified from previous protocol (Schrimpe-Rutledge, Codreanu et al. 2016)

2.2.2.2 Targeted Metabolomics

Targeted metabolomics is an important part of metabolomics research as an extension and expansion of global metabolomics research. Compared with untargeted metabolomics analysis, targeted metabolomics has several characteristics such as high specificity, high detection sensitivity and accurate quantification. Through the enrichment and accurate quantitative and qualitative analysis of a specific metabolite in blood, urine or other body fluids and tissues, it can reveal the relevant molecular biological mechanism of action in combination with other experimental data on the one hand, and provide strong support for the subsequent in-depth research and development of metabolic molecular markers on the other hand. While untargeted metabolomics focuses on the relative content of metabolites in the samples, targeted metabolomics measures the absolute content of metabolites in the samples. Its methodology focuses on quantitative analysis using natural and biologically variable samples, validating pre-identified metabolites, also relying on analytical standards.

The general analytical process for targeted metabolomics is: (i) Data collection and standards obtaining. The standards should be synthesized if they are not available. The MRM data of the metabolites are determined by optimizing the product ion collision energy, mobile phase ratio and other parameters, to obtain the signal by QQQ. (ii) Quantification. MRM data are next processed with quantitative analysis to determine the absolute content of each targeted metabolite. (iii)Statistical analysis and interpretation. The quantitative results are generated by applying statistical analysis method, such as t-test or ANOVA, to determine the dysregulation intensity and significance (Lu, Bennett et al. 2008) **(Fig. 2.9).**

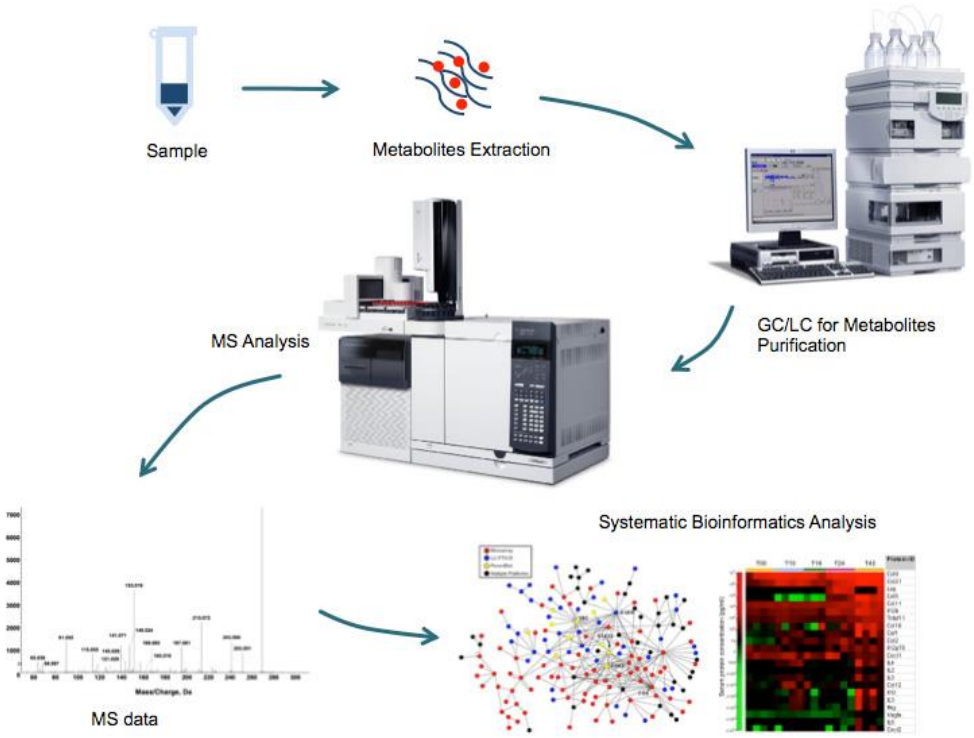

Fig. 2.9 Typical workflow of a targeted metabolomics research

2.2.3 Review on the Instrumentation techniques of Metabolomics Study

2.2.3.2 Gas chromatography–mass spectrometry (GC-MS)

Gas chromatography–mass spectrometry (GC-MS) is a chromatographic technique for the separation and analysis of volatile components. Gas chromatography works on the principle that an inert gas (usually helium) is blown through the column at a high temperature. Sample injected thus evaporates and volatile molecules are pushed through the column, where they interact with the column's coating materials. Each compound interacts differently with the coating as it passes through the column, resulting in different retention times and thus providing an effective separation of the volatile molecules before they are introduced into the mass spectrometer. Gas chromatography–mass spectrometry (GC-MS) is a method that combines the properties of gas chromatography and mass spectrometry to identify different

substances for analysis in a specimen. A major advantage of this method is the ability to design columns to separate specific analytes of interest, but a limitation and prerequisite for GC is the analytes' tendency to volatilize and stabilize at high temperatures. Metabolite coverage can be improved by chemical derivatization of non-volatile molecules, but at the cost of introducing another variable into the metabolite histology data. However, many metabolites remain non-volatile and therefore difficult to quantify by GC-MS (M.R, S et al. 2019) **(Fig. 2.10).**

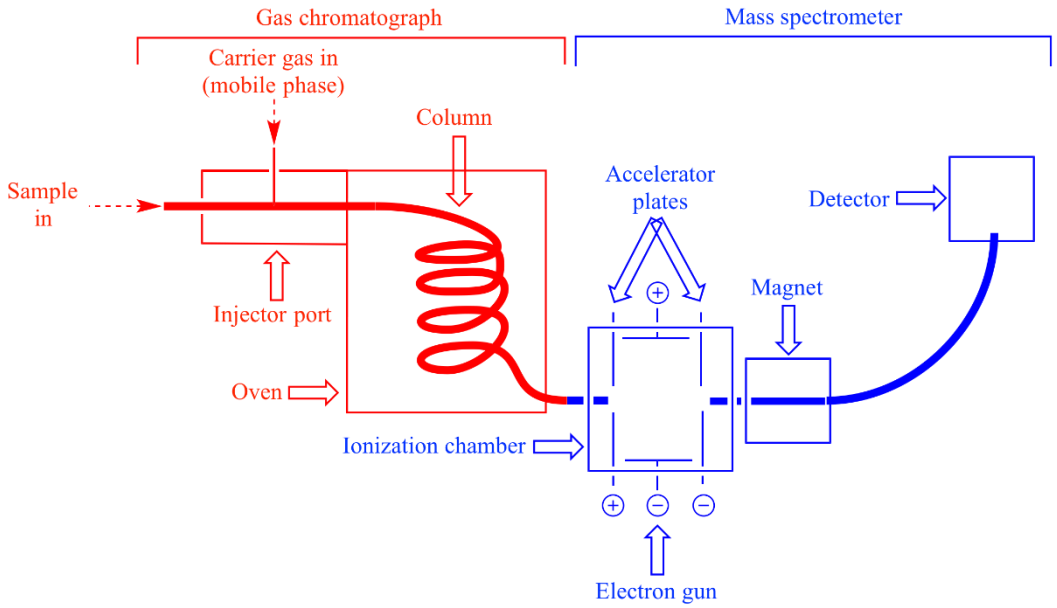

Fig. 2.10 Typical working principal for GC-MS instrumentation

.

The drawback of GC-MS based metabolomics is that it requires derivatization of the sample, which increases the sample preparation time. The advantages are its high sensitivity, its clear advantages in chromatographic reproducibility, resolution and reproducibility of mass spectral fragments obtained by electron bombardment of the ionization source, and its low influence by matrix effects (Beale, Pinu et al. 2018).

2.2.3.3 High Performance Liquid chromatography–mass spectrometry (HPLC-MS)

Liquid chromatography (LC) uses a liquid mobile phase, usually a mixture of water and organic solvents, that operates under high pressure. Similar to GC, in HPLC, a given sample is forced through a column by a liquid under high pressure. The column itself contains a solid adsorbent material that, depending on its degree of interaction with the adsorbent material, will slow down the passage of compounds, thereby separating individual substances and providing different retention times. By changing the column and mobile phase, different types of substances can be separated and then introduced into the mass spectrometer. HPLC-MS is a very powerful analytical technique in metabolomics research with comparably high sensitivity and selectivity. HPLC-MS is also used for the analysis of natural products, and for the analysis of secondary metabolites of plants and animal specimens. The most frequently used HPLC method is reversed-phase high performance liquid chromatography (RP-HPLC), also hydrophilic interaction liquid chromatography (HILIC) has been developed for the analysis of charged polar metabolites (Pitt 2009) **(Fig. 2.11).**

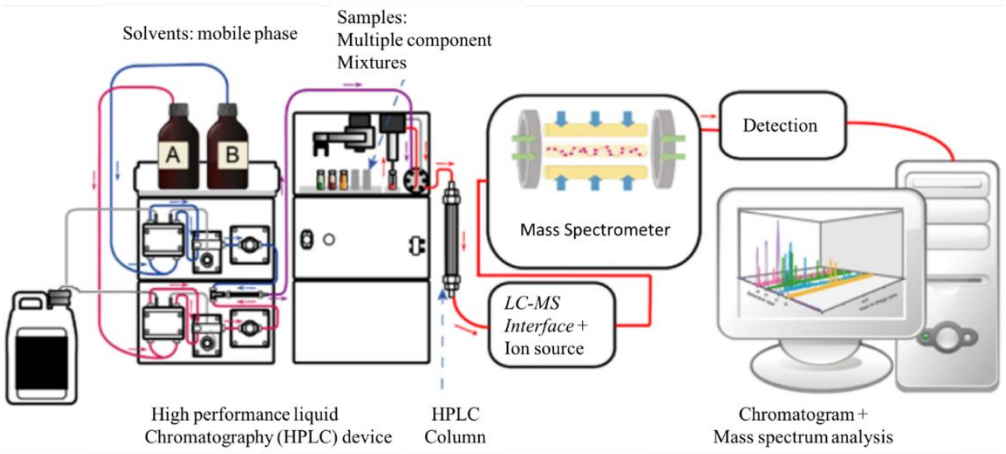

Fig. 2.11 Typical working principle for HPLC-MS instrumentation

The advantages of HPLC-MS based metabolomics are outstanding analytical sensitivity and specificity of the metabolite targets, more accurate identification of the structure of the metabolites, reliable qualitative and quantitative results, and greatly improved analytical efficiency. The disadvantages are the high price and maintenance costs, as well as the variation in detection sensitivity, and the fact that different parameters and instruments do not yield identical data for HPLC-MS. Another problem faced by HPLC-MS based metabolomics techniques is the influence of the liquid phase flow on the operating conditions of the mass spectrometry, and also the influence of the temperature of the mass spectrometry ion source on the analytical source of the liquid chromatography (Matuszewski, Constanzer et al. 2003).

2.3 Literature Review on Dose-response Research

2.3.1 Dose-response relationship: definition and applications

Dose-response relationship is an assessment of the relationship between the dose of xenobiotics entering the organisms and the severity of the adverse effects induced (Altshuler 1981). The adverse outcomes are commonly annotated as toxicology endpoints. The values of the toxicological endpoints are derived from toxicity tests by specific measurements taken during or at the end of the test. They measure the severity of biological dysfunctions including mortality, behavior, reproductive status or physiological and biochemical changes (Sass 2000). Assessment of dose effects according to endpoints often requires extrapolation from animal studies to human responses and from high doses to low doses. Therefore, the assessment of dosing effect requires appropriate fitting models to predict the occurrences of the effect and to define its statistical and biological meanings.

In practice, it is widely acknowledged by scientists to apply dose-response curves for the relationship visualization and characterization. A dose-response curve is a coordinated graph that relates the magnitude of a stimulus to the response of a biological event. The measured dose is typically plotted on the X-axis and the response is plotted on the Y-axis. In some cases, the logarithm value of the dose is applied, in which case the curve is usually sigmoidal, with the steepest part in the middle. A biological dose-response model is considered with preference using the logarithm doses. Statistical analysis of dose-response curves can be performed by regression methods, such as probit models, logistic models, or other empirical fitting methods (Hamilton, Russo et al. 1977). Empirical models based on nonlinear regression are usually better than using some transformation of the data that linearizes the dose-response relationship (Ritz 2010, Andrzejczyk, Greer et al. 2020).

2.3.2 Review on the Dose-response models

2.3.2.1 Linear

A linear dose-response relationship, also known as threshold dose-response, is the relationship between dose and biological response in a straight line. In other words, at any dose, the rate of change (slope) of the response is the same. A typical linear dose response formula is shown as **Equation (i)*** and **Fig. 2.12**: (x stands for concentration level, and y stands for observed effect intensity)

$$y = d + bx \qquad \text{(i)}$$

** b: slope; d: signal at control*

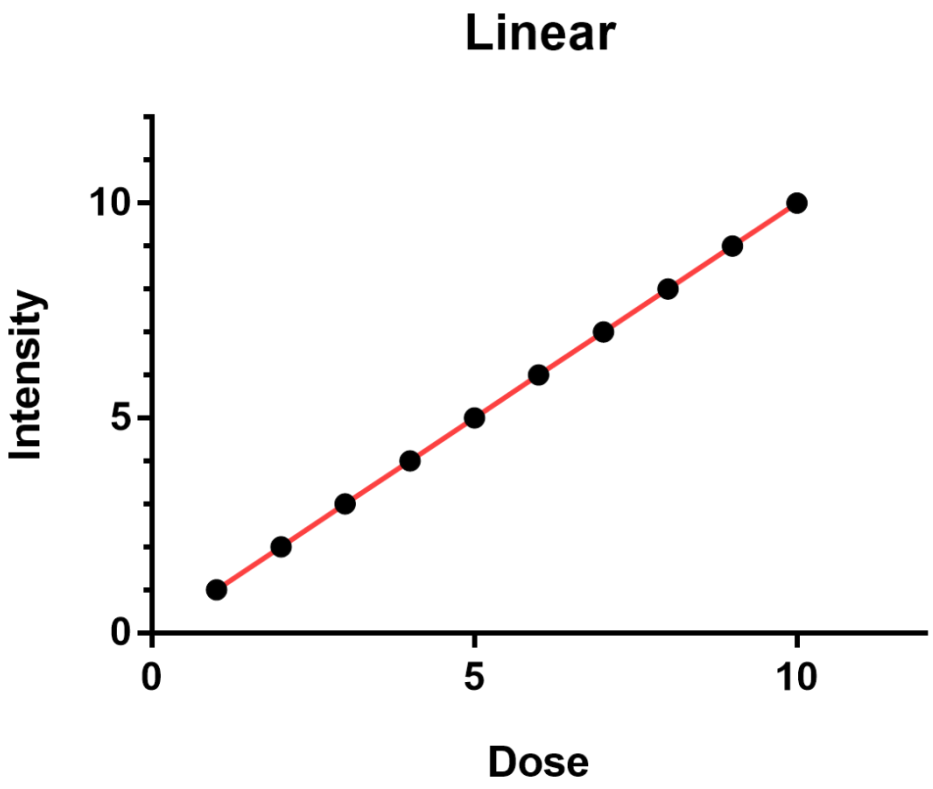

Fig. 2.12 A typical linear dose response curve

In a linear dose-response relationship, as the dose increases, the intensity of the effect or response also increases or decreases with proportional and monotonic trend. However, in biological organisms, a linear relationship is less frequent and exists only in certain in vitro experiments and within a certain dose range. For example, below no-observed-adverse-effect level (NOAEL). Recently, studies have raised about whether a linear model better suits the reality than the non-linear dose-response curve (Seong, Seo et al. 2016).

2.3.2.2 Logistic

Logistic dose-response relationship, also called as sigmoid, is one of the most featured and widely-applied model in dose-response study. The logistic equation

assumes that the conversion rate is proportional to the converted and unconverted substrates. It is founded upon the hypothesis that conversion initially proceeds exponentially, then slows down and eventually saturates, producing the characteristic S-curve. A typical four-parameter logistic dose response formula is shown as **Equation (ii)**[*]:

$$y = \frac{Kde^{bx}}{K + d(e^{bx} - 1)} \quad \text{(ii)}$$

** K: signal at maximum; b: slope; e: Euler number; d: signal at control*

The Logistic formula was originally an optimal mathematical model to describe the growth pattern of a population under resource-limited conditions. It is interesting to note that this equation has been well applied for the dose-response relationship in many endpoints' characterization, though their meanings are completely different. For fitting convenience, researchers developed four-parameter logistic dose response formula which is shown as **Equation (iii)*** and **Fig. 2.13:**

$$y = d + x^b \frac{a - d}{x^b - c^b} \quad \text{(iii)}$$

** a: signal at highest value; b: slope; c: medium effect concentration (EC_{50}); d: signal at control*

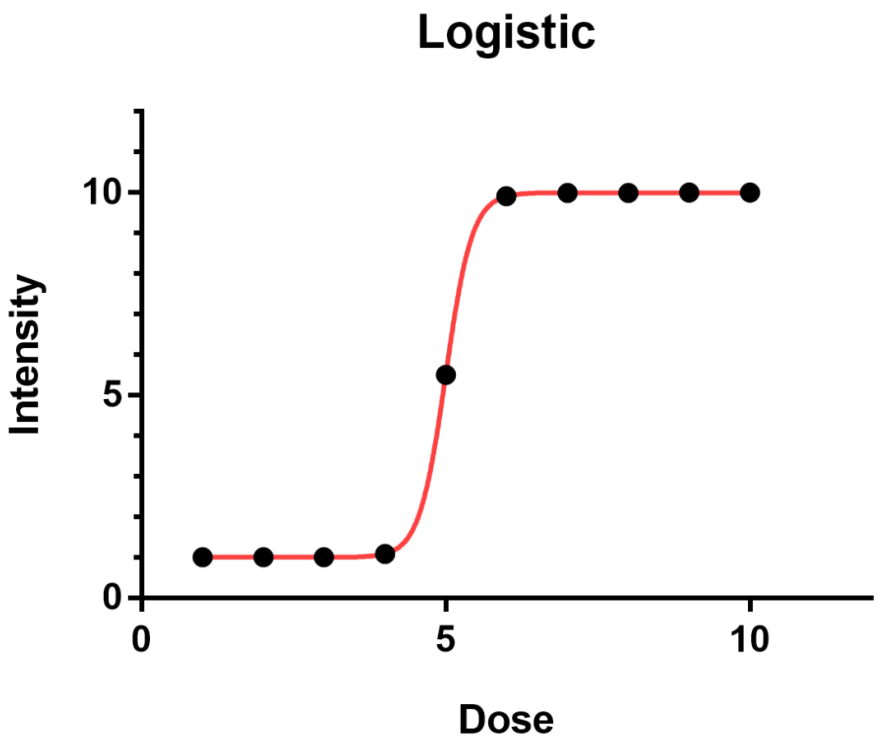

Fig. 2.13 A typical four-parameter logistic dose response curve

Logistic equation is often used combined with log-transformed dosing levels. It is a widely applied theory in statistics, physics, ecology, machine learning, medicine, even economics. From the reasoning model reflecting a linear limiting relationship of nutrition on population growth in ecology, to the sensitivity of stochastic behavior to initial values in the evolutionary process from order to chaos in quantum mechanics, all these elements are contained in the logistic difference equation, revealing the knowledge richness embedded in the depth of the logistics theory (Ritz, Baty et al. 2016).

2.3.2.3 Exponential

The exponential dose-response model is one of the most widely used models in the field of quantitative microbial community characterization, and was originally

developed based on mathematical assumptions in microbiology regarding the number of pathogens consumed and the variability of the infection process. As for the rapid development population boost of microbes under suitable culturing atmosphere, the observed effects are preferably described by models with exponential algorithms (Schmidt, Pintar et al. 2013). A typical exponential dose-response relationship is shown as **Equation (iv)*** and **Fig. 2.14:**

$$y = d + b(\exp\left(\frac{x}{e}\right) - 1) \qquad \text{(iv)}$$

** b: shape parameter I; d: mean signal at control; b: shape parameter II ;*

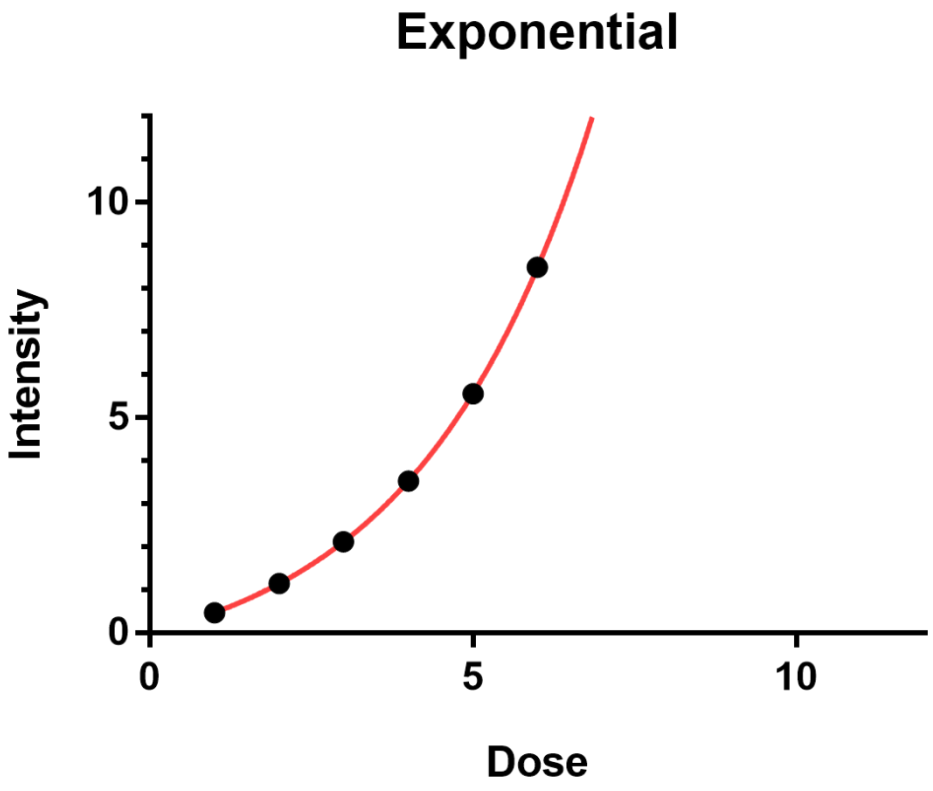

Fig. 2.14 A typical exponential dose-response curve

Similar to Beta-Poisson distribution, in the exponential dose-response model, the number of pathogens consumed during the exposure is assumed to be Poisson distributed, and the probability that each consumed pathogen survives and begins infection in the host-pathogen response is constant. The equation shows the likelihood function, which describes the joint probability of the data which are conditional on uncertainty about the parameter values (Teunis and Havelaar 2000).

2.3.2.4 Weibull

The Weibull distribution was initially used in reliability engineering, especially for the distribution of accumulation failure of electromechanical products. It is a compensatory model for logistic dose-response under certain conditions in toxicology research. Since it can be easily inferred from its distribution parameters using probability values, it is widely used in data processing for various biological endpoints distribution modelling (Ritz, Baty et al. 2016). Weibull distribution is shown as **Equation (v)* and Fig. 2.15:**

$$y = \begin{cases} c + (d - c)\exp\left(-\exp\left(b(\log(x) - \log(e))\right)\right), & Weibull\ I \\ c + (d - c)\left(1 - \exp\left(-\exp\left(b(\log(x) - \log(e))\right)\right)\right), & Weibull\ II \end{cases} \quad (v)$$

** b: slope; d: signal at highest value; c: mean signal at control; e: the dose where the inflection point locates.*

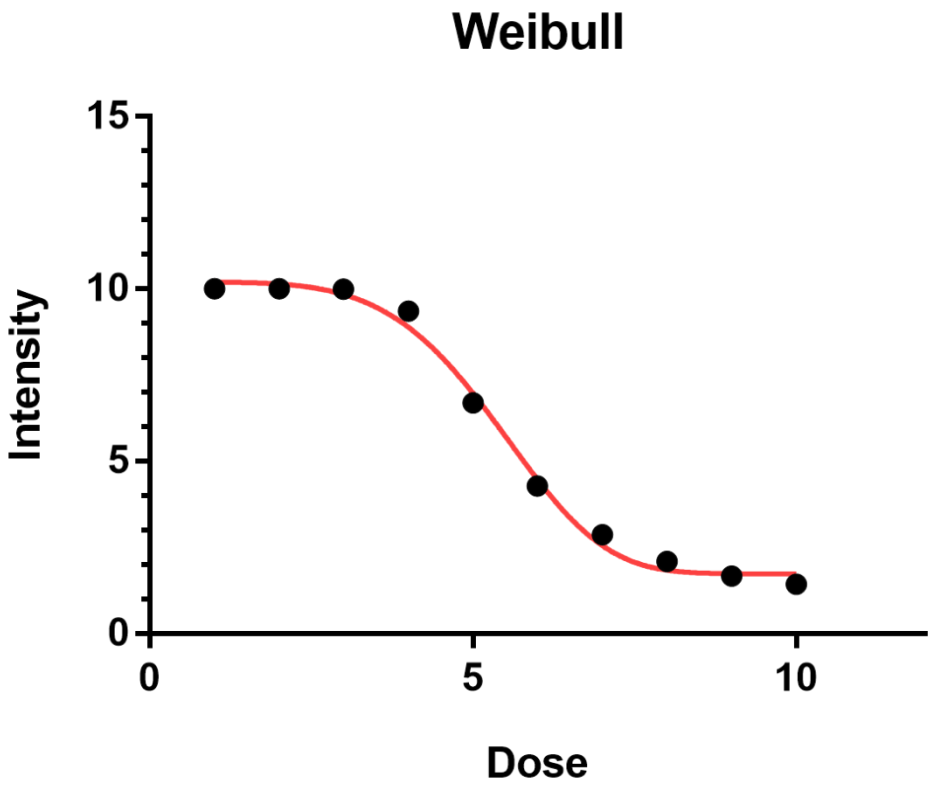

Fig. 2.15 A typical Weibull dose-response curve

Weibull dose-response curve is divided into two parts, which are asymmetry to each other. In the dosage range of lowest limit of Weibull I model area, and the highest limit of Weibull II area, Weibull model shows nearly identical result with log-logistic dose-response curve. Weibull dose-response relationship show slightly different modifications to logistic model, which suits the observed endpoints distribution behavior in the high dosage range more appropriately (Carlborg 1981). Yet, it is seldomly used nowadays as for the generalizability of logistic modelling.

2.3.2.5 Polynomial

Polynomial dose-response model is a data-based empirical approach to explore biphasic nonlinearities. It's founded with the theory that each exposure value is

reformulated as a polynomial of certain degree (eg. 3,4,5), producing an estimated model with multiple predictors. The main advantage is that it produces a single overall relational model. The disadvantage is that the fit can be poor over a selected range of exposure doses, particularly over the highest and lowest exposure dose ranges (Zetzsche and Nuding 2005). Over the years, multiple correction models have been established based on the basic idea of polynomial dose-response model, like fraction polynomial and splines (Lewis, Micke et al. 2012). A typical 3rd order polynomial dose-response model is shown as **Equation (VI)* and Fig. 2.16:**

$$y = d + cx + bx^2 + ax^3 \qquad \text{(vi)}$$

** a, b, c, d are the fitting parameters for 3rd order term, 2nd order term, 1st order term and constant, respectively;*

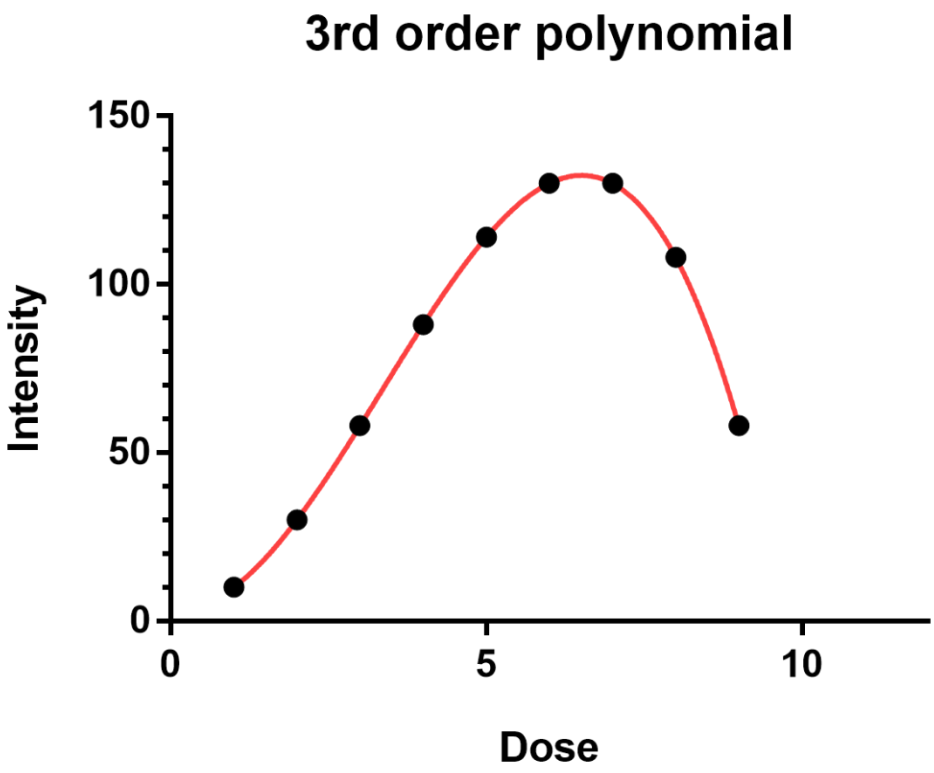

Fig. 2.16 A typical 3rd order polynomial dose-response curve

The most appealing characteristic of polynomial model is its capacity to simulate biphasic dose-response curve (U-shaped) even with more inflection features, though sometimes this would lead to quite uncertainties in certain dosage range. With a higher order equation, it allows to describe the trend in a more complicated model with more inflection points, also with high fitting goodness. Yet, as for the intrinsic data limitation, it would also result in drawbacks like ambiguous statistical meaning (too complex model) and overfitting (too few data points) (Faes, Geys et al. 2003). Up to now, limited research has regarded the methodology in traditional toxicological endpoints characterization (May and Bigelow 2006). Still, as for no single approach is universally appropriate, the polynomial model may be promising and suitable in several future dose-response relationship establishment (Sunde, Nilsen et al. 2007, Herwibawa and Kusmiyati 2017).

2.3.3 Review on the Dose-response modelling strategies

Dose-response curves' establishment can be easily accomplished with automation software, like GraphpadPrism and Matlab. However, to achieve higher quality in confidence level and prediction performance, one still needs to make certain modification and optimization on the modelling strategies, which is mainly concerned with the data transformation and model selection (Seong, Seo et al. 2016).

Firstly, about the log-transformed dose values. The rationale for log-transformed data processing is quite straightforward. In toxicity studies, test doses range widely from non-effect-observed dose levels to toxic dose levels. Log-transformation of the concentration data effectively stabilizes the variance, and regression analysis of the log-transformed data allows quantitative assessment of the magnitude of the nonlinear kinetics of the test compounds in toxicity studies (Igarashi 1995).

Secondly, about the normalized toxicity effect values. The normalizing process means to constrain the datasets within the range of 0%-100%, which specifies two fundamental parameters for dose-response curves: bottom and top plateau. This is of extreme importance in study intended to define the best-fit EC_{50}. On one hand, the constraint only makes effect when 0% and 100% are defined by reliable control group, which means they should cover the whole dosage range along a complete dose-response relationship. On the other hand, only when several different dose-response curves are comparable can one plot them on one graph with normalized feedbacks (Carpenter 1986).

Thirdly, about the hill slope. Many dose-response curves follow the identical pattern as receptor binding, a log-logistic dose-response model. The hill slope determines how sharp it is in the steepest range. Models with a higher absolute-value of slope factor tend to be sharper than the standard one (slope = 1), and vice versa (**Fig. 2.17**).

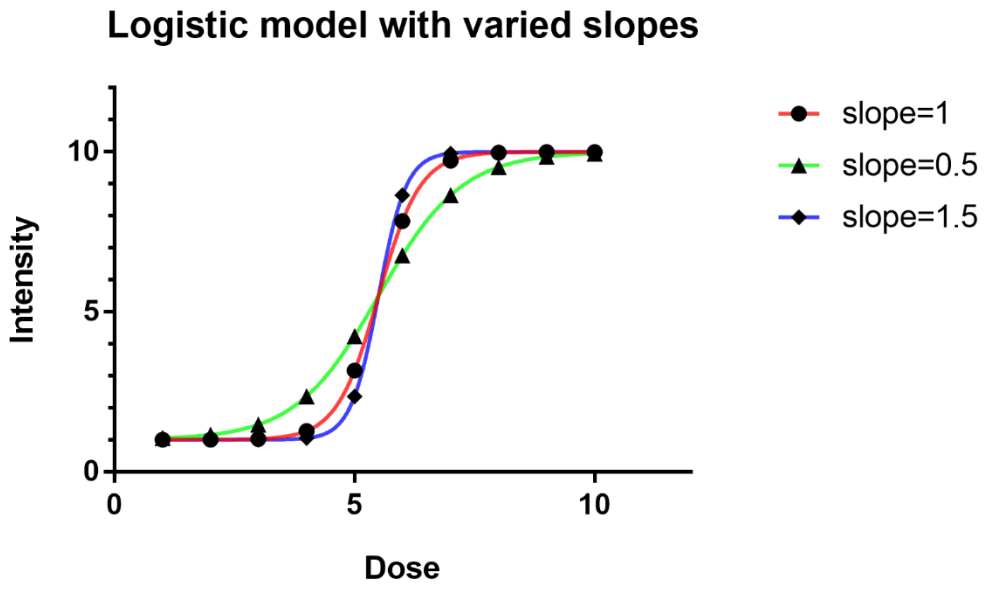

Fig. 2.17 Logistic dose-response model with different slope factors

Additionally, as for the modelling interpretation index (adjusted R squared, confidence & prediction interval, standard deviation, etc.) is a rather comprehensive topic, it requires further investigation and promotions to contribute to for a higher model performance, goodness, stability and robustness (Carpenter 1986).

2.3.4 Review on the Dose-response Omics study

Plenty of research have been regarding dose-response relationship characterization in the omics regulation pattern. On one hand, dose-response omics study is implemented to complement and explain specific biological phenomena and toxicological regulatory mechanisms. Crizer et al. observed a concentration-dependent metabolomic response of liver injury compounds based on the benchmark concentration analysis (Crizer, Ramaiahgari et al. 2021). Zhan et al. investigated the dose-dependent metabolomics effects of Cd stress and presumed an adaptive strategy of metabolic responses (Zhan, Wang et al. 2021) **(Fig. 2.18)**.

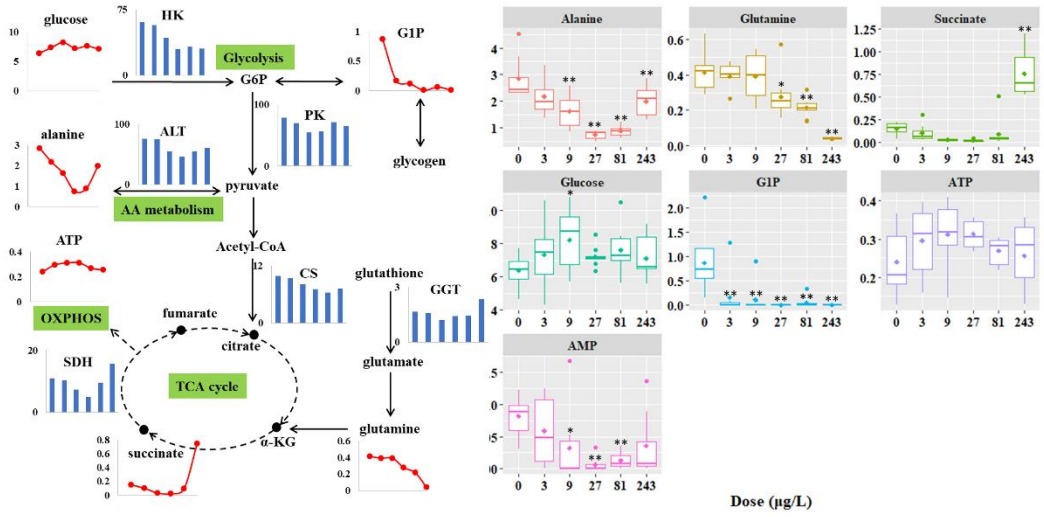

Fig. 2.18 Dose-response metabolite dysregulation and metabolic pathway patterns in clam under Cd stress (modified from (Zhan, Wang et al. 2021))

Several trans-omics studies have also adopted dose-response research strategies to achieve multi-omics integration analysis and comprehensive interpretation of given biochemical phenomenon. Bernhard et al. reported ethoxyquin, a food additive, with dose-response induction effect of lipid metabolism dysfunction and purine metabolism disorder, on a metabolomics and transcriptomics level (Bernhard, Rasinger et al. 2019). Significant elevation of GSH was observed with dose-response manner, which indicated the NRF2-mediated oxidative stress also enhanced detoxification process. Sano et al. investigated the dose-response effect of insulin release on differential gene expression in hepatic cancer cell line (Sano, Kawata et al. 2016). It is interesting to note that the up-regulated genes responded faster than down-regulated ones in a high insulin dose; and vice versa. Typically, genes involved in cholesterol biosynthesis were stimulated while gluconeogenesis-related ones were heavily suppressed. What' more, Kawata et al. constructed a trans-omics data network to assess dose-response relationship of insulin action (Kawata, Hatano et al. 2018). Induced and basal insulin signals were distinguished between high and low doses of

insulin secretion due to distinct sensitivity. The mentioned dose-response omics studies provided researcher with a comprehensive horizon also mechanistic insight into the surveyed biological dysfunctions.

On the other hand, researchers have put great emphasis on the dose-response modelling strategies development. Due to the large data dimension in omics result, dose-response omics has been challenging with its data processing and automation. Several R-packages and platforms have been proposed under the circumstances. In transcriptomic field, Larras et al. reported DRomics R-package as an automated tool for analysis of concentration-dependency in genomics and transcriptomics data (Larras, Billoir et al. 2018). In DRomics, researchers applied four steps to achieve omics data dose-response relationships establishment and automated ecological risk assessment (**Fig. 2.19**). Step 1: to normalize omics data by quantile, scale and cyclic loess method. This aims to eliminate the differences between varied transcriptomic microarrays. Step 2: to filter out the responsive omics data of dose-response characteristics. This helps to remove the large-scale data points without sensitive dose-response features, and examine the desired ones with supervised monotopic or biphasic model fittings. Step 3: to decide the best-fitting models for omics data dose-response characterization. The basic selection pipeline is Akaike Information Criterion (AIC) and false discovery rate (FDR), and the model pool included models as follows: linear, exponential, log-Gaussian-probit and Hill. Step 4: to extrapolate Effect Concentrations (EC) and Benchmark Dose (BMD) values by established dose-response models. This provides an insightful tool to pick sensitive biomarkers from omics data, which can be furtherly applied in chemical ecological risk assessment. In total, DRomics showed great advantages in dose-response omics data automation and process. It is dedicated to perform dose-response characterization with multiple models and provide direct risk assessment suggestions. Similarly, Yang et al. proposed BMDExpress as a solution to characterizing transcriptional and genomic

alterations with dose-dependent manners (Yang, Allen et al. 2007, Phillips, Svoboda et al. 2019), which allows to identify specific biological meanings for dose-response curves in relation to perturbed cellular processes. Ewald et al. established FastBMD as an rapid dose-response benchmark tool for transcriptomic data analysis (Ewald, Soufan et al. 2021).

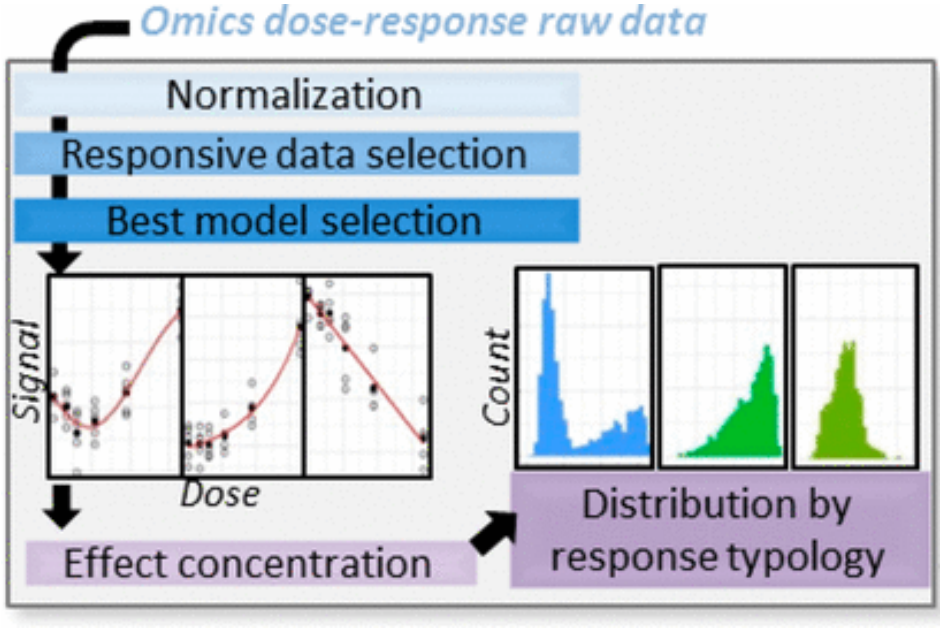

Fig. 2.19 Workflow for DRomics dose-response transcriptomics data dose-response characterization. (Larras, Billoir et al. 2018)

In proteomics field, Schmidt et al. developed ProteomicsDB, a database tool to explore quantitative relationships from proteomics data obtained from MS, in order to provide guidance on drug development (Schmidt, Samaras et al. 2018). Throw the three-layer design, it provided researchers a systematic overview to investigate dose-response correlations between proteomics data and certain biological functions (**Fig. 2.20A**). Specifically, ProteomicsDB focused on three biochemical topics: inhibitor potency analysis, cell viability analysis and protein-drug interactions analysis. For inhibitor potency analysis (**Fig. 2.20B**), ProteomicsDB integrated dose-dependent

competitive-binding data to explore potential protein targets for a given chemical or drug. By fitting omics data in dose-response curves, researchers can predict and calculate EC_{50} range to determine relative binding potency in supplement to other bioassays (e.g., isothermal titration calorimetry, molecular docking, surface plasmon resonance). For cell viability analysis (**Fig. 2.20C**), ProteomicsDB provided an inspection for comparable sensitivity to specific drugs between different cell line assays, which offered researchers instructions on *in vitro* model selection in drug development. And for protein-drug interactions analysis (**Fig. 2.20D**), dose-dependent effects of multiple drugs on multiple protein targets were investigated. This assisted to identify mixture effect for drug-combination in order to achieve best target inhibition and prognosis therapy. In total, ProteomicsDB is a useful and practical tool which integrated dose-response proteomics data for target fishing and drug development (Lautenbacher, Samaras et al. 2022). Similar work like FastBMD, a rapid dose-response tool to perform benchmark concentration analysis from transcriptomic data (Ewald, Soufan et al. 2021).

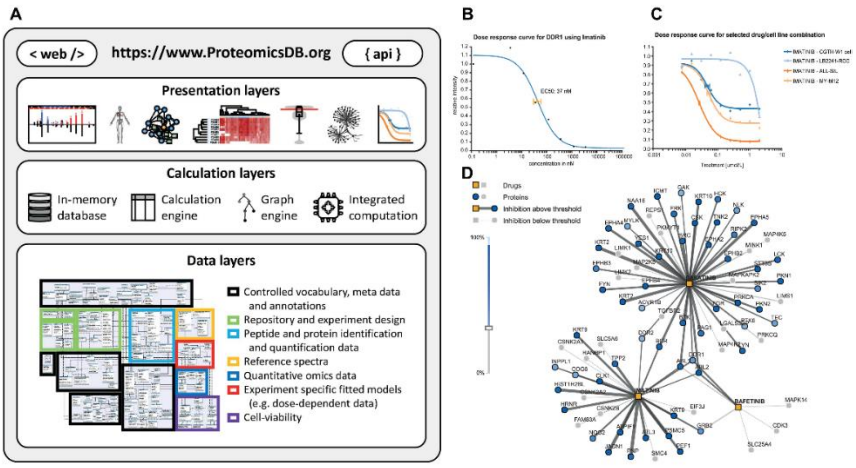

Fig. 2.20 ProteomicsDB interface for dose-response proteomics data process. (A) Three layers framework for ProteomicsDB data analysis logic; (B) Inhibitor potency/ selectivity analysis; (C) Cell availability analysis; (D) Protein-drug interactions analysis. (Modified from (Schmidt, Samaras et al. 2018))

In metabolomics field, it is worth-noted that TOXcms, a newly developed omics-analysis tool focuses on dose-response metabolomics has drawn significant research interests (Yao, Wang et al. 2020). In supplement to the transcriptomic and proteomic dose-response characterization studies, TOXCms focused on metabolites' dose-dependent behavior as for they are tightly related to cellular phenotypes. TOXcms is a LC-MS data processing platform under XCMS framework, which implements three steps automation algorithms to achieve dose-dependent features' identification and biological principles' interpretation (**Fig. 2.21**). Firstly, raw LC-MS data was converted into peak tables by detection and alignment algorithms. Secondly, intensity vs. dose diagrams were plotted, and statistical analysis was applied to examine the significance, further to filter out inflection and scattering features. Finally, the features that were recognized with statistically significant monotopic dose-response relationship were clustered and their EC_{50} values were extrapolated. On top of that, the researcher tested TOXcms performance in the relative off-target effects between metformin and etomoxir. Although the two drugs were both initially designed for liver carnitine pamitoyltransferase-1 (CPT1) inhibition, etomoxir in this study exhibited inhibitions to both CPT1 activity and mitochondrial respiration with numerous dose-response metabolites identified, which suggested its severe off-target effect. Although TOXCms is at first designed for metabolic fingerprints picking with dose response dysregulation manner, it is also promising in finding off-target effects for drugs, binding affinity calculation and biomarkers identification. Though TOXcms is promising for dose-response feature selecting automation, yet challenging in recognizing features with inflection dose-response characteristics (Zhao, Liu et al. 2021).

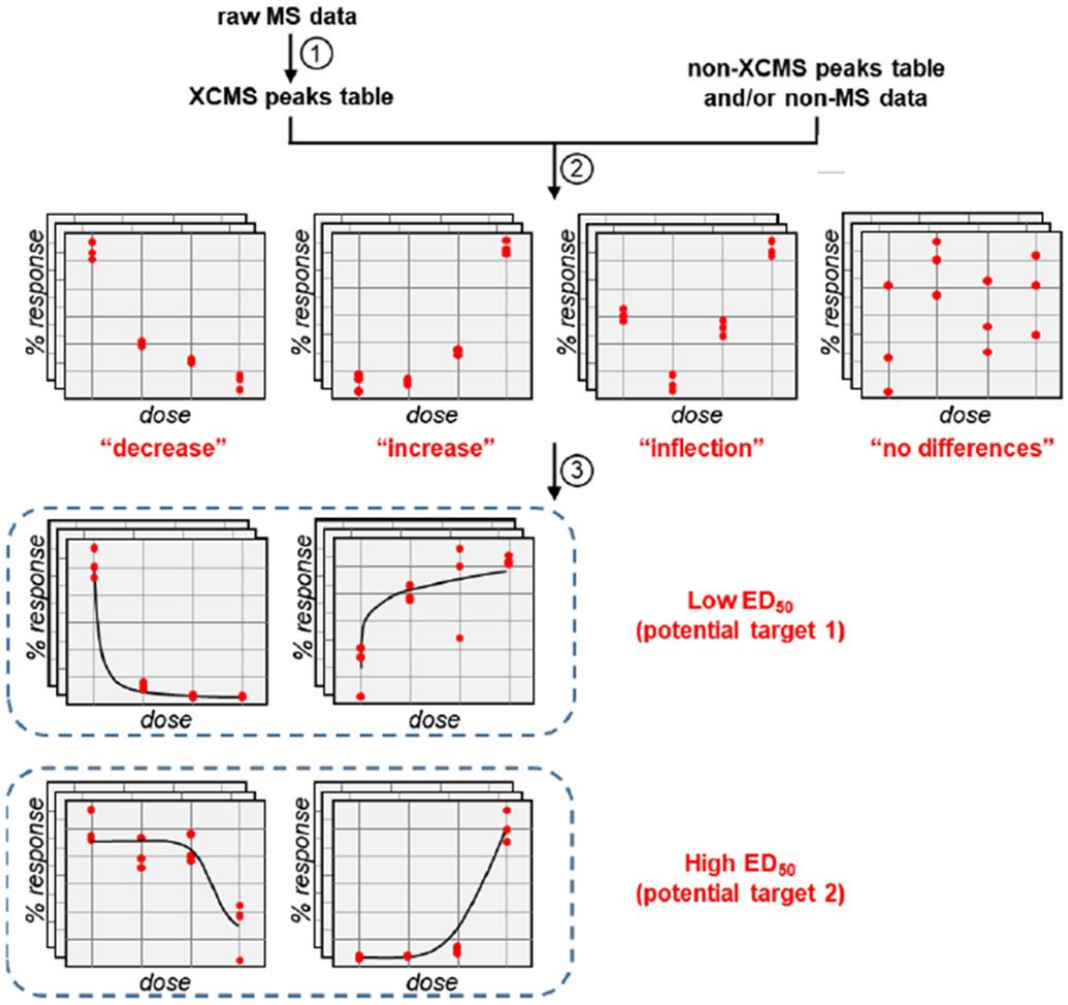

Fig. 2.21 Workflow for TOXcms dose-response metabolomics to identify drug off-target effects. (Yao, Wang et al. 2020)

In summary, omics-scale dose-response characterization studies have been widely utilized to guide data-driven mechanistic analysis and interpret biological phenomenon. This is based on the factor that quantitative relationships underlie most measurable cellular phenomena. Still, the studies mentioned above have certain limitations in model effectiveness, also ambiguous explanation for the toxicity mode of action on an omics-study level. It is also essential to develop novel modelling strategies for omics-data research, to demonstrated the biochemical interpretation embedded in trivial dysregulation change (Smetanova, Riedl et al. 2015, Crizer,

Ramaiahgari et al. 2021). Totally, there is a knowledge gap to standardize the dose-response analysis of metabolomics data by involving compensatory validation experiments (Ritz 2010).

2.4 Literature Review on Time-resolved Metabolomics Research

2.4.1 Review on the Time-resolved Omics study

Time-resolved omics is another topic of importance to draw attention in dynamic omics regime. Similar to the dose-response omics strategy, time plays an indispensable coordinate in full set transcriptome/ metabolome characterization, as for the intracellular metabolome is ever-changing and real-time metabolic balance state is vulnerable (Buchweitz, Yurkovich et al. 2020). Traditional static-state metabolomics only yield the snapshot of the metabolite dysregulation pattern in single timepoint, while time-resolved metabolomics is advancing in depiction and interpretation of complex biological process regarding time change, including metabolic concentration, activity and availability (Link, Fuhrer et al. 2015, Costello and Martin 2018). Across years, though not as mature as dose-response omics techniques, time-resolved metabolomics has already been widely applied in agronomy, toxicology, systems biology, engineering biology, clinical diagnostics fields, and will continue to play a prominent role in the development of dynamic metabolomics and active metabolomics regime (Lee, Jedrychowski et al. 2017, Rinschen, Ivanisevic et al. 2019).

In practice, acting as an indispensable technique under dynamic metabolomics framework, time-resolved metabolomics plays an important role in providing information about mechanisms of metabolic disorders, guidance on drug development and prognostic advice (Spegel, Sharoyko et al. 2013, Kowalski, De Souza et al. 2015, Geng, Misra et al. 2016, Krycer, Yugi et al. 2017, Halama, Aye et al. 2019). Hannes et al. constructed a sampling system which allows to inject *E. coli* directly into LC-MS, to monitor hundreds of metabolites' real-time dysregulation behavior every 15 seconds within several hours (Link, Fuhrer et al. 2015). By the time-dependent control of substrate availability, a "switch-like" inhibition effect of nucleotide synthesis was shown which suggested salvage pathway is preferred rather

than *de novo* for less energy consumption (**Fig. 2.22**). The real-time metabolomics study firstly illustrated significant metabolic transitions within *E. coli*, to satisfy temporal cellular requirements in adaptions to ambient nutritional conditions.

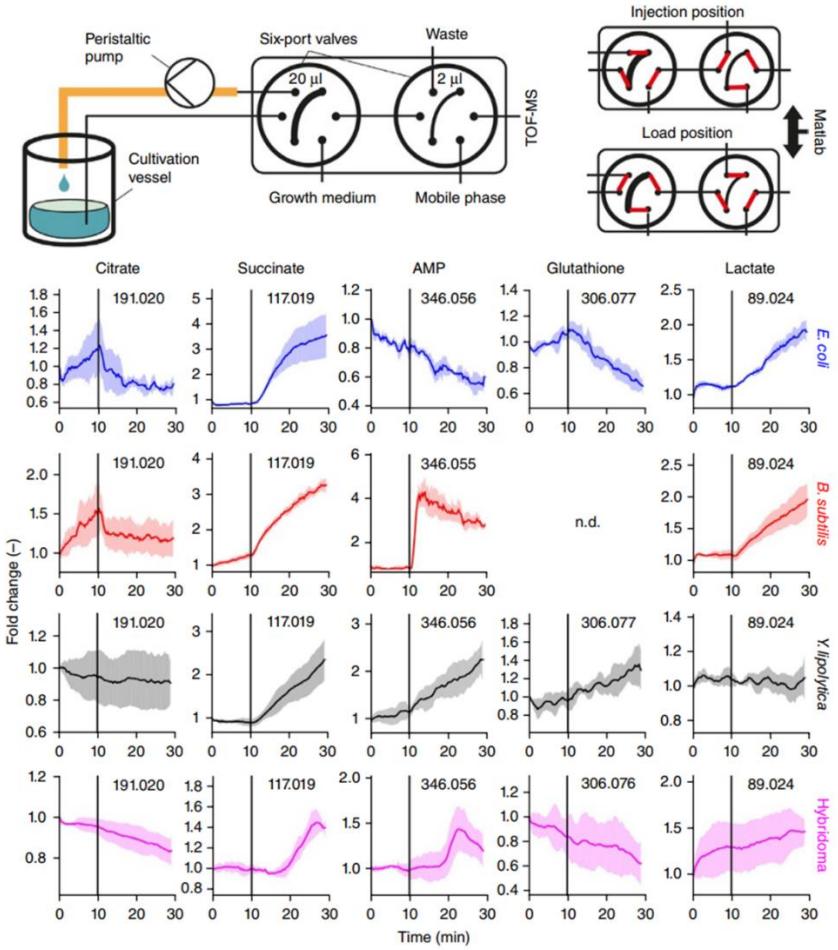

Fig. 2.22 System for real-time metabolome profiling, with time-resolved metabolites' dysregulation pattern presented. (Link, Fuhrer et al. 2015)

Similarly, Jain et al. identified strong positive correlation between glycine consumption with cancer cell proliferation (Jain, Nilsson et al. 2012). With time-dependent glycine reliance from carbon incorporation to purine ring biosynthesis, researcher proposed glycine pathway as a potential metabolic vulnerable target in tumor cells. Lee et al. applied time-resolved proteomics and metabolomics approaches to correlate changes in metabolism and physiology with cancer cell cycle,

and observed multiple metabolic response alterations with reference to time which indicates cell's canceration procedure, including upregulation of nucleotide biosynthesis and downregulation of oxidative phosphorylation as well as the epigenome maintenance breakdown (Lee, Jedrychowski et al. 2017). Li et al. implemented time-series metabolomics strategies to investigate 3,5-diethoxycarbonyl-1,4-dihydrocollidine post-exposure effect in mice, with multiple serum metabolites dynamic dysregulation pattern decided (Li, Xue et al. 2021). Downregulation of docosahexaenoate, arachidonate and linoleate were proposed as the key factors to progressive cholestatic liver injury and fibrosis induction. Herold et al. investigated the differentially expression genes and substrate usage behavior among WWTP microbial community with time-resolved population adaptions (Herold, Martínez Arbas et al. 2020). In another research regarding cell cycle (**Fig. 2.23**), Hartl et al. monitored more than four hundred metabolites dysregulation pattern in bacteria within 160 min, and reported glutathione as the key metabolite playing roles in potassium homeostasis and cell division, which was potentially linked to glycolysis and Glutamate/Glutamine (GABA) cycle (Hartl, Kiefer et al. 2020).

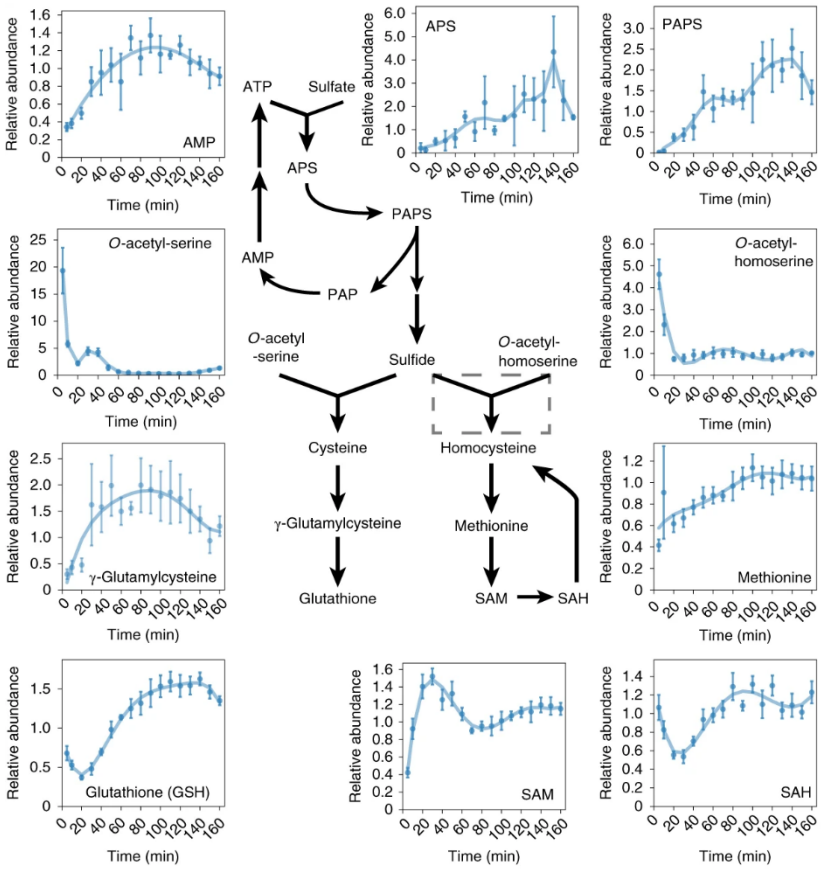

Fig. 2.23 Cell cycle dependency of sulfur metabolism and glutathione identified by time-resolved omics strategies. (Hartl, Kiefer et al. 2020)

Tandon et al. studied fructo-oligosaccharides, a prebiotic supplement, with time-dependent induction effect of selective proliferation of certain gut microbial species (Tandon, Haque et al. 2019). Dai et al. reported severe metabolism and cytokines disturbances in rat exposed to lipopolysaccharide, with significant temporal distinctions in progressive oxidative stress and energy metabolism (Dai, Gao et al. 2016). In engineering biology and synthetic biology field (Vavricka, Hasunuma et al. 2020), time-series metabolomics is also frequently applied to determine key factors interrelated to wheat's growth and production (Li, Xue et al. 2021). Sano et al. investigated temporal transcriptional responses to insulin excretion at different time points (Sano, Kawata et al. 2016). Time-resolved models identified significant

distinctions between two different stages: insulin signaling to transcription and insulin signaling to transcription and mRNA stability.

Besides, it is quite ubiquitous to allocate antimalaria drug performance from dynamic metabolomics study, to achieve the mode of action determination as well as pharmacokinetics optimization (Allman, Painter et al. 2016, Cobbold, Chua et al. 2016, Cobbold and McConville 2019).

2.4.3 Review on Time-resolved Metabolomics' Model strategies

In order to process the huge amount of omics data, modeling strategies play important roles in time-resolved metabolomics study. Unlike the clear biochemical meaning proposed by dose-response relationship, metabolite' time-resolved dysregulation kinetics can hardly be interpreted by stereotypic models (Zampieri, Sekar et al. 2017, Costello and Martin 2018). To process the massive amount of time-resolved metabolomics data, various solutions have been established to parameterize and interpret underlying biological principles (Zampieri, Sekar et al. 2017). Costello et al. developed an unsupervised machine-learning based protocol to unbiasedly predict time-series metabolic pathway dynamics, which proves a supreme performances compared with traditional Michaelis–Menten kinetics fitting (**Fig. 2.24**) (Costello and Martin 2018). Firstly, time-dependent metabolomics raw data were acquired, with various metabolite presented in phase space. Then, the dynamic traces of metabolite were smoothed and differentiated by differential equations. Afterwards, machine learning algorithms (scikit-learn) were applied to learn and generalize models based on the training set data, which included Support Vector Machine (SVM), Random Forest (RF), gradient boosting (GB), k-means and Density-based spatial clustering of applications with noise (DBSCAN). Finally, the generated models were applied to search for virtual features with metabolic significance, as well as provide mechanistic insights about metabolome changes. The implicit methodology is heavily data-driven,

which contains no predefined interactions with particular biology meaning, to improve the prediction performance substantially.

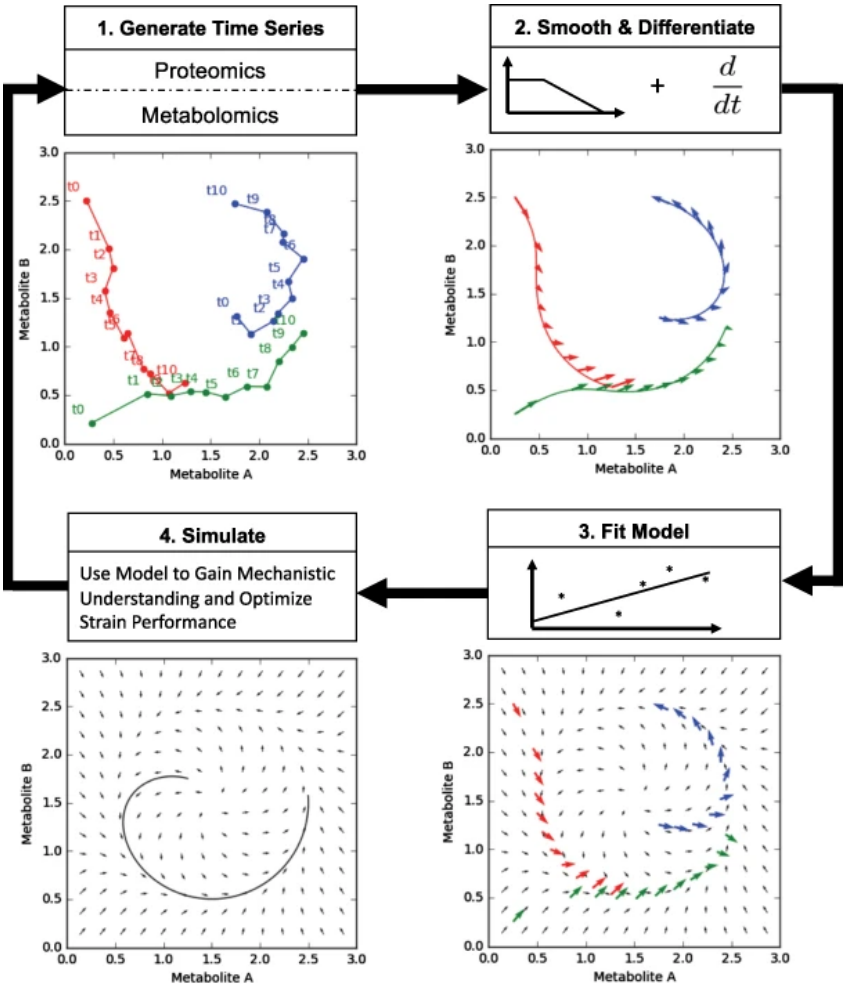

Fig. 2.24 Workflow for a machine-learning based proteomics or metabolomics data processing. (Costello and Martin 2018)

On top of that, Nyamundanda et al. proposed an automated regression algorithm to identify biomarkers with time-resolved dysregulation importance (Nyamundanda, Gormley et al. 2014). And Buchweitz et al. developed a visualization technique to present dynamic metabolome changes within desired biological pathways, by integrated time-course metabolites' changing layouts to generate animations (Buchweitz, Yurkovich et al. 2020). Up to date, researchers are paying increasing attention on effective time-induced information extraction with high performance,

ranging from tensor factorizations, smooths, mean-variation-weighted, and dimension-reducing principal component analysis, etc. (Smilde, Westerhuis et al. 2010, Zhang, Zhou et al. 2015, Li, Hoefsloot et al. 2021)

One of the most prominent and widely implemented time-resolved techniques is referred as Metabolic Flux Analysis (MFA), originated back to 1985 (Papoutsakis and Meyer 1985). MFA starts with stable isotope labeling of specific compounds as carbon source or nitrogen source. By analyzing the stable isotope labeling pattern of downstream metabolites, their kinetic characteristics in the intracellular metabolic pathway can be deduced, ranging from direction, turnover rate, and distribution pattern. Subsequently, the activity level of specific metabolic pathways of organisms can be obtained, thus describing the metabolic activity of cells at the dynamic level (Lee, Park et al. 2011, Shimizu 2013). As a time-and-spatial-resolved targeted metabolomics approach, MFA aims to uncover the main metabolic abnormal pathways and their biological functions with real-time applicability, and reveal their upstream and downstream inter-regulatory mechanisms, which provide a strong scientific basis for understanding the mechanism of disease occurrence and drug target discovery (Papoutsakis and Meyer 1985, Shimizu 2013, Stewart, Dhungana et al. 2015, Kundu, Chakravarty et al. 2019, Chou, Xiong et al. 2021).

Currently, MFA has been widely accommodated in physiological studies, gene and protein function studies, pathological studies (e.g., tumor, obesity and diabetes metabolism), and microbial engineering (Antoniewicz 2021). The common MFA application includes the study of glycolytic pathway, tricarboxylic acid cycle pathway, pentose phosphate pathway, amino acid metabolism (Glutamine, Serine, Tryptophan, Leucine, isoleucine and Valine, etc.), fatty acid metabolism, folate metabolism, methionine cycle, nucleotide metabolism, Nicotinamide adenine dinucleotide phosphate (NADPH) metabolism, etc. (Stewart, Dhungana et al. 2015, Kundu, Chakravarty et al. 2019) MFA can quantitatively characterize the dynamic changes in

cellular metabolism *in vivo* and the fine distribution of flow in metabolic pathways, reveal changes in major metabolic pathways during disease development, and promote the understanding of physiological or pathological mechanisms (Yang, Liu et al. 2007). It can also search for key genes in signaling pathways for cell growth and value-added processes, and characterize metabolic networks in combination with the kinetic properties of enzyme reactions (Lee, Park et al. 2011, Shimizu 2013). Development in time-course metabolomics and flux studies have inspired researchers' interest to combine both methodology for dynamic omics characterization. Unsteady-state flux balance analysis (uFBA), provided a novel quantitative strategy to compute real-time intercellular metabolic changes at cellular scale (**Fig. 2.25**) (Bordbar, Yurkovich et al. 2017). Firstly, time-course metabolomics profiling data were reorganized into discontinuous time-intervals (each indicated a special metabolic state) by PCA analysis. Then, metabolite changing rates at each state were linearly fitted and calculated by MFA principles (confidence intervals, significance). Lastly, metabolic flux was extrapolated and further utilized for dynamic metabolic flow characterization. In this study, parameterized vector is applied as constraints, which shows supreme model performance and robustness than traditional single use MFA or time-resolved metabolomics.

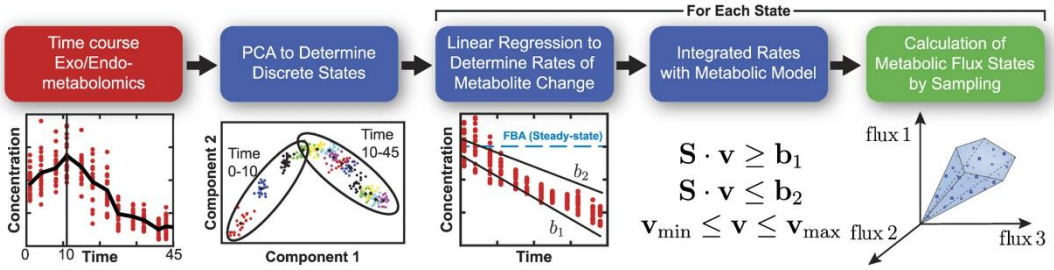

Fig. 2.25 uFBA working principle (Bordbar, Yurkovich et al. 2017)

2.4.3 Review on Time-resolved Metabolomics' major challenges

Several challenges have been revealed during the development of time-resolved

metabolomics research. One is the non-invasive sampling design. Since time-resolved omics study is parameterized with time, the homogeneity and reliability of the metabolomics acquisition data which are determined by different time points of sample collection are of great importance. Though it is easier to accomplish with isotope-labelled MFA techniques and suspension cell system auto-sampling device, challenges still exist for research carried out by adherent cell samples collected *in situ* (Pereira Braga and Adamec 2019). Bishnubrata et al. developed a microfluidic device containing spheroids sensors, which were directly connected to an optimized NMR probe, to achieve real-time metabolome monitoring (Patra, Sharma et al. 2021). The process exhibits no damage to the cell system as for NMR analysis process is comparably non-invasive for observation in live system. In bacteria field, Hannes et al. constructed a system which allows to inject yeast directly into LC-MS, to monitor hundreds of metabolites' real-time change every 15 seconds within several hours (Link, Fuhrer et al. 2015). In a specific case, to investigate the health state in upper gastrointestinal organs, time-series samples were collected by a diameter tube linked patient's stomach to external environment (Folz, Shalon et al. 2021). The findings were further applied to offer therapeutics strategies and prognostic advice.

What's more, the huge sample amounts lead to long-term data acquisition process. To avoid unwanted intra- and inter-batch variations, Kim et al. designed a workflow by which one can quantify and counterbalance the unwanted batch-run deviations under hierarchy framework (**Fig. 2.26**) (Kim, Tang et al. 2021). The protocol included two steps: (i) within batch signal drift adjustment with robust smoothers; (ii) adjustment of the datasets with an unwanted variation in a hierarchical approach. Firstly, with the help of pre-defined intra-batch sample, one can normalized the whole LC-MS data matrix by fitting a linear smoother. By comparing with inter-batch as well as QC samples, this process can include calculation and process of standard adjustment, loess and linear line fitting with pooled QC samples. After that,

correction of multiple batches was performed by using either balanced tree or concatenating approach. The newly developed methodology removed unwanted batch-run variations, in the same time preserved metabolic signals with clear biological meaning, which provided guidance on large-scale omics-data process and design strategies.

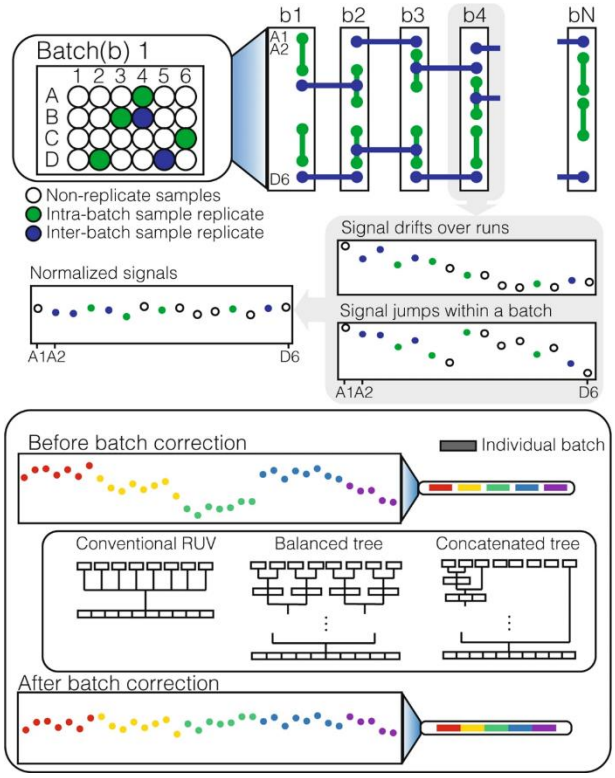

Fig. 2.26 Schematic illustration of the batch-run correction and normalization process. (Kim, Tang et al. 2021)

Nowadays, though ambiguities and false positive results happened occasionally, the generated time-resolved omics processing algorithms along with prediction models have brought novel and promising insights into the underlying correlation of metabolic features with disease status and prognostic impacts regarding time influence (Zhang, Zhou et al. 2015). Still, problems remained on how to avoid false positive and over-fitting models, which require more emphasis in the time-resolved metabolomics data processing field (Smilde, Westerhuis et al. 2010).

2.5 Summary of literature review

From the literature review, the following study progress and research gaps are identified:

1) The occurrences of BPA are ubiquitous both in environmental compartments and organism specimens. It is widely acknowledged that BPA is with multiple adverse health effects ranging from acute to chronic toxicity. However, it is rather challenging to analyze BPA omics-toxicity with its mode of action identified. Hence, a precise and automated method should be developed especially for BPA omics-toxicity identification.

2) Dose-response relationship have been widely applied in toxicological behavior characterization. Different models reported have been reviewed, with model establishing strategies summarized. Yet, insufficient studies have regarded the xenobiotics post-exposure omics-dysregulation pattern with dose-response relationship behavior. What's more, little is known regarding BPA dose-dependent metabolomic dysregulation pattern. More studies are needed to investigate the biological events in the cellular response of BPA to elucidate the underlying mechanism, further to quantify the prediction of metabolomic biomarkers concentration for intended exposure situation

3) Dynamic metabolomics techniques like time-resolved metabolomics MFA provides a promising perspective in real-time metabolome monitoring and dynamic hazard identification. Yet, dynamic metabolomics is poorly implemented in chemical risk assessment, which is of great value in future research. Besides, time-resolved metabolome dysregulation pattern shall provide a mechanistic insight into the dynamic metabolic emphasis with alterations in biological function requirements, which is of great importance in characterizing BPA's toxic mode of action.

CHAPTER 3. DOSE-RESPONSE METABOLOMICS AND PATHWAY SENSITIVITY TO MAP MOLECULAR CARTOGRAPHY OF BISPHENOL A EXPOSURE

ABSTRACT:

In the toxicological regime, the toxicological endpoint and its dose-response relationship are two of the most prominent characters in conducting a risk assessment for chemical exposure. Systems biological methods have been used to comprehensively characterize the impact of toxicants on the biochemical pathways. However, the majority of the current studies are only based on single-dose, and limited information can be extrapolated to other doses from these experiments, regardless of the sensitivity of each endpoint. This study aims to understand the dose-response metabolite dysregulation pattern and metabolite sensitivity at the system-biological level. Here, we applied bisphenol A (BPA), an endocrine-disrupting chemical (EDC), as the model chemical. We first employed the global metabolomics method to characterize the metabolome of breast cancer cells (MCF-7) upon exposure to different doses (0, 20, 50, and 100 μM) of BPA. The dysregulated features with a clear dose-response relationship were also effectively picked up with an R-package named TOXcms. Overall, most metabolites were dysregulated by showing a significant dose-dependent behavior. The results suggested that BPA exposure greatly perturbed purine metabolism and pyrimidine metabolism. Interestingly, most metabolites within the purine metabolism were described as a biphasic dose-response relationship. With the established dose-response relationship, we were able to fully map the metabolite cartography of BPA exposure within a wide range of concentrations and observe some unique patterns. Furthermore, an effective

concentration of certain fold changes (e.g., EC+10 means the dose at which metabolite is 10% upregulated) and metabolite sensitivity were defined and introduced to this dose-response omics information. The result showed that the purine metabolism pathway is the most venerable target of BPA, which can be a potential endogenous biomarker for its exposure. Overall, this study applied the dose-response metabolomics method to fully understand the biochemical pathway disruption of BPA treatment at different doses. Both dose-response omics strategy and metabolite sensitivity analysis can be further considered and emphasized in future chemical risk assessments.

3.1 INTRODUCTION

Toxicological endpoint and its dose-response relationship are two of the most prominent characters in conducting the risk assessment for chemical exposure (Altshuler 1981). Traditional dose-response studies in toxicology usually focused on a single toxicological endpoint such as carcinogenicity, mutagenicity, teratogenicity, or certain protein receptors (Fritsche, Grandjean et al. 2018). Over the past decades, omics strategies including transcriptomics, proteomics, and metabolomics as well as their integration are effective tools to provide insights into the mode of action and adverse outcome pathways in an unbiased and systematic manner (Larras, Billoir et al. 2018, Ewald, Soufan et al. 2021, Xu, Zhao et al. 2021). For example, metabolomics, a method to understand metabolic regulations by studying small molecule metabolites under environmental stress, is an ideal way to address downstream phenotypes related biochemical pathway disruption and provide valuable information for risk assessment (Zhang, Keerthisinghe et al. 2018, Liu, Jia et al. 2019, Keerthisinghe, Yang et al. 2021). Due to the high cost and complex data analysis for global omics, the majority of the previous studies only investigated the omics change under the treatment of a single or a couple of concentrations. However,

very few studies have investigated the dose-dependent characteristic on omics scale, which is important to greatly enhance our understanding on the health impact at different exposure levels. To completely understand the health impacts at different exposure levels, the acquisition of the dose-response information from the omics results is essential. Furthermore, the establishment of a suitable metabolite dose-response relationship is also important to understand the intrinsic toxicological mechanisms and estimate the metabolite dysregulation pattern under untested scenarios. Additionally, the dose-response systematic biological omics approaches are promising for applications in novel endogenous biomarkers identification and mixture effect assessment on both molecular and ecotoxicology levels (Smetanova, Riedl et al. 2015).

Several previous studies, though limited, have already indicated that the dose-response relationship in metabolic change is quite common. For example, Cizer et al. observed a concentration-dependent metabolomic response of liver injury compounds based on the benchmark concentration analysis (Crizer, Ramaiahgari et al. 2021). Zhan et al. investigated the dose-dependent metabolomics effects of cadmium stress and presumed an adaptive strategy of metabolic responses (Zhan, Wang et al. 2021). Due to the large data dimension in omics results, dose-response omics have been challenging with their data processing and automation. With regards to the dose-response relationship characterization aspect, progress has been made in model fitting like threshold and biphasic, which shows better accuracy and robustness in comparison to traditional monotonic ones (Calabrese and Baldwin 2003, Vandenberg, Colborn et al. 2012). However, most of these fitting models rely on the traditional monotonic or several known non-monotonic algorithms. Therefore, a knowledge gap to fill is to standardize the dose-response analysis of metabolomics data by involving more validation experiments.

One purpose of the current study is to understand the dose-response relationship of

metabolomics and possible cellular disturbances using bisphenol A (BPA) as one model compound. BPA is a widely applied bisphenol material that is commonly used as a bisphenol plasticizer in epoxy resins and polycarbonate plastics manufacturing industries (Cabaton, Canlet et al. 2013). The global production volume of BPA reached approximately 1.03 million metric tons in 2019 (Garside 2020), which has been greatly consumed by daily products, food packages, plastic bottles, and medical equipment (Fernandez, Arrebola et al. 2007). BPA is reported to occur extensively in the indoor environment, dense industrial areas, and agricultural soil (Wang, Abualnaja et al. 2015, Gao, He et al. 2021, Zaborowska, Wyszkowska et al. 2021). Apart from environmental samples, BPA has also been detected in the human placenta, fetal serum, and milk in pregnant women (Sun, Irie et al. 2004). Many toxicological studies have raised increasingly safety concerns about the aforementioned huge amount of BPA usage and exposure. Due to the structure-activity relationship theory, BPA is regarded as an estrogen analogue and plenty of research has confirmed its interaction with other chemicals (Zhang, Liu et al. 2020), also with estrogenic perturbation effect on signaling, immune and reproduction system (Alonso-Magdalena, Morimoto et al. 2006, Alonso-Magdalena, Ropero et al. 2012, Engin and Engin 2021). Exposure to BPA is linked with pleiotropic toxic effects such as affecting estrogenic, androgenic, thyroid, retinoid, and prostaglandin signaling pathways as well as cholesterol and lipid homeostasis (Ortiz-Villanueva, Navarro-Martín et al. 2017). On the omics scale, although BPA was found to result in perturbation of metabolic pathways including amino acids metabolism, glycolysis, tricarboxylic acid cycle (Yue, Yu et al. 2019), as well as induction of DNA methylation and broad protein degradation (Chen, Zhou et al. 2014), yet little is known regarding its dose-dependent metabolomic behavior. Human breast cancer cells (MCF-7), a hormone-responsive cell line, acts as an ideal *in vitro* model to study BPA's endocrine-disruption effect. MCF-7 has been proven to be an ER positive

epithelial cell, coming from the breast which is a typical target tissue of BPA (Aghajanpour-Mir, Zabihi et al. 2016). Sufficient evidence has proven BPA's adverse effect on the MCF-7 cell line, ranging from induction of cell proliferation, binding with serum proteins, increase of cell signaling gene expression and activation of the progesterone receptor, etc (Samuelsen, Olsen et al. 2001, Singleton, Feng et al. 2004, Matsumoto, Adachi et al. 2005, Zhang, Fang et al. 2012, Aghajanpour-Mir, Zabihi et al. 2016). More studies are needed to investigate the biological events in the cellular response of BPA to elucidate the underlying mechanism and to further quantify the prediction of metabolomic biomarkers concentration for the intended exposure situation (Fang, Peng et al. 2020).

In this study, we seek to understand the possible cellular disturbances induced by different levels of BPA exposure to MCF-7 using a combination of global metabolomics and dose-dependent metabolomics approach. We first identified the metabolic profiles of BPA and its affected biochemical pathways at multiple doses to understand the underlying mechanism on a system-biological level. To maximize the extracted number of metabolic features with a known and unknown dose-response pattern, we have applied multiple group analyses of global metabolomics and TOXcms dose-response metabolomics, which is an R-package to pick up the dysregulated features with a known dose-response relationship (Yao, Wang et al. 2020). Furthermore, the prediction models of dysregulated metabolites within the application domain are characterized, to provide a solid real-time full range mapping of metabolite dysregulation and disturbed biological pathway changing patterns under given exposure situations. Additionally, the multiple sensitive effective concentrations (EC) of metabolites were calculated and ranked to pinpoint potential endogenous biomarkers of BPA exposure.

3.2 MATERIAL AND METHOD

3.2.1 Cell Culture and Reagent Preparation

MCF-7 cell line was obtained from the American Type Culture Collection (ATCC, Rockville, MD, USA). Cells were stored in the liquid nitrogen vapor phase and were revived and maintained in humidified 37°C atmosphere containing 5% CO_2. Dulbecco's modified eagle medium (DMEM; with 4.5 g/L glucose, 10% fetal bovine serum (FBS), and L-glutamine) (Gibco, Thermo Fisher Scientific, Singapore) was applied as the growth medium. BPA chemical applied for cell treatment was purchased from Sigma-Aldrich (Singapore). The single-compound stock solution was prepared in dimethyl sulfoxide (DMSO, Thermo Fisher, Singapore).

3.2.2 BPA Exposure and Metabolite Extraction

MCF-7 cells were seeded in 6-well plates with a density of 0.4×10^6 in each well. After the cell reached 60 ~70% confluency, they were exposed to BPA (each level with four replicates, N=4) with varying concentrations (0 µM, 20 µM, 50 µM, and 100 µM) in the culture medium for 24 hours. Non-treated control samples were prepared by adding DMSO with a final concentration of 0.1%. Metabolite extraction was a modified version that was used in our previous studies (Fang, Ivanisevic et al. 2015, Beyer, Fang et al. 2018). Cell metabolites were extracted with 1.6 mL ice-cold methanol: acetonitrile: water (2:2:1, *v/v/v*) and then collected by a cell scraper. The intracellular metabolites were extracted by freeze-thaw steps conducted thrice using liquid nitrogen followed by sonication in an ice bath for 10 min. Afterward, the samples were placed at -40 °C for 1 hour, followed by 15-min centrifugation at a speed of 13,000 rpm at 4 °C to precipitate proteins. The protein concentration of the cells was measured in the final pellet after centrifugation using Pierce BCA assay (N=3) according to kit protocols. A 100µL diluted sample (100 times) was mixed with 100 µL of working reagents in 96-well plates and incubated at 37 °C for 4 hours.

The absorbance was measured at 562 nm on a plate reader. The resulting supernatant was removed and evaporated to dryness by a CentriVap centrifugal vacuum concentrator (Labconco, USA). The dried extracts were then reconstituted in the appropriate volume of acetonitrile: water (1:1, v/v), normalized by the protein concentration with the lowest concentration of 50 µL, sonicated for 10 min, and centrifuged for 15 min at 13,000 rpm and 4 °C to remove insoluble debris. The supernatants were transferred to HPLC vials with inserts and stored at -40 °C before analysis.

3.2.3 Metabolite Profiling and QA/QC

Instrumental analysis was performed using a High-performance Liquid Chromatography (HPLC) system (1200 series, Agilent Technologies) coupled to a 6550 quadrupole Time-of-Flight (qToF) mass spectrometer (Agilent Technologies, Singapore). Details of the profiling method were modified based on our previous study (Fang, Ivanisevic et al. 2015, Beyer, Fang et al. 2018). For instrumental analysis, the method was slightly modified from an earlier method (Wang, Cui et al. 2018) using UPLC (Ultra performance liquid chromatography) Acquity BEH amide (1.7 µm, 2.1×100 mm) in negative mode (ESI-) with an injection volume of 10 µL, with a reduction in the run time from 50 to 12.5 min per sample (12 min of processing and 0.5 min of post-run). Briefly, mobile phase A was 25 mM NH_4OH and 25 mM NH_4OAc in water, and mobile phase B was acetonitrile. The flow rate was 0.5 mL/min and the column temperature was 25 °C. The linear gradient was set as follows: 0~0.5 min: 95% B; 0.5~7 min: 95% to 65% B; 7~8 min: 65% B to 40% B; 8~9 min: 40% B; 9~9.5 min: 40% B to 95% B; 9.5~12.5 min: 95% B. Other parameters were set as follows: gas temperature: 225°C; gas flow: 14 L/min; sheath gas temperature: 275°C; sheath gas flow: 11 L/min; nozzle voltage: 1000 V; nebulizer pressure: 35 psig; capillary voltage: 3500V for positive mode (ESI+, electrospray ionization);

nozzle voltage: 1000 V; fragmentor: 175 V, collision energy: 0 V and scan rate: 1 spectra/second. To correct the mass, retention time, and response drift, a mix of metabolites (QC sample) was prepared by pooling all treated and control cell samples. QC analysis was conducted once for every six injections of biological samples and a blank sample (acetonitrile: water, 1:1, v/v). Data-dependent acquisition (DDA) auto-MS/MS and targeted MS/MS of selected precursors were run with the QC sample to confirm the identity of metabolites. To compare the metabolic changes under different dosing levels, one-way *ANOVA* and *Duncan post-hoc* analysis were used to test whether one treatment group is statistically different from non-treated controls; an FDR-adjusted p-value ≤ 0.05 was considered statistically significant.

3.2.4 Metabolite Identification and Metabolic Pathway Analysis

The metabolite profiling data were converted to mzXML files using Agilent Masshunter Acquisition Software 6.0 and then uploaded to the cloud-based XCMS Online platform (Smith, Want et al. 2006) (http://xcmsonline.scripps.edu). After alignment and annotation, the significant features were first screened with p-value ≤ 0.05, maximal intensity >10,000, and fold change >1.1 or fold change <0.9. Metabolite identification was carried out using a few filters including MS/MS fragment match (auto/targeted MS/MS), accurate mass match, and in-house retention time match if available. Moreover, the metabolite standard verification by the identical HPLC method was applied to support the metabolite identification process if available. Additionally, metabolite features were searched against several open-source platforms, including METLIN (Smith, Maille et al. 2005) (https://metlin.scripps.edu/), KEGG (http://www.genome.jp/kegg/), and HMDB (www.hmdb.ca/). Pathway analysis was conducted using Metaboanalyst (http://www.metaboanalyst.ca). Joint network analysis was performed by metabolome data mapping with a previous transcriptomics study with Cytoscape

(Mesnage, Phedonos et al. 2017). Graphs were plotted using GraphPad Prism (version 7) and statistical analyses were performed by SPSS Statistics (version 22).

3.2.5 TOXcms Metabolomics and dose-response relationship characterization

TOXcms dose-response metabolomics study was applied for the data mentioned above according to the protocol (http://pattilab.wustl.edu/software/toxcms/toxcms.php). Briefly, the metabolite profiling data were converted to CSV files by Agilent Masshunter Acquisition Software 6.0 and then processed with TOXcms R-package. The features that were recognized with statistically significant dose-response relationship by TOXcms were selected and further taken into comparison with global metabolomics results and off-target unknown identification. Metabolite dose-response relationship was established based on the fold changes of the significantly dysregulated metabolites, with dose levels ranging from 0 μM to 100 μM continuously. The best dose-response fitting methods were chosen for each metabolite from a comprehensive regression model set, which includes linear, hill, exponential, polynomial, and Gauss-probit, as instructed in a previous study (Larras, Billoir et al. 2018). Metabolite full dose mapping cartography was plotted based on these prediction models, with normalized fold change value versus dosage in convenience for relative sensitivity comparison. Additionally, effective concentrations which showed significant response degree (e.g., e.g., EC_{+10} means the dose at which metabolite is 10% upregulated) were derived from the prediction models and summarized in a sequential rank. A tiered approach is plotted in **Fig. 3.1**, with the workflow starting from the exposure experiment, dose-response metabolome, and metabolite identification to the metabolite dose-response relationship characterization.

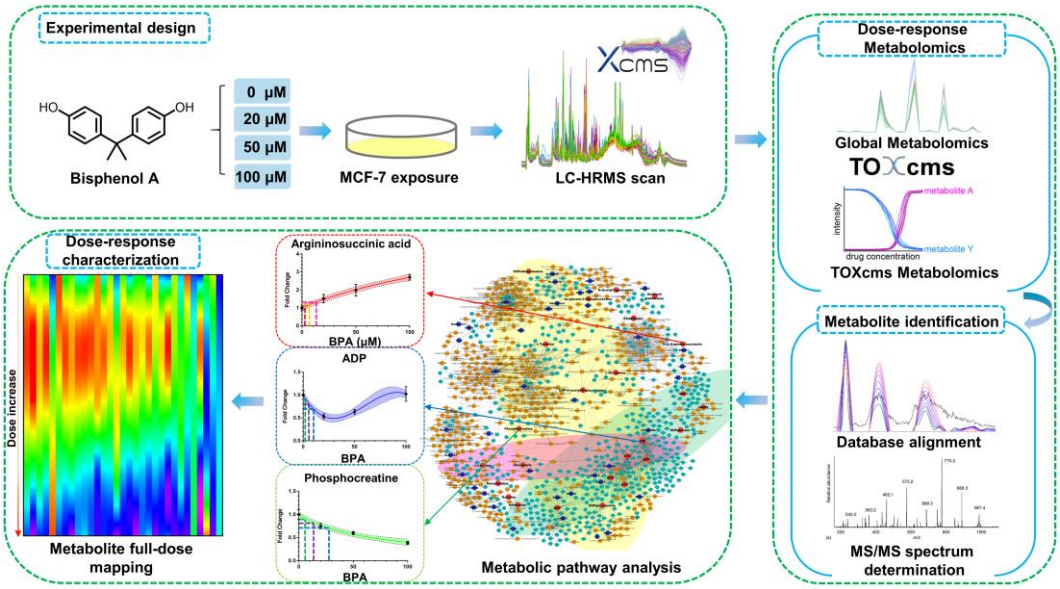

Fig. 3.1. Tiered workflow of this study with a combination of global metabolomics and dose-response metabolomics approach. Experimental design: MCF-7 was treated with different levels of BPA, with metabolites extracted and detected in liquid chromatography–high-resolution mass spectrometry (LC-HRMS). Dose-response metabolomics: Both global metabolomics and TOXcms metabolomics were utilized to select statistically significant changed features, followed by applying metabolite identification and pathway analysis. Dose-response characterization: Dose-response relationships were characterized with full-dose mapping cartography established, with multiple EC values calculated.

3.3 Results and Discussions

3.3.1 Metabolomics Profiling

We semi-quantitatively evaluated the dose-response effect of BPA using manually confirmed feature numbers and automatically feature detection by TOXcms (**Fig. 3.2A-B**). Overall, increasing dosing concentrations of BPA induced more responsive

metabolite features in ESI negative mode. We also summarized the overlapping and distinct feature numbers for 25, 50, 100 µM of BPA from TOXcms in a *Venn* diagram. Among all treatment groups, the overlapped percentage for dysregulated features were significantly distinct for 25 µM, 50 µM and 100 µM BPA (100%, 57% and 69%; respectively), while the coverage of TOXcms only accounted for 55%. The coverage discrepancy is mainly attributed to the differences in feature selection criteria and statistical analyses, though it can be also potentially related to the over-fitting problem in TOXcms modelling process. The results also showed that the dose-response relationship of many features cannot be picked with either dose-response metabolomics or global metabolomics. Both metabolomics strategies are compensatory for each other.

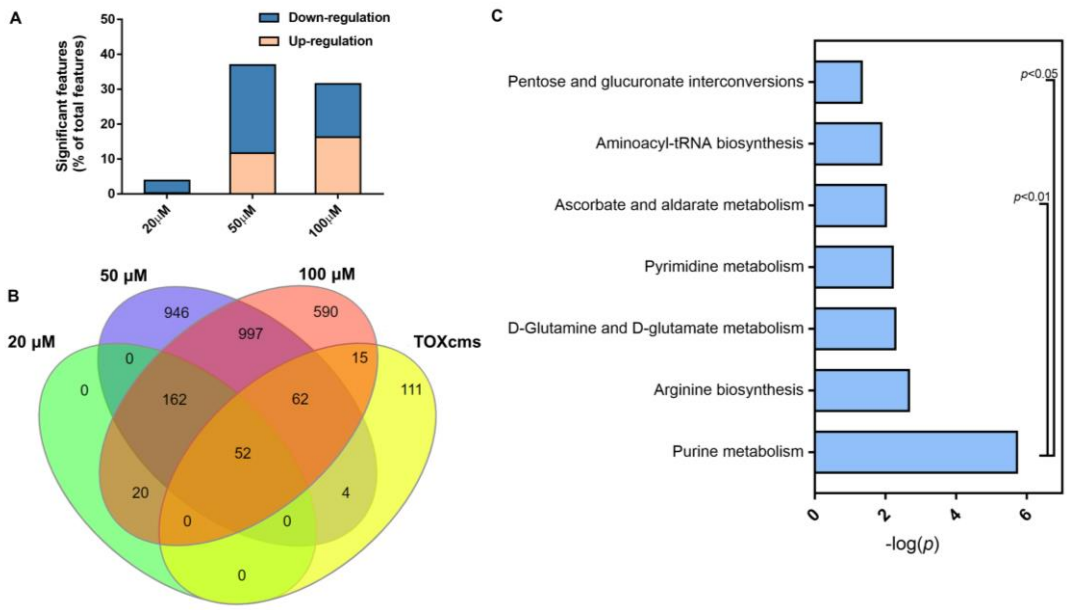

Fig. 3.2. A. Up and down-regulated features detected by global profiling (the percentage was calculated based on total detected feature numbers); **B.** Classic Venn diagram summarizing the number of shared and distinct features of TOXcms and global metabolome at 25 µM, 50 µM, and 100 µM; **C.** Metabolite enrichment analysis

of cells exposed to 100 μM BPA. ($p \leq 0.05$).

3.3.2 Dysregulated Metabolite Identification

In total, we have identified 29 significantly dysregulated metabolites across all treatment conditions, including nucleoside phosphate compounds, fatty acids, and amino acids **(Table A1, A2)**. Among them, 82.8% were identified using the multiple group global metabolomics analysis, and 17.2% were found with TOXcms. TOXcms has provided an output of 12 features with reasonable peak shape, while 7 of them cannot be identified although clear dose-response relationships were observed. The discrepancy is mainly attributed to the fact that TOXcms only applied the sigmoid model and the features with inflection characteristics are ignored (Yao, Wang et al. 2020). The metabolite heatmap along with the bar graph was presented in **Fig. 3.3**. Many amino acids and their precursors were interrupted in higher doses of (100 μM) BPA, such as the upregulation of o-succinyl-l-homoserine, tyrosine, proline, and leucine. It is also noteworthy that, plenty of metabolite dysregulation trends showed a biphasic (U-shaped) mode (**Fig. 3.3**), which means downregulation in lower dosage and upregulation in higher ones. For example, CTP presents the highest fold change (FC=1.5) 100 μM, while the lowest (FC=0.5) at 20 μM within the applicable dose range. The relative exposure sensitivity can be effectively curated from this trend.

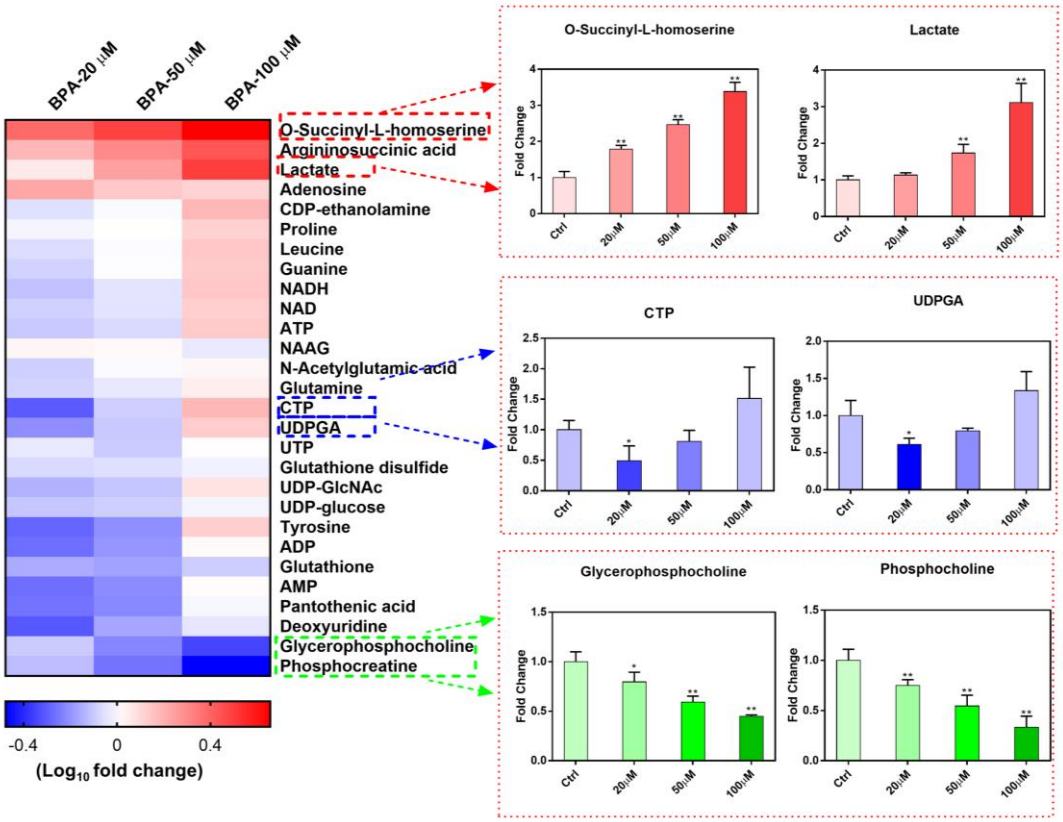

Fig. 3.3. Heatmap of the identified metabolites for different concentrations of BPA regarding the combination of TOXcms dose-response metabolomics and multiple group global metabolomics. Scales in coloured key represent $\log_{10}$ transferred fold change value of metabolites. Red indicates upregulation; Blue indicates downregulation. Bar graphs represent the dysregulation of metabolites as examples in treatment (y-axis is the fold changes by comparing the treatment to the control). "*" and "**" represent $p \leq 0.05$ and $p \leq 0.01$. [Abbreviations: Cytidine diphosphate ethanolamine (CDP-ethanolamine); Nicotinamide adenine dinucleotide (NAD); 1,4-Dihydronicotinamide adenine dinucleotide (NADH); Spaglumic acid (NAAG); Adenosine 5'-monophosphate (AMP); Adenosine 5'-diphosphate (ADP); Adenosine 5'-triphosphate (ATP); Cytidine 5'-triphosphate (CTP); Uridine 5'-diphosphate (UDP); Uridine 5'-triphosphate (UTP); UDP-N-acetylglucosamine (UDP-GlcNAc); UDP-glucuronate (UDPGA).]

Among these metabolites, o-succinyl-l-homoserine showed the highest fold change (FC=3.4) at 100 µM, while phosphocreatine hits the minimum (FC=0.4). It is interesting to note that the dysregulating patterns of specific metabolites after exposure were quite similar. For example, the upregulation for lactic acid, o-succinyl-l-homoserine**,** argininosuccinic acid, and the downregulation of glycerophosphocholine and phosphocholine. The upregulation of NADH and lactic acid at 100 µM suggested that the post-exposure biological activities may be associated with sugar/energy metabolism (Kawai, Harada et al. 2020). The accumulation of NADH implied the reduced expression of the mitochondrial electron transport system, which also facilitated anaerobic glucose metabolism that further resulted in excess lactic acid (Vemuri, Eiteman et al. 2007). Since glycerophosphocholine is a metabolite precursor of phospholipids, its depletion after exposure to BPA (50 µM and 100 µM) suggested a possible impact on lipid metabolism (Xiao, Rossignol et al. 2021). The toxicity differences between different levels of BPA could be explained by the gradient increasing estrogenic activity. Numerous other evidences could further facilitate this explanation. For example, UDPGA (FC=1.3) was an indicator of cell proliferation and was found upregulated after 100 µM BPA exposure. Additionally, a high level of BPA exposure has comparably resulted in more amino acid dysregulation in the amino acyl-tRNA synthesis pathway in 100 µM. The upregulation of amino acids after BPA exposure was probably due to the need for these nutrients in proliferating cells (Vander Heiden, Cantley et al. 2009). As one of the most prominent estrogenic biomarkers, proline was observed with an upregulation (FC=1.3 for 100 µM), which could clearly be related to estrogenic exposure and concomitant ERα-mediated induction of proliferation (Potratz, Tarnow et al. 2017). Overall, higher BPA dosage has triggered significant dose-response metabolome changes for many metabolites.

3.3.3 Biological Pathways Analysis and Omics Integration

Pathway analysis was further conducted through pathway mapping of dysregulated metabolites for BPA post-exposure. The top interfered pathways were purine metabolism, arginine biosynthesis, glutamine and glutamate metabolism, as well as pyrimidine metabolism **(Fig. 3.2C)**. This is in line with an earlier study suggesting that developmental toxicants such as BPA exposure can induce arginine and proline metabolism, citrate cycle, and glutamate metabolism (West, Weir et al. 2010). Among these pathways, the dysregulated metabolites in global metabolomics outcomes could be well mapped with the purine metabolism pathway and were significantly enriched as exposure gradient rises **(Fig. 3.3)**. The perturbation of aminoacyl-tRNA synthesis was also consistent with earlier studies demonstrating an increase in amino acid concentrations in BPA treated-embryos (Huang, Benskin et al. 2017, Ortiz-Villanueva, Navarro-Martín et al. 2017).

We further applied transcriptome-metabolome integration network analysis to confirm those disrupted pathways. The transcriptomics data was retrieved from the RNA sequencing result from one previous study which used MCF-7 cells and one similar treatment dose of BPA (Mesnage, Phedonos et al. 2017). As shown in **Fig. A1**, purine metabolism ($p = 7\times10^{-6}$), glycolysis or gluconeogenesis ($p = 0.01$), and pyrimidine metabolism ($p = 0.047$) were found with comparably more hits in the mapping result, which is consistent with a previous proteomics study (Huang, Zhu et al. 2020). The perturbation in sugar metabolism also indicates BPA's potential induction effect on proliferation trends in cancer cell lines (Wang and Dong 2019). Though lacking RNA data for each dose level, this further enlightened us on the potential existence of certain dose-dependent pathway regulation patterns, which provide information on pathway sensitivity determining metabolic stimulation or inhibition (Liu, Jia et al.).

3.3.4 Metabolite Dose-response Relationship Characterization and Cartography Prediction

Furthermore, we managed to determine the dose-response relationship and fitted the dose-response curve for each metabolite dysregulation pattern. The full dosage mapping of the identified metabolites models within the applicable range is present in **Fig. 3.4A.** The heatmap showed great regional specificity, which indicates a certain intrinsic correlation between specific metabolites regulatory profiles. Several metabolite prediction models are shown in **Fig. 3.4B**. Traditional monotonicity dose-response methods can hardly be eligible for all metabolites behaviour description, as for the subtle fold change and up-and-downstream intercorrelation regulation along the metabolism pathway (Larras, Billoir et al. 2018). Thus, a third-order polynomial was applied to determine several biphasic curves with better performance and robustness, for instance, CTP and UDPGA. Most of the models showed a reasonable coefficient of determination and acceptable confidence level, while several posed certain degrees of ambiguity in the 50-100 µM range, with wider confidence and prediction bands. This has mainly resulted from few dose levels for high concentration areas.

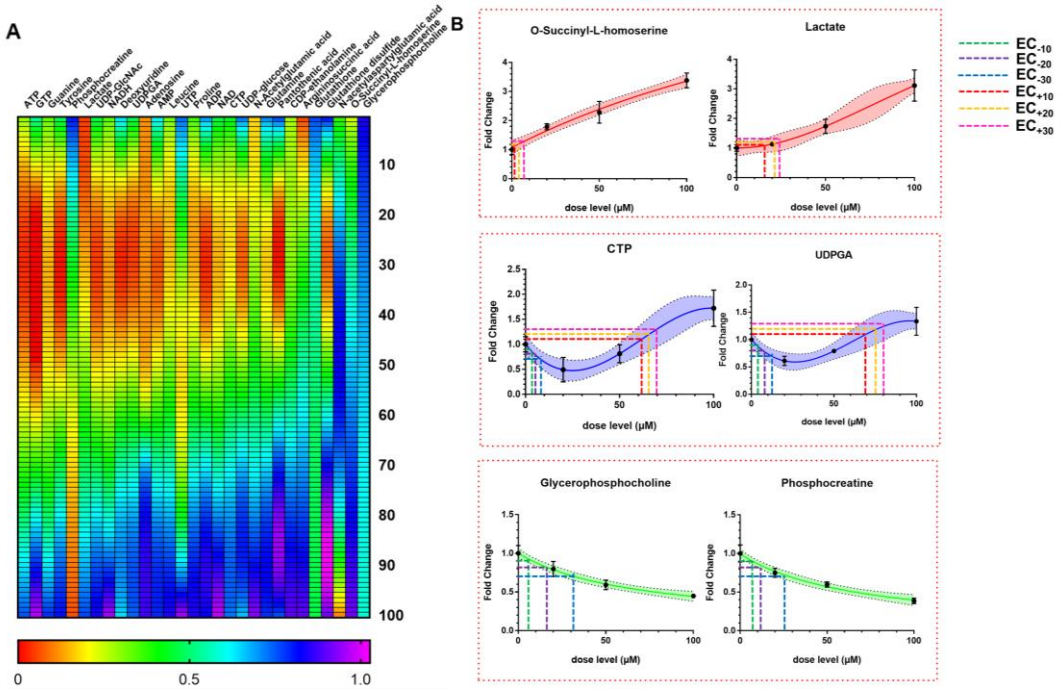

Fig. 3.4. A. Full-dose mapping of the identified metabolites models. The columns represent the metabolites category, while rows stand for normalized fold changes of dysregulated metabolites ranging from 0-100 μM continuously. **B.** Metabolite models established with fold change versus dose levels. The dose-response fitting methods include but are not limited to: Agonist vs. response variable slope (four parameters), Inhibitor vs. response (three parameters), and Polynomial third order. Graphs and dose-response equation fitting are performed using GraphPad Prism (version 7). Effective concentration (EC) values for each pinpoint are labelled with dash lines in characteristic colours, respectively. Areas in light colour present the fitting model confidence level (α=0.05).

3.3.5 Metabolite EC Value Calculation

The models are further applied to specify certain endpoints to quantify effective concentrations of importance during metabolite changes. Hereby, two benchmark indicators, metabolite 10% downregulation effective concentration (EC_{-10}) and 10%

upregulation effective concentration (EC_{+10}), were firstly defined to provide information on metabolite regulation sensitivity to exposure stress (**Table A3**). As suggested in previous studies, 10% change (*i.e.,* fold change of 1.1 or 0.9) is usually used for the benchmarking concentration of toxicants (Crizer, Ramaiahgari et al. 2021). Nevertheless, due to the uncertainties of metabolomics results, higher fold changes of 20% and 30% were also introduced with the pinpoint of EC_{+20}, EC_{+30}, EC_{-20}, EC_{-30}, as shown in **Table A3**. These pinpoint indicators helped certify the effective concentration with a certain degree of regulation of metabolite theoretically, which can be further applied to characterized metabolites dysregulation patterns and compared different metabolite sensitivity within the application domain (Crizer, Ramaiahgari et al. 2021).

Fig. 3.5 plots the sequential rank of different EC values (EC_{+10}, EC_{+20}, EC_{+30}, EC_{-10}, EC_{-20}, EC_{-30}). Generally, the lower the EC value, the more sensitive the metabolite is upon exposure event. Those substances with lower EC values can be the potential biomarker for BPA metabolic perturbation effect. We observed GTP is the metabolite with the lowest EC_{-10}, while o-succinyl-l-homoserine shows the minimum EC_{+10}value. Although proline has been reported in previous *in vivo* studies as a BPA exposure biomarker (Heinzmann, Brown et al. 2010), it only presented moderate EC_{+10} and relatively high EC_{-10} value in this study, ranking 57.1% and 95.8%, respectively. Still, proline showed an absolute sensitive EC_{-10}, albeit with a comparatively low ranking. This suggests that compared with proline, metabolites such as GTP and CTP may possess greater potential to perform as perturbation biomarkers. Moreover, it is worth noticing that the EC_{-10} showed a generally lower and flatter trend than EC_{+10}, which indicated BPA's induction effect towards global metabolites downregulation. As for EC_{20} and EC_{30}, the metabolite sensitivity ranking pattern was similar in comparison with EC_{10}, yet the prediction coverage converged due to the application domain limitation. This is reasonable as the prediction model

is both continuous and unambiguous.

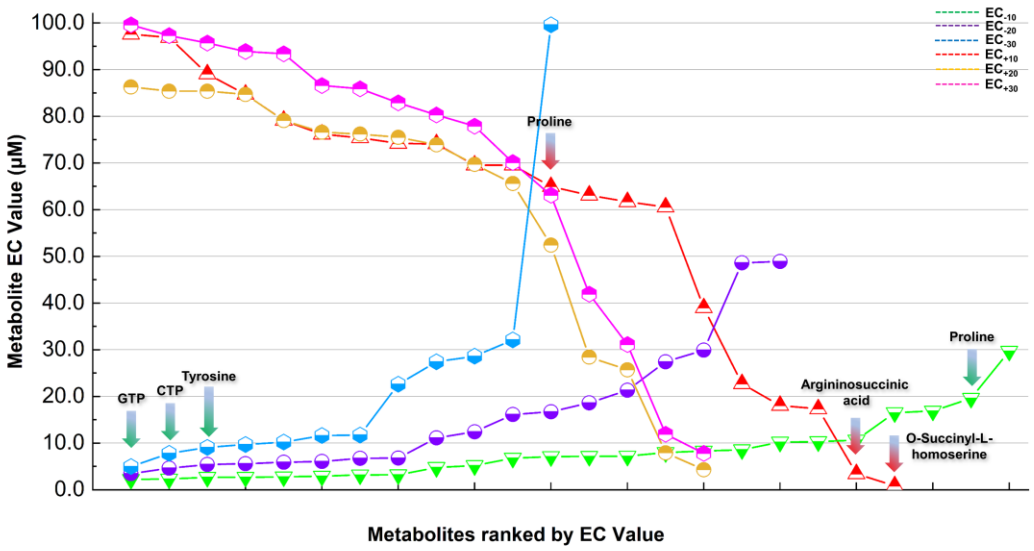

Fig. 3.5. The sequential rank of predicted EC_{+10}, EC_{+20}, EC_{+30}, EC_{-10}, EC_{-20}, EC_{-30} value. Several typical metabolites with high sensitivity are labelled.

Specifically, we summarized the dose-response features of significantly dysregulated metabolites in the purine metabolism pathway (**Fig. 3.6)**. All metabolites showed a characteristic biphasic dysregulation pattern along the exposure gradient, indicating the pathway goes through suppression in low dose and then rescued in higher levels. Our results implied that purine metabolism is suppressed at low BPA dosage areas, which may be resulted from impairing the antioxidation system and increasing lipid peroxidation (Meng, Tian et al. 2019, Sun, Wang et al. 2021). Interestingly, the downstream metabolites' EC_{-10} is commonly lower than the upstream ones (AMP < Adenosine, ADP < ATP < Glutamine, Guanine < glutamine), where dysregulation is more likely to take place within trivial dosage. From this perspective, several endogenous biomarkers ranging from cell proliferation (proline), immunoreactivity impairment (tyrosine), and inflammation-related (GTP), can be derived as for the

comparably low effective concentration value (Ishido, Masuo et al. 2004, Potratz, Tarnow et al. 2017, Song, Park et al. 2017). This dose-dependent metabolomics study shall provide implications for active metabolomics to provide a solid framework for elucidating metabolite upstream and downstream dependencies (Rinschen, Ivanisevic et al. 2019).

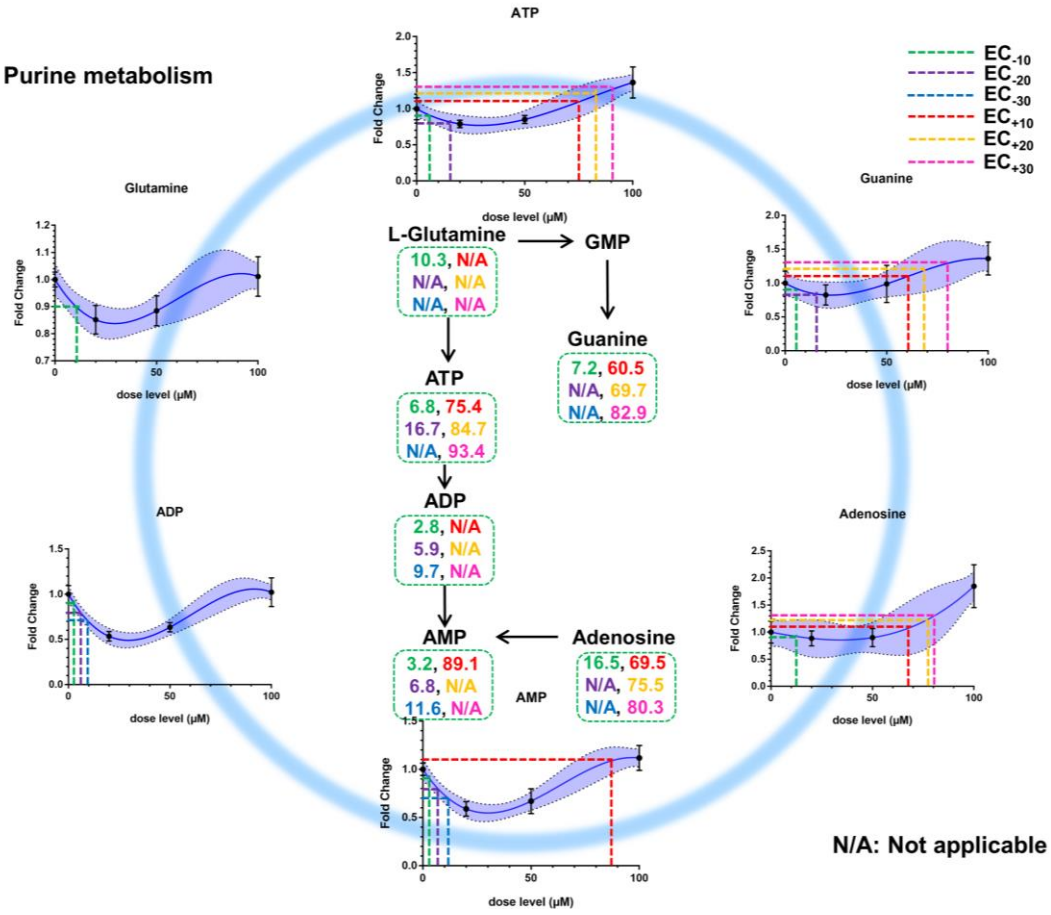

Fig. 3.6. Up and down regulation of metabolites at different concentrations (20, 50 and 100 μM of BPA) in the purine metabolism pathway fitted by GraphPad Prism. EC_{+10}, EC_{+20}, EC_{+30}, EC_{-10}, EC_{-20}, EC_{-30} value points are labelled with dash lines of characteristic color, respectively. GMP is under the detectable limit in this study.

3.4 Conclusions

In summary, we characterized the cellular metabolome changes upon exposure to different levels of BPA. The metabolomics studies suggested that BPA exposure perturbed specific biochemical pathways such as purine metabolism and pyrimidine metabolism. The dysregulated metabolites and affected metabolic pathway results are consistent with several previous studies (Potratz, Tarnow et al. 2017, Cabaton, Poupin et al. 2018, Zhao, Tang et al. 2019). Interestingly, we observed that the sensitivities were varied for different metabolites. However, the metabolites on the same pathways are more likely to behave in similar manners. Metabolite dose-dependent relationships were established based on the applied dosage range. These relationships were further used to predict and describe the dysregulation pattern of metabolites under untested scenarios. We also calculated respective EC values at specific points, which can provide useful information on metabolite relative sensitivity and propose some endogenous biomarkers for BPA exposure. Overall, the results showed that both TOXcms dose-response metabolomics and multiple group global metabolomics are compensatory mutually, and essential for the dose-response interpretation.

Limitations of this study are further addressed as follows. Dose-response relationship-directed analysis such as TOXcms is promising for dose-response feature selecting automation, yet challenging in recognizing features with inflection dose-response characteristics. Nevertheless, to avoid overfitting issues resulting from relatively few dosage levels, the statistical methods may need additional modifications. In addition, relatively limited dosage levels were applied due to workload and cytotoxicity concerns, which may not cover the full range for certain metabolites dysregulation pattern. Some metabolites were observed with incomplete dose-response dysregulation manner, and this may also be attributed to somehow narrow dose range. What's more, comparably high concentrations of chemicals (at μM level) were adopted in this study to obtain observable results, and a single cancer

cell line is adopted. In vivo and other in vitro models should also be considered in future study, to investigate and validate the metabolite dose-response models. Some conclusion reached may need future validations, such as the metabolome comparison of intracellular and extracellular samples to examine the mechanism of observed amino acid upregulation. Overall, the dose-response metabolomics study is promising for elucidation of the toxicological mode of action and omics-integration analysis, yet still challenging in omics data analysis principles, model's automation and optimization, also experiment's reproducibility and scalability.

CHAPTER 4. TIME-RESOLVED METABOLOMICS UNCOVER DYNAMIC METABOLIC ADAPTIONS TO BISPHENOL A EXPOSURE *IN VITRO*

ABSTRACT:

The biochemical consequences induced by xenobiotics stress are featured with dose-response and time-resolved landscapes. Understanding the dynamic process of cellular adaptions is crucial in conducting the risk assessment for chemical exposure. As one of the most phenotypes-related omics, metabolome in response to environmental stress can vary from seconds to days. Up to now, very few dynamic metabolomics studies have been conducted to provide time-dependent mechanistic interpretation in understanding xenobiotics induced cellular adaptation. This study aims to explore the time-resolved metabolite dysregulation manner and dynamically perturbed biological functions in MCF-7 cell exposed to bisphenol A, a well-known endocrine-disrupting chemical. By sampling at 11 time points from several minutes to hours, 37 significantly dysregulated metabolites were identified, ranging from amino acids, fatty acids, carboxylic acids and nucleoside phosphate compounds. The metabolites in different pathways basically showed distinct time-resolved changing patterns, while ones within the common class or same pathways showed similar and synchronized dysregulation behaviors. The pathway enrichment analysis suggested that purine metabolism, pyrimidine metabolism, aminoacyl-tRNA biosynthesis as well as glutamine/glutamate (GABA) metabolism pathways were heavily disturbed. As exposure event continued, MCF-7 cells went through multiple sequential metabolic adaptions from cell proliferation to energy metabolism, which indicated an

enhancing cellular requirement for elevated energy homeostasis, oxidative stress response and ER-α mediated cell growth. We further focused on the time-dependent metabolite dysregulation behavior in purine and pyrimidine metabolism, and identified excessive NADH accumulation as the primary contribution to impairing glycolysis and oxidative phosphorylation by redox imbalance. Lastly, we established a restricted cubic spline-based model to fit and predict metabolite's full range dysregulation cartography, with metabolite' sensitivity comparisons retrieved and novel biomarkers suggested. Overall, the results indicated that 8 hr BPA exposure leaded to global dynamic metabolome disturbances including amino acid, nucleoside and sugar metabolism disorders, and the dysregulated metabolites with interfered pathways at different stages are of significant temporal distinctions.

4.1 INTRODUCTION

Biological systems are highly refined processes subject to dynamic metabolism regulation (Chen, Mias et al. 2012, Link, Fuhrer et al. 2015). Being the terminal products of transcriptomic and proteomic activities, intercellular metabolites' change in response to metabolic syndrome factors can vary from seconds to days (Yanes, Clark et al. 2010, Jain, Nilsson et al. 2012, Link, Kochanowski et al. 2013). Given that metabolites are among the most phenotype-relevant cellular components under environmental stress (Moreno-Sanchez, Saavedra et al. 2008), dynamic metabolomics study exhibits its advantages in characterizing the real-time metabolome dysregulation pattern both comprehensively and comparatively (Paris, Johnson et al. 2016, Clement, Wong et al. 2019, Song, Lam et al. 2020, Vavricka, Hasunuma et al. 2020). Although techniques like quantitative metabolic flux provides a promising perspective for time-dependent omics exploration, acquisition of high-quality dynamic metabolomics data remains challenging in regard to non-invasive *in situ* sampling, improper labeling, insufficient model options and intensive workload (Zamboni, Fendt et al. 2009, Link, Fuhrer et al. 2015, Tugizimana, Djami-Tchatchou

et al. 2019). Time-resolved metabolomics, acting as an indispensable compartment under dynamic metabolomics framework, plays an important role in providing unbiased information about mechanisms of metabolic disorders, guidance on drug development and prognostic advice (Spegel, Sharoyko et al. 2013, Kowalski, De Souza et al. 2015, Geng, Misra et al. 2016, Krycer, Yugi et al. 2017, Halama, Aye et al. 2019, Lu, Chen et al. 2020). Hannes et al. constructed a time-of-flight mass spectrometry (TOF-MS) auto-sampling system which enables bacteria's metabolome real-time monitoring (Link, Fuhrer et al. 2015), and observed an inhibition effect of nucleotide synthesis under starvation which suggested salvage pathway is preferred than *de novo* for less energy consumption. Lee et al. investigated multiple metabolic response alterations along cell's canceration procedure, including upregulation of nucleotide biosynthesis, downregulation of oxidative phosphorylation and epigenome maintenance breakdown (Lee, Jedrychowski et al. 2017). In practice, researchers have allocated antimalaria drug's performance from time-resolved metabolomics study, to achieve the mode of action determination as well as pharmacokinetics optimization (Allman, Painter et al. 2016, Cobbold, Chua et al. 2016, Cobbold and McConville 2019).

As time-resolved metabolomics being utilized as a potential tool, new challenges have been posed by the annotation and information extraction from the massive amount of dynamic omics data generated (Liang, Rasmussen et al. 2020). Up to date, various solutions have been established to parameterize the time-resolved metabolomics, furtherly to interpret the underlying biological principles (Zampieri, Sekar et al. 2017). Zak et al. developed a supervised machine-learning based protocol to unbiasedly predict time-series metabolic pathway dynamics, which proves a supreme performance compared with traditional Michaelis–Menten kinetics fitting (Costello and Martin 2018). Nyamundanda et al. proposed an automated regression algorithm to identify biomarkers with time-resolved dysregulation importance

(Nyamundanda, Gormley et al. 2014). On top of that, researchers are paying increasing attention on multi-omics informatics development, ranging from tensor factorizations, smooths, mean-variation-weighted, and dimension-reducing principal component analysis, etc (Smilde, Westerhuis et al. 2010, Zhang, Zhou et al. 2015, Li, Hoefsloot et al. 2021). Though ambiguities and false positive conclusion reached occasionally, the generated algorithm along with prediction models have brought novel and promising insights into the underlying correlation of metabolic features with disease status and prognostic impacts regarding time influence (Zhang, Zhou et al. 2015). However, very few studies are concerned with environmental factors' contributions through time-resolved metabolomics. Furthermore, one knowledge gap to fill is the derivation of chemical exposure's metabolic toxicokinetics and extrapolation modelling from time-series metabolomics data consequently (Fu, Scheidegger et al. 2021, Liu, Jiang et al. 2021, Luan, Zhao et al. 2021).

Bisphenol A (BPA), an endocrine disrupting chemical of great public health concern, is an ideal model compound of toxicological research interest due to its multiple molecular targets (Howdeshell, Hotchkiss et al. 1999, Chen, Zhou et al. 2014). Sufficient evidence has demonstrated BPA's estradiol-mimic effect which induces pleiotropic toxicity by affecting endocrine, immune and reproduction system (Alonso-Magdalena, Morimoto et al. 2006, Alonso-Magdalena, Ropero et al. 2012, Engin and Engin 2021). In our recent study, multi-omics research has reported BPA exposure with consequences on metabolic pathways perturbation including glycolysis, purine metabolism, tricarboxylic acid cycle with a clear dose-response dependence (Yue, Yu et al. 2019, Zhao, Liu et al. 2021). Yet, no previous research has adopted time-resolved metabolome strategies to carry out BPA's dynamic hazard identification and risk assessment.

Here, we adopted time-resolved untargeted metabolomics to characterized global temporal metabolite profiles during 8 hr BPA exposure. The dysregulated metabolites

and interfered pathways were firstly identified, with the biochemical mechanisms interpreted. We further detailed the time-resolved metabolism patterns with distinct predominant pathways derived on each stage, and observed significant metabolic transitions which related to varying cellular events. Furthermore, the fitting models of dysregulated metabolites within application domain are established, to provide a solid real-time full range prediction of metabolite dysregulation, as well as an insight into the relative sensitivity extrapolation and novel biomarkers discovery. Collectively, this dynamic metabolomics study demonstrated a unique time-resolved metabolome dysregulation behavior and explored the distinct metabolic adaptions due to temporal cell function requirements.

4.2 MATERIAL AND METHOD

4.2.1 Cell Culture and Reagent Preparation

MCF-7 cell line was purchased from the American Type Culture Collection (ATCC, Rockville, MD, USA). Cells were kept in liquid nitrogen vapor phase until reviving, and then maintained in humidified 37°C atmosphere containing 5% CO_2. Dulbecco's modified eagle medium (DMEM; supplemented with 4.5 g/L glucose, 10% fetal bovine serum, 4 mM L-glutamine, 2 mM sodium pyruvate) was applied as the growth medium. BPA chemical applied for cell treatment was purchased from Sigma-Aldrich (Singapore, purity > 97%), and BPA stock solution was prepared in dimethyl sulfoxide (DMSO, 99.8%, Thermo Fisher, Singapore). All of the analytical reagents applied in this study are of high performance liquid chromatograph grade or higher unless otherwise stated.

4.2.2 BPA Exposure and Metabolite Extraction

MCF-7 cells were seeded in 6-well plates with initial density of 0.3×10^6 for each well.

As the cells reached about 80% confluency, they were exposed to BPA with final concentration of a fixed 100 μM at ten varying time points (each time point with four replicates). The selection of this concentration was based on our previous study and most metabolic dysregulation yet no obvious toxicity has been observed (Aghajanpour-Mir, Zabihi et al. 2016, Zhao, Liu et al. 2021). Cells (n = 4 replicates for each) after treatment with duration of 0.25 hr, 0.5 hr, 0.75 hr, 1 hr, 1.5 hr, 2 hr, 3 hr, 4 hr, 6 hr, and 8 hr, respectively were quickly quenched and stored in -80° C fridge (one sample at 1 hr was lost due to centrifuge operations). As reported previously, the doubling time for MCF-7 proliferation ranges from 31.2-80 hours (Sweeney, Swarbrick et al. 1998, Jain, Nilsson et al. 2012, Cowley, Weir et al. 2014). It can be derived that the theoretically maximum proliferation rate falls around 7%-18% at T = 8 hr, which is supported by our prelimimary survival test (**Fig. B1**). Taking cell cycle, observable outcomes and nutrient limit into consideration, we finally decided that 8 hr was used as final exposure point. As expected, the effect of undulated cell counts at each time point have been treated as marginal and negligible. Control samples (n = 3) were prepared by adding quenching solution instantly after BPA was exposed. Metabolite extraction protocol was modified based on our previous studies (Fang, Ivanisevic et al. 2015, Beyer, Fang et al. 2018, Liu, Jia et al. 2020, Zhao, Liu et al. 2021). After rinsing with PBS twice rapidly, intercellular metabolites were collected with 1.6 mL ice-cold methanol: acetonitrile: water (2:2:1, *v/v/v*) and harvested by a cell scraper. To preserve and extract the pure metabolite, freeze-thaw steps were conducted thrice using liquid nitrogen followed by sonication in an ice bath for 10 min. After placed at -40 °C for 1 hour, the samples were violently vortexed and centrifuged for 15-min at a speed of 13,000 rpm at 4 °C to precipitate proteins. The supernatant was collected and evaporated to almost dryness by a CentriVap centrifugal vacuum concentrator (Labconco, USA). The resulting extracts were then reconstituted by 100 μL acetonitrile: water (1:1, v/v), sonicated on ice for

10 min, and centrifuged for 15 min at 13,000 rpm and 4 °C to remove insoluble debris. The final metabolite products were transferred to HPLC vials with insert and stored at -40 °C for further instrument analysis

4.2.3 Metabolite Profiling and QA/QC

Instrumental analysis was performed on High-performance Liquid Chromatography (HPLC) system (1200 series, Agilent Technologies) coupled with 6550 Quadrupole Time-of-Flight (QTOF) mass spectrometer (Agilent Technologies, Singapore). Details of the profiling method was a modified version from our previous study (Fang, Ivanisevic et al. 2015, Beyer, Fang et al. 2018, Zhao, Liu et al. 2021). In our previous study, most of the altered metabolites were shown in the HILIC negative mode (ESI-), and thus we only used this method due to the large number of samples analyzed. For instrumental analysis, the samples were analyzed in negative mode (ESI-) with an injection volume of 10 µL coupled with UPLC (Ultra performance liquid chromatography) Acquity BEH amide column (1.7 µm, 2.1×100 mm), with a running time of 12.5 min per sample (12 min of processing and 0.5 min of post-run). Briefly, mobile phase A was 25 mM NH_4OH with 25 mM NH_4OAc in water, and mobile phase B was acetonitrile. The flow rate was 0.5 mL/min and the column temperature was 25 °C. The linear gradient was set as follows: 0~0.5 min: 95% B; 0.5~7 min: 95% to 65% B; 7~8 min: 65% B to 40% B; 8~9 min: 40% B; 9~9.5 min: 40% B to 95% B; 9.5~12.5 min: 95% B. Other parameters were set as follows: gas temperature: 225°C; gas flow: 14 L/min; sheath gas temperature: 275°C; sheath gas flow: 11 L/min; nozzle voltage: 1000 V; nebulizer pressure: 35 psig; capillary voltage: 3500V for negative mode (ESI-, electrospray ionization); nozzle voltage: 1000 V; fragmentor: 175 V, collision energy: 0 V and scan rate: 1 spectra/second. To correct the mass, retention time, and response drift, a mix of metabolites (QC sample) was prepared by pooling all treated and control cell samples. QC analysis was conducted once for

every six injections of biological samples and a blank sample (acetonitrile: water, 1:1, v/v). Data-dependent acquisition (DDA) auto-MS/MS and targeted MS/MS of selected precursors were run with the QC sample to confirm the identity of metabolites.

4.2.4 Metabolite Identification, Metabolic Pathway Analysis and Data Visualization

The metabolite profiling data (MS1 full scan) were converted to *.mzXML files using Agilent Masshunter Acquisition Software 6.0 and uploaded to cloud-based XCMS Online platform (Smith, Want et al. 2006) (http://xcmsonline.scripps.edu). After alignment and annotation, the significant features were firstly screened with signal-to noise (S/N) ratio >10, maximal intensity >10,000, and fold change >1.1 or fold change <0.9. To compare the metabolic changes at various time points, one-way *ANOVA* and *Duncan post-hoc* analysis were used to test whether the treatment group is statistically different from non-treated controls; an FDR-adjusted p-value ≤ 0.05 was considered statistically significant. After filtering out the metabolic features of interest, metabolite identification was carried out using a few filters including accurate mass match, MS/MS fragment match (auto/targeted MS/MS) and in-house retention time match. Additionally, metabolite features were searched against several open-source platforms, including METLIN (Smith, Maille et al. 2005) (https://metlin.scripps.edu/), KEGG (http://www.genome.jp/kegg/), and HMDB (www.hmdb.ca/).

Metabolic Pathway Enrichment Analysis were conducted using Metaboanalyst (http://www.metaboanalyst.ca) and Metamapp (https://metamapp.fiehnlab.ucdavis.edu/). The calculated nodes and edges were extracted and visualized by Cytoscape. To characterized time-resolved metabolites' dysregulation tendency and interspecies correlation, restricted cubic spline fitting

(RCS) modelling was applied as previously stressed (Inoue, Ritz et al. 2020, Johannesen, Langsted et al. 2020). Other data visualization such as heatmap, principal component analysis, rose diagram and correlation plot were completed using R-studio (version 4.0.1) (Vienna, Austria) and GraphPad Prism (version 7), while statistical analyses were performed by SPSS Statistics (version 22). All data were processed and optimized in advance (log-transformed, FDR-adjusted normalized, Pareto scaling, etc.) as suggested in the workflow summarized in **Fig. 4.1**.

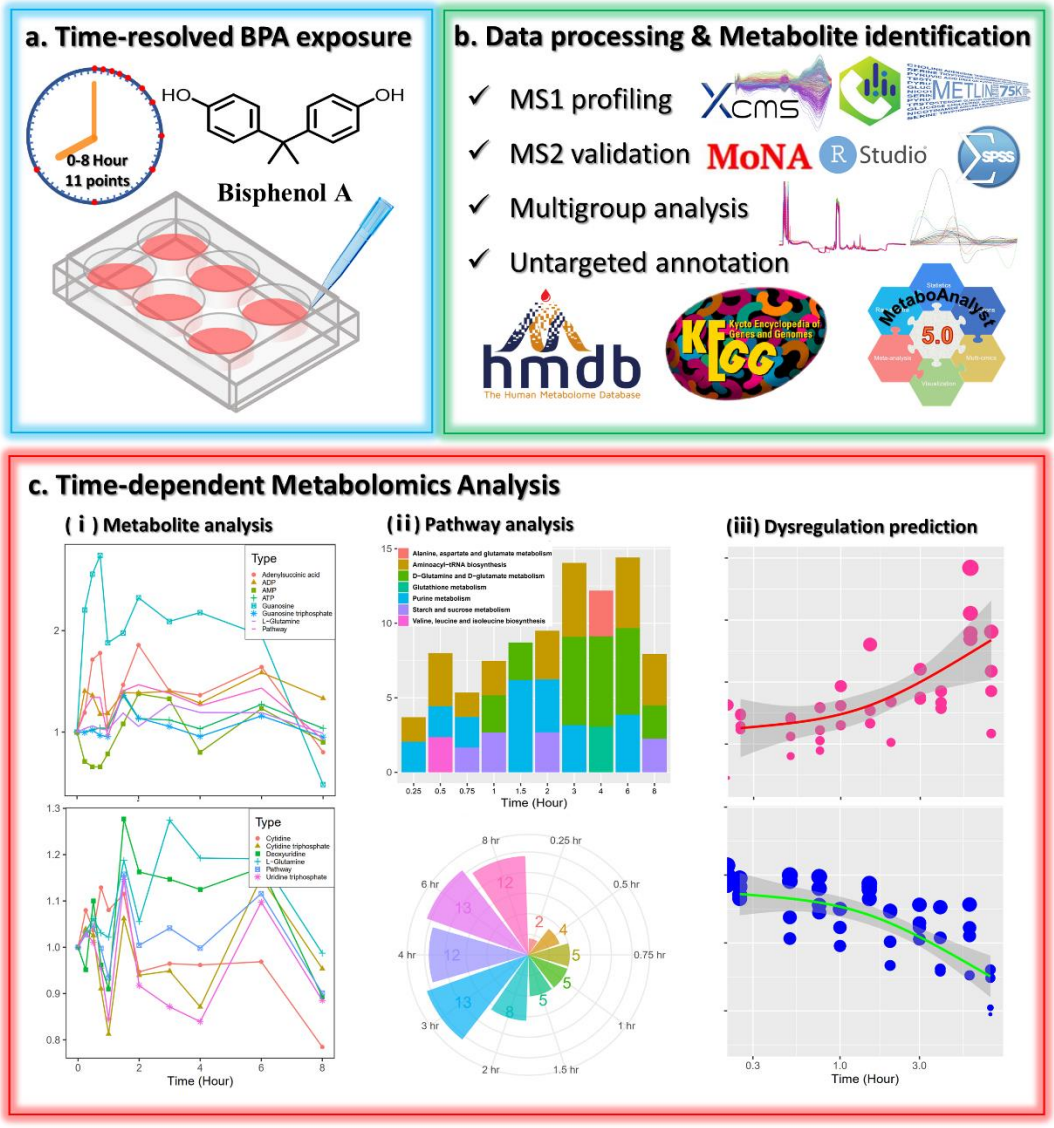

Fig. 4.1. Tiered approach of the time-resolved metabolomics study. a. Experimental workflow to harvest MCF-7 cells exposed to Bisphenol A at 11 varying time points (0 hr, 0.25 hr, 0.5 hr, 0.75 hr, 1 hr, 1.5 hr, 2 hr, 3 hr, 4 hr, 6 hr, and 8 hr), with intercellular metabolites extracted and analyzed by HPLC-MS. b. Data processing and metabolite identification under untargeted metabolomics framework. The applied methodology included but not limited to: MS1 profiling, MS2 validation, RT shifted correction, in-house standard library alignment, one-way *ANOVA*, t-test, pathway enrichment analysis, etc. c. Time-resolved metabolomics was implemented to uncover metabolite time-dependent dysregulation behavior, including metabolite dysregulation analysis, temporal pathway enrichment and restricted cubic spline-based prediction.

4.3 Results and Discussions

4.3.1 Metabolomics Profiling

To uncover the metabolites of time-dependent dysregulation interest, we conducted untargeted metabolomics analysis by initiating with semi-quantitatively aligning the features across all samples and conducting the multiple group analysis. In total, 6143 significant features were identified with FDR-adjusted *p*-value $\leqslant$ 0.05 calculated by one-way *ANOVA*. Overall, a positive correlation was observed between exposure time with significant feature numbers (**Fig. 4.2C**), and the upregulated features were ubiquitously outnumbered than the downregulated ones. PCA analysis exhibits quite well grouping pattern (**Fig. 4.2A**), and the percentage of explained variances reaches approximately 32.9% and 20.2% for the first two components; respectively (**Fig. 4.2B**), which suggests a characteristic distinction for the time-resolved metabolome change.

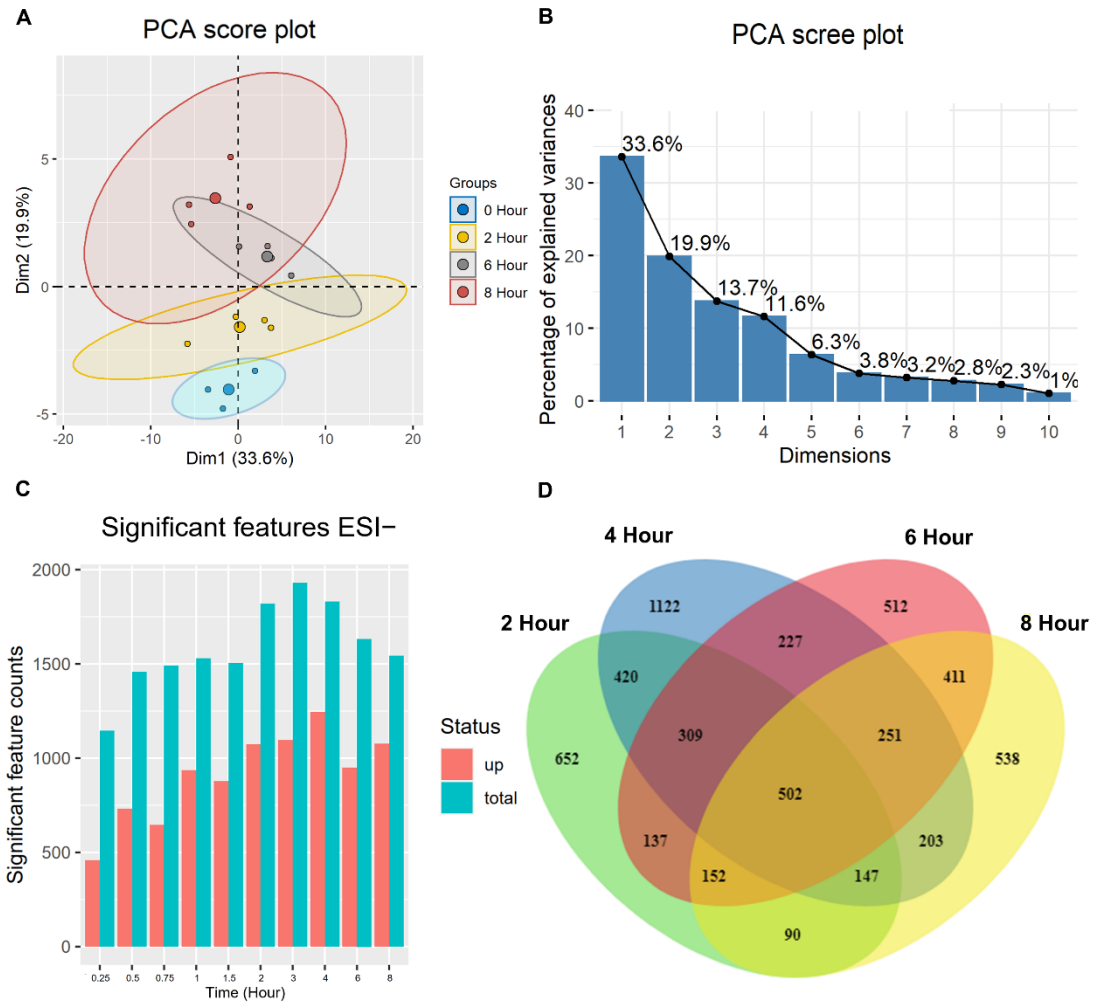

Fig. 4.2. A. Principal component analysis score plot of aligned features at 0 hr, 2 hr, 4 hr, and 8 hr (3 control samples + 1 mean point at 0 hr; 4 treated samples + 1 mean point at 2 hr, 4 hr, and 8 hr); **B.** Principal component analysis scree plot of total ion features at 0 hr, 2 hr, 4 hr, and 8 hr; **C.** Up and down-regulated significant features of 10 time point detected by global profiling (pairwise comparison with control samples); **D.** Venn diagram summarizing the number of shared and distinct features of total metabolome features at 0 hr, 2 hr, 4 hr, and 8 hr (multigroup analysis).

We also summarized the overlapping and distinct features at 2 hr, 4 hr, 6 hr and 8 hr in a *Venn* diagram (**Fig. 4.2D**). Among all treatment groups, the overlapped percentage for dysregulated features were significantly distinct (72.9% for T =2 hr, 64.7% for T =4 hr, 79.5% for T = 6 hr and 76.5% for T= 8 hr, respectively). The coverage discrepancy may imply certain intrinsic relationships between features' alteration tendency as exposure time increasing.

4.3.2 Dysregulated Metabolite Identification

Based on the feature alignment and annotation results, we manually curated the shifted m/z and retention time. Combined with in-house standard library matching and MS/MS fragmentation validation, 37 significantly dysregulated metabolites were confidently identified at either level 1 confirmed structure or level 2 probable structure (**Fig. B1**) (Schymanski, Jeon et al. 2014), ranging from amino acids, fatty acids, carboxylic acids and nucleoside phosphate compounds **(Table B1)**. Hierarchical clustering heatmap of 37 metabolites was presented in **Fig. 4.3**. The clustering pattern exhibits quite reasonable dynamically-distinct features, as well as the simultaneous/ synchronized dysregulation characteristic for certain metabolites within one shared category, which is consistent with our previous report (Zhao, Liu et al. 2021) .

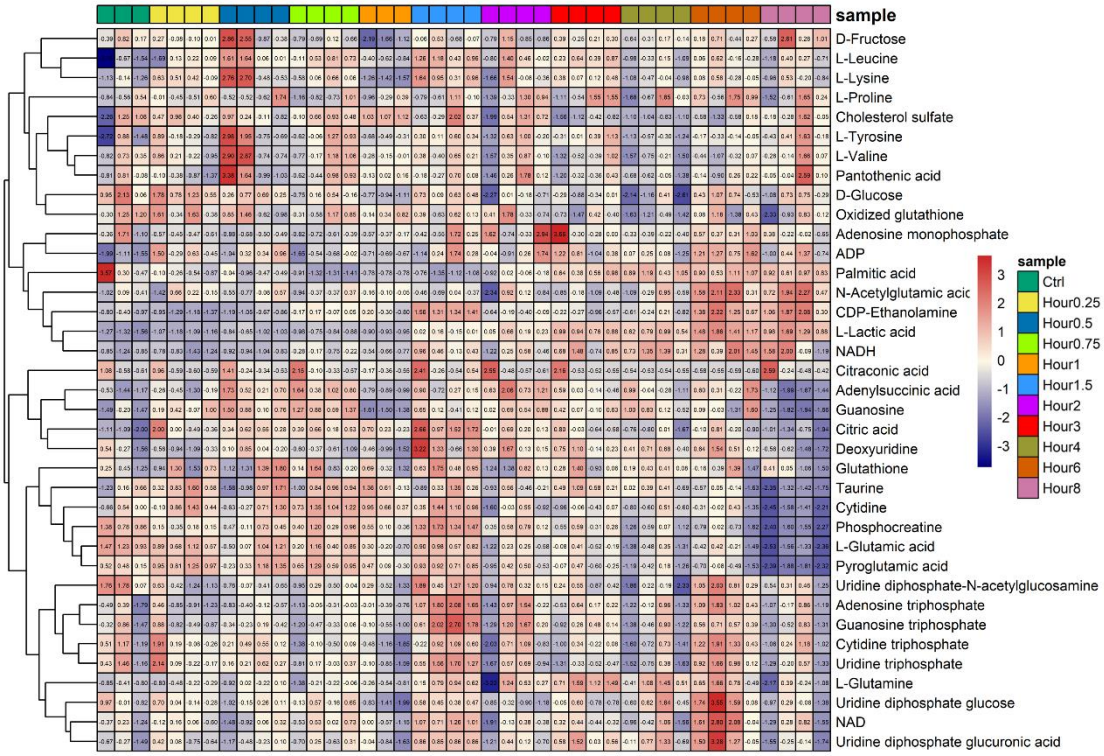

Fig. 4.3. Clustered heatmap of 37 significant dysregulated metabolites. Scales in colored key represent z-score scaled fold change value of metabolites. Red indicates upregulation; Blue indicates downregulation. [Abbreviations: Nicotinamide adenine dinucleotide (NAD); 1,4-Dihydronicotinamide adenine dinucleotide (NADH); Adenosine 5'-diphosphate (ADP).]

Based on the clustering, a few different patterns can be observed. For one thing, different metabolites exhibited distinct temporal dysregulation patterns. Among all the identified metabolites, lactic acid showed the highest fold change (FC=4.0) at 8 hr, while citraconic acid hits the minimum (FC=0.1) at 6 hr. The intercellular accumulation of lactic acid implied an enhanced glucose uptake due to Warburg effect (Brodsky, Odenwelder et al. 2019). Several metabolites were significantly upregulated to certain degree after 8 hr exposure (NADH, N-Acetylglutamic acid,

lactic acid, CDP-ethanolamine, etc.), while others exhibited a monotonic downregulation tendency (glucose, glutamic acid, phosphocreatine, pyroglutamic acid, etc.), which is consistent with previous studies (Potratz, Tarnow et al. 2017, Liu, Jia et al. 2020, Zhao, Liu et al. 2021). The decrease of glucose and phosphocreatine indicated a higher metabolic requirement for sugar and energy consumption, which suggests BPA exposure induced disturbances in TCA cycle and glycolysis (Azevedo, Porto Dechandt et al. 2019). It is also worthy to note that a few metabolites were behaving a global oscillation behaviour. For example, UDP-glucose plays indispensable roles in polysaccharides biosynthesis by gluconeogenesis and glycogen metabolism, also extracellular signalling as inflammatory responses (Lazarowski 2003, Zimmer, Barycki et al. 2021), which suggested a multi-factor and crossed-pathway co-regulation manner (Kerkhofs, Haijes et al. 2020).

For another, similar or synchronized dysregulation patterns were observed for certain metabolites within one common class, which implied a certain intercorrelated dysregulation principle. For example, the dysregulation pattern for amino acids (leucine, lysine, proline, tyrosine, valine) as well as nucleotide triphosphates (ATP, GTP, CTP, GTP). The dysregulated amino acids play important roles in the promotion of energy metabolism, protein biosynthesis, hormone production and inhibition of protein degradation (Slominski, Zmijewski et al. 2012, Acevedo, Davis et al. 2013, Duan, Li et al. 2016). In addition, the disturbed nucleotide triphosphates were explicitly related to purine/pyrimidine metabolism dysfunction (Liu, Jia et al. 2020), cell cycle maintenance, as well as potentially linked to BPA provoked DNA damage and degradation (Mokra, Kuźmi ń ska-Surowaniec et al. 2016). The differences of metabolomic effect between exposure time could be partially explained by the gradient increasing estrogenic activity (Zhao, Liu et al. 2021). Overall, the time-dependent regulation of amino acids, nucleosides and sugar suggested global metabolome disturbances, as a consequent from environment estrogen exposure and

concomitant ERα-mediated induction of cell proliferation (Potratz, Tarnow et al. 2017). The lasting BPA exposure has triggered more significant time-resolved metabolome changes for many metabolites.

4.3.3 Time-series Metabolomic Pathway Analysis

Metabolomic pathway analysis was further conducted by pathway enrichment of the dysregulated metabolites. The top interfered pathways within 8 hr exposure were purine metabolism, pyrimidine metabolism, aminoacyl-tRNA biosynthesis as well as glutamine/glutamate metabolism **(Fig. 4.4A)**. The result is also in line with several earlier studies suggesting that exposure to developmental toxicants such as BPA can induce disturbances in arginine and proline metabolism, citrate cycle and glutamate metabolism (West, Weir et al. 2010, Zhao, Liu et al. 2021). The perturbation of aminoacyl-tRNA biosynthesis was also supported by studies which observed an increase in amino acid concentrations in BPA treated-embryos (Huang, Benskin et al. 2017, Ortiz-Villanueva, Navarro-Martín et al. 2017). What is more, nucleotide phosphate levels were elevated through both *de novo* synthesis (glutathione) (Yuan, Zhang et al. 2016, Fan, Hou et al. 2020) and salvage pathway (Vahdati Hassani, Abnous et al. 2018) as reported. Other pathways include amino sugar and nucleotide sugar metabolism, galactose metabolism and TCA cycle indicated an upregulation of glucose oxidation reactions, elevated levels of proteolytic metabolism and energy consumption (Liu, Jia et al. 2020). In total, the enriched pathways revealed an enhancing proliferation trend for MCF-7 cells through BPA's estrogenic effect, with multi-pathway and multi-ending adverse effects involving global amino acid, glucose and lipid metabolism dysfunctions. Compared to previous studies (24~48 hour *in vitro*), this study demonstrates that short-term exposure to BPA can produce similar and observable disorders in varieties of amino acids, nucleotide phosphates and metabolism intermediates.

Fig. 4.4. A. Metabolite enrichment analysis of 37 significant dysregulated metabolites ($p \leqslant 0.05$); **B.** Temporal diagram of the top 3 mostly enriched pathway (with minimum *p*-value) at each time point; **C.** Rose diagrams which present the number of significantly changed metabolites and significantly disturbed pathway ($p \leqslant 0.05$) at each time point; **D.** Average abundance profiles of detected metabolites for four pathways (purine metabolism, pyrimidine metabolism, aminoacyl-tRNA

biosynthesis, alanine, aspartate and glutamate metabolism). The pathway value was set as the mean of the involved metabolite within specified pathway. All abundance levels are normalized to their mean values at 0 hr.

On top of that, we further specified the time-series regulatory patterns for certain pathways, in order to specifically describe the dynamic changes of selected biological processes with reference to exposure time. To demonstrate the featured pathway during 8-hour BPA exposure, we identified the top 3 mostly enriched pathway at each time point (**Fig. 4.4B)**. From 0.25 hr to 2 hr, purine metabolism features the most dominant regulating pathway, which indicated a temporal metabolic emphasis on one-carbon unit biosynthesis and tumor cell proliferation (Yin, Ren et al. 2018). The enriched upregulation of nucleotide phosphates (AMP, ADP, ATP) was greatly attributed to enhanced de novo purine biosynthesis (Lv, Wang et al. 2020), as well as the blockage in nucleotides degradation consequently (Xu, Wang et al. 2021). From 2 hr to 6 hr, glutamate/ glutamine metabolism shows the top enrichment, which suggested a metabolic alteration to elevated energy requirement. Glutamine is an essential component in ATP biosynthesis which fuels TCA cycle and nitrogen metabolism (Mazat and Ransac 2019). Its upregulation suggested a higher intercellular energy demand from enhanced sugar metabolism after 2 hr BPA exposure. The observed metabolic adaption from cell growth to energy metabolism interpreted the intercellular metabolic adaptions due to temporal cell function requirements, which is of great significance in understanding xenobiotics' toxicology mode of action, as well as providing an insight into the time-resolved biochemical hazard identification (Kalkhof, Dautel et al. 2015).

We further managed to plot the average abundance profiles of detected metabolites within four pathways individually (**Fig. 4.4D),** which showed tangible distinctions mutually. Rose diagram showed the number of significantly affected metabolites as

well as pathways soared with lasting exposure time, and the metabolic disruption severity continuously increased (**Fig. 4.4C)**. Totally, the results suggested that multiple pathways were distinctly activated, or inhibited with reference to time. Time-resolved changes in metabolic pathway profiles were achieved through co-regulation of various metabolites (Metallo and Vander Heiden 2013).

4.3.4 Time-resolved Metabolite Dysregulation Pattern Spotlight

To accurately describe the time-response relationship of metabolites and investigate the time-induced microscale effects on biological functions, we furtherly focused on the metabolites in purine metabolism and pyrimidine metabolism pathways (**Fig. 4.5)** as they were comparably abundant and globally pathway-enriched. As the primary catabolism compartment for intercellular signalling, energy transfer and DNA/RNA production, purine and pyrimidine metabolism are among the rapidest responding biological processes dealing with xenobiotic exposure (Liu, Jia et al. 2020). ATP is the basic cellular fuel component, whose dysregulation pattern shows an increasing energy consumption demand. AMP is a crucial composition for coenzyme (CoA, NAD, etc.), from which we inferred an enhancing oxidative phosphorylation and cellular respiration. UTP acts as the energy source for glucose/ galactose metabolism, and CTP involves energy transfer in membrane lipid metabolism. The time-resolved regulation of the mentioned purine/ pyrimidine nucleotides showed a global elevated energy homeostasis, which may be related to membrane lipid biosynthesis, protein glycosylation and upregulated cell cycle progression (Moffatt and Ashihara 2002, Quemeneur, Gerland et al. 2003, Liu, Jia et al. 2020). This is reasonable as MCF-7 is a hormone-sensitive cell line, for which BPA can induce environmental estrogenic effect (Blom, Ekman et al. 1998, Gould, Leonard et al. 1998). Another evidence is that the oxidized-glutathione and glutathione metabolism dysfunction indicated an increasing oxidative stress that cells experience. This is consistent with multiple

literature suggesting BPA exposure has led to several antioxidant enzymes depression, including glutathione reductase and glutathione peroxidase (Meli, Monnolo et al. 2020). Besides, tumor cells often tend to enhance glycolysis with extra ATP produced, as a protection against the inflammatory damage from xenobiotic intrusion (Brand and Hermfisse 1997). And it is validated by an earlier trans-omics study which reported plenty of inflammatory-related genes along Nrf2-ARE pathway were substantially expressed in MCF-7 cell undergoing BPA exposure (Liu, Jia et al. 2020). To prove this, we focused on two pairs of metabolites: NAD with NADH, and glutathione (GSH) with oxidized GSH (GSSG) to check cell's oxidative stress and redox metabolism status (**Fig. 4.6B-C**). NAD/ NADH ratio maintains redox balance in mitochondrial activity through electron transport chain. The observed excess NADH is linked with reactive oxygen species (ROS) production by inhibiting pyruvate dehydrogenase complex, which leads to DNA/ protein damage and various metabolic syndromes (Wu, Jin et al. 2016). GSH/ GSSG ratio is another important indicator in the assessment of redox state and cellular antioxidant capacity (Owen and Butterfield 2010). Unlike the monotonic drop in NAD/ NADH ratio, the observed GSH/ GSSG value showed an oscillating behavior. For 0.25 hr to 2 hr, the upregulation of GSH is potentially attributed to the cell proliferation events (Wu, Fang et al. 2004) (DNA replication, protein biosynthesis, signal transduction, etc.). This result suggested rather GSSG, the overloaded NADH is the predominant contribution to increased cellular oxidative stress, in turn resulted in oxidative phosphorylation and glycolysis dysfunctions (Moreira, Hamraz et al. 2016), which is supported by earlier study indicating that BPA exposure induced malate-aspartate shuttle functioning disorders (aspartate aminotransferase, glutamate-aspartate transporter, etc.) to break the NADH balance between cytosol and mitochondrial (Kunz, Camm et al. 2011).

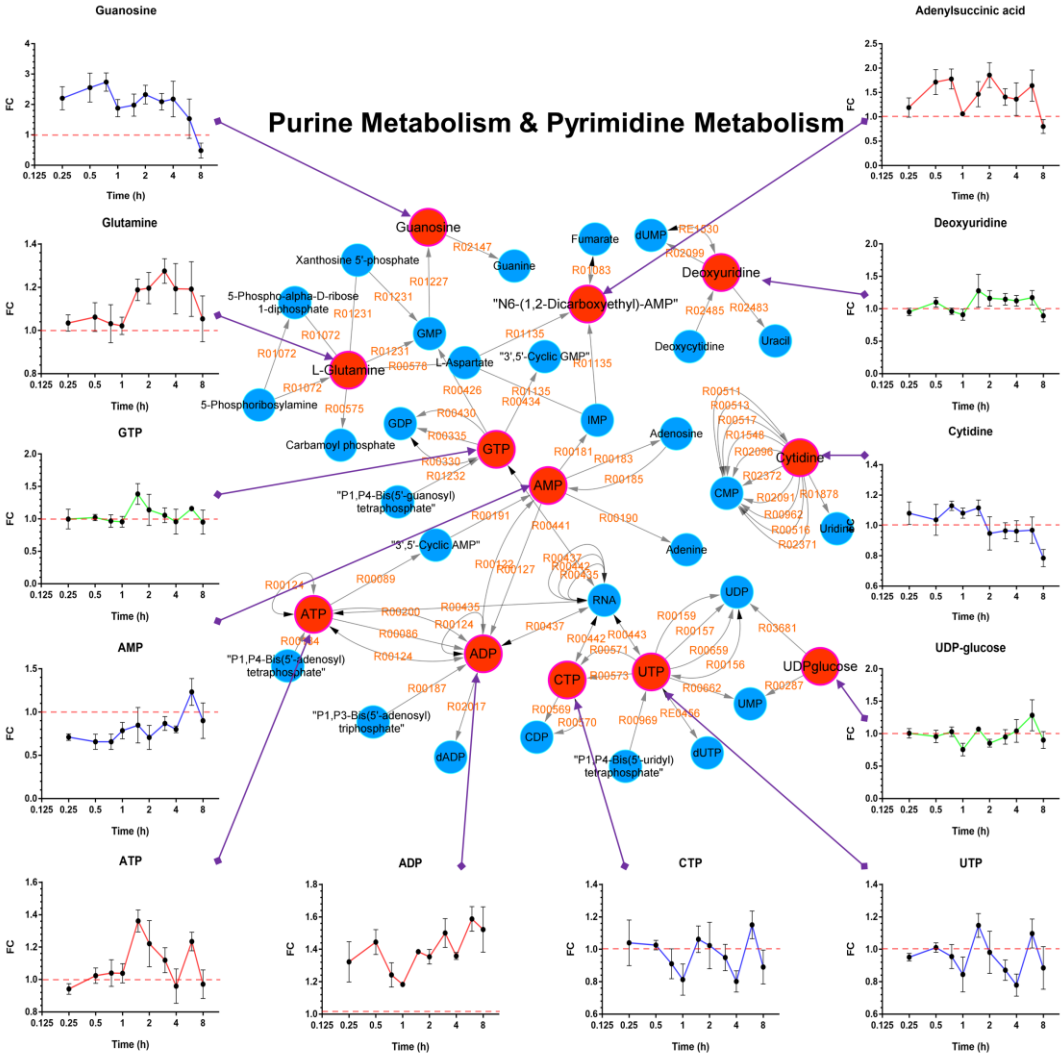

Fig. 4.5. Metabolomic analysis of purine metabolism and pyrimidine metabolism. The time-response plot for detected metabolites were shown (fold change vs. time), with red dashed line stands for control (FC = 1).

4.3.5 Metabolite Time-response Model fitting

To investigate the intrinsic relationship between different metabolites' dysregulation patterns, Pearson correlation matrix was adopted to explore the characteristic linear association (**Fig. 4.6A**). Most metabolites exhibited weak co-dysregulation dependencies, while several showed regional clustering features. For example, N-

Acetylglutamic acid (C00624) demonstrated quite positive regulation correlations with L-Glutamic acid (C00025), Pyroglutamic acid (C01879) and Citric acid (C00158). This is reasonable as for the consumption and regeneration between glutamic acid and its derivative maintains a dynamic balance from GABA cycle to TCA cycle (Petroff 2007). Similarly, significant negative correlations were observed between UTP (C00075) with UDP-glucose (C00029) and UDPGA (C00043), which may suggest that BPA exposure triggered an enhanced conversion from UTP to UDP-glucose which fuels TCA cycle as well as fulfills cell proliferation requirements (Kim, Choi et al. 2010). Scatterplots of fold changes at the adjacent time steps for 37 metabolites were further presented in **Fig. B2**. Typically, the metabolite changes between neighboring time points are performing positive correlations, yet the dysregulation pattern and intensity varies between each period (Lee, Jedrychowski et al. 2017). The results also indicated a characteristic dysregulation rate for different metabolites, and the derivation of accurate and robust time-resolved models are essential for full-period cartography prediction.

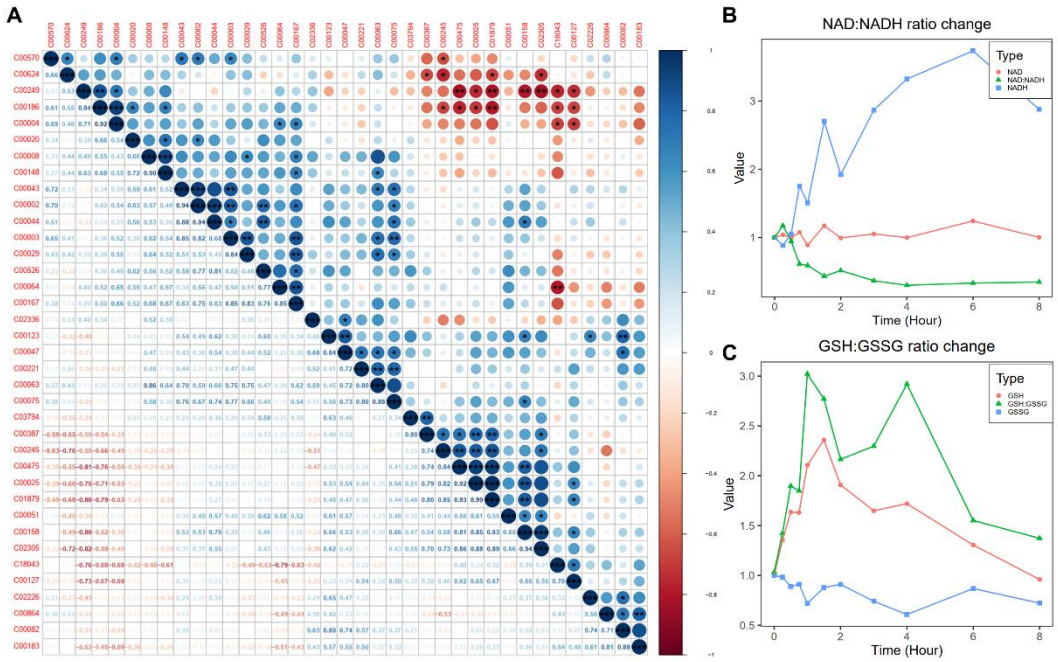

Fig. 4.6. A. Pearson correlation matrix of 37 metabolites. Dots in color stands for correlation coefficient from -1(red) to 1 (blue), with significance level presented ("*" for $p < 0.05$; "**" for $p < 0.01$; "***" for $p < 0.001$, respectively). ; **B.** Schematic diagram of dynamically changing NAD:NADH ratio; **C.** Schematic diagram of dynamically changing GSH:GSSG ratio.

To systematically evaluate the time-resolved dysregulation pattern for various metabolite, as well as interpolating their interspecies regulatory correlations, time-response relationship for each were fitted and several curves were presented (**Fig. 4.7**). Traditional monotonic dose-response methods can hardly be eligible for the time-resolved metabolism behavior characterization. Hereby, we implemented a restricted cubic spline fitting (RCS) protocol, as for its advantage in non-linearity continuous description and successful application in multiple public health issues (Desquilbet and Mariotti 2010, Inoue, Ritz et al. 2020, Johannesen, Langsted et al. 2020). The established models not only provide an insightful tool to predict the

metabolite dysregulation behavior in untested scenarios, also illustrate metabolites' relative sensitivity which leads to novel biomarkers identification (Zhao, Liu et al. 2021). For example, the four presented metabolites (AMP, citrate, guanosine, glutamic acid) are performing different biological functions in separate metabolic pathways. At 1 hr, the predicted FC values for each are 0.75, 1.86, 2.28 and 0.9, respectively, which suggested metabolites' sequential relative sensitivity to BPA exposure (guanosine > citrate > AMP > glutamic acid). The information could furtherly be adopted for potential biomarkers identification, for metabolites with higher dysregulation sensitivity (GTP, CTP, proline, etc.) (Zhao, Liu et al. 2021). The time-resolved dynamic metabolomics study shall provide insights into active metabolomics to construct a solid framework for elucidating metabolite real-time dysregulation pattern, also promising in the application of dynamic metabolome monitoring, prediction and extrapolation (Rinschen, Ivanisevic et al. 2019, Lai, Liu et al. 2021, Peng, Zhao et al. 2022).

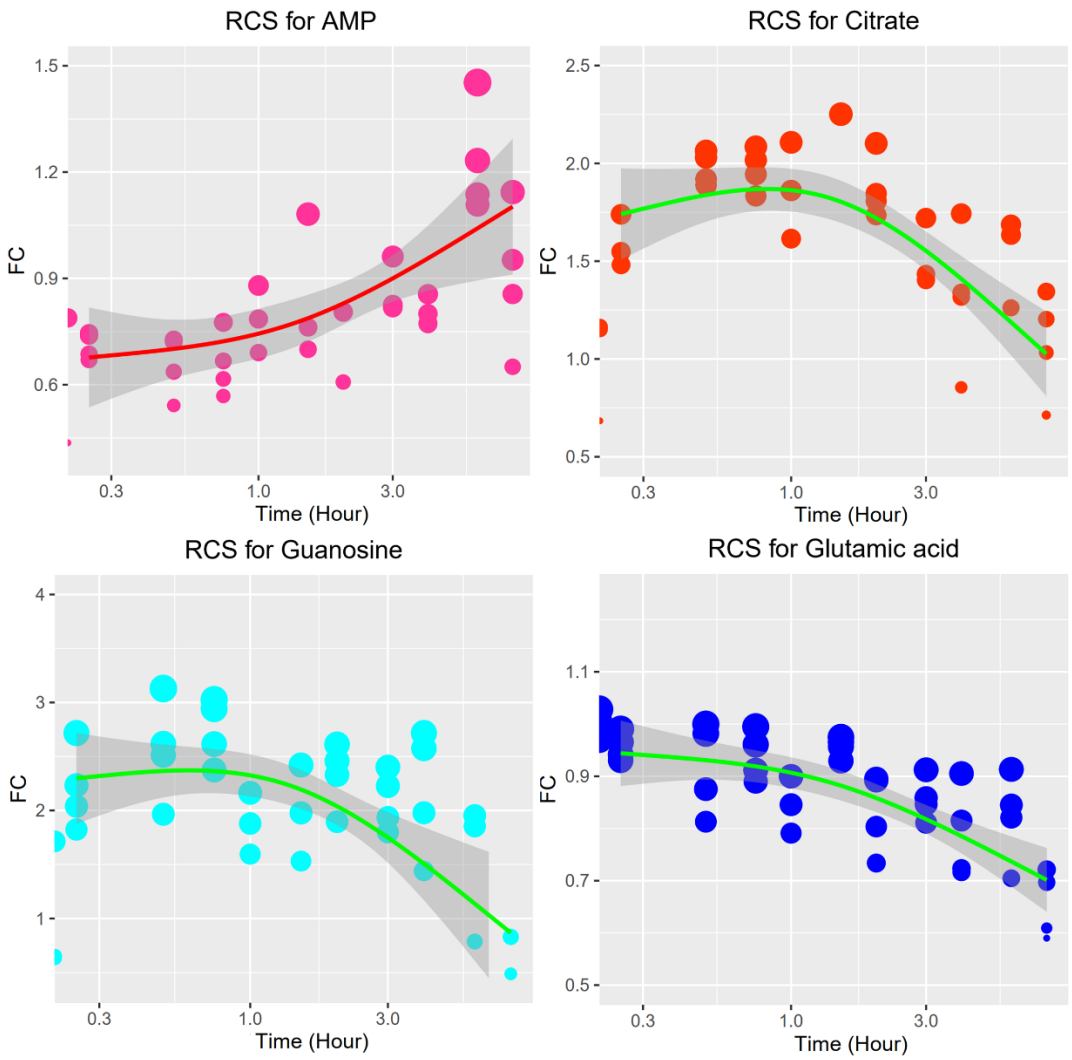

Fig. 4.7. Restricted cubic spline fitting curve of four metabolites, with confidence level indicated in grey ($p < 0.05$).

4.4 Conclusions

In summary, this study characterized the time-resolved cellular metabolome changes under xenobiotics exposure. Thirty-seven significantly dysregulated metabolites were identified, ranging from amino acids, fatty acids, carboxylic acids and nucleoside phosphate compounds. Different metabolites basically showed distinct time-resolved changing patterns, while ones within common class showed similar

and synchronized dysregulation manners. The pathway enrichment analysis suggested that purine metabolism, pyrimidine metabolism, aminoacyl-tRNA biosynthesis as well as glutamine/ glutamate metabolism pathways were heavily disturbed. As exposure event lasting, MCF-7 cells went through clear sequential metabolic adaptions from cell proliferation to energy metabolism, which indicated an enhancing cellular requirement for elevated energy homeostasis, oxidative stress response and ER-α mediated cell growth. We further focused on the time-dependent metabolite dysregulation behaviour in purine metabolism and pyrimidine metabolism, and identified excessive NADH accumulation as the primary contribution to impairing glycolysis and oxidative phosphorylation by redox imbalance. Lastly, we established a restricted cubic spline-based model to fit and predict metabolite's full range dysregulation cartography, with metabolite' sensitivity comparisons retrieved and novel biomarkers suggested. Overall, the results indicated that 8 hr BPA exposure leads to dynamic global metabolome disturbances including amino acid, nucleoside and sugar metabolism disorders, and the dysregulated metabolites with interfered pathways at different stages are of significant sequential distinctions.

Limitations of this study are further addressed as follows. As we investigated the metabolomic effect of BPA exposure within 8 hr, the observed time-response dysregulation pattern may be incomplete. Also, the selection of time points isn't intensive enough to acquire real-time metabolome monitoring data, which may lead to key stages' neglections at which metabolic transition happens. Comparably high concentrations of chemicals (100 μM) were adopted in this study to obtain observable results, and a single cancer cell line is adopted. *In vivo* and other *in vitro* models should also be considered in future study, to investigate and validate the metabolite time-response models (Xu, Chen et al. 2021). The reached conclusion requires further validation, like chemical proteomics and flux studies (Xu, Lim et al. 2020, Xu, Zhao et al. 2021). And the RCS modelling strategies can hardly be applied to all

metabolites as for some were exhibiting an oscillation dysregulation behavior. Overall, the time-resolved metabolomics study is promising for elucidation of the time-dependent metabolome dysregulation and identification of the sequential biochemical anomalies, yet still challenging in the interpretation of toxicological mechanisms, as well as experiment's reproducibility and scalability.

CHAPTER 5 CONCLUSION AND RECOMMENDATIONS

5.1 Conclusion

This study adopted dose-response metabolomics to characterize metabolites' dysregulation behaviour under BPA exposure. In summary, we characterized the cellular metabolome changes upon exposure to four different levels of BPA. The metabolomics studies suggested that BPA exposure perturbed specific biochemical pathways such as purine metabolism and pyrimidine metabolism. The dysregulated metabolites and affected metabolic pathway results are consistent with several previous studies. Interestingly, we observed that the sensitivities were varied for different metabolites. However, the metabolites on the same pathways are more likely to behave in similar manners. Metabolite dose-dependent relationships were established based on the applied dosage range. These relationships were further used to predict and describe the dysregulation pattern of metabolites under untested scenarios. We also calculated respective EC values at specific points, which can provide useful information on metabolite relative sensitivity and propose some endogenous biomarkers for BPA exposure.

This study also characterized the time-resolved cellular metabolome changes under xenobiotics exposure. Thirty-seven significantly dysregulated metabolites were identified, ranging from amino acids, fatty acids, carboxylic acids and nucleoside phosphate compounds. Different metabolites basically showed distinct time-resolved changing patterns, while ones within common class showed similar and synchronized dysregulation manners. The pathway enrichment analysis suggested that purine metabolism, pyrimidine metabolism, aminoacyl-tRNA biosynthesis as well as glutamine/ glutamate metabolism pathways were heavily disturbed. As exposure event lasting, MCF-7 cells went through clear sequential metabolic adaptions from cell proliferation to energy metabolism, which indicated an enhancing cellular

requirement for elevated energy homeostasis, oxidative stress response and ER-α mediated cell growth. We further focused on the time-dependent metabolite dysregulation behaviour in purine metabolism and pyrimidine metabolism, and identified excessive NADH accumulation as the primary contribution to impairing glycolysis and oxidative phosphorylation by redox imbalance. Lastly, we established a restricted cubic spline-based model to fit and predict metabolite's full range dysregulation cartography, with metabolite' sensitivity comparisons retrieved and novel biomarkers suggested. Overall, the results indicated that 8 hr BPA exposure leads to dynamic global metabolome disturbances including amino acid, nucleoside and sugar metabolism disorders, and the dysregulated metabolites with interfered pathways at different stages are of significant sequential distinctions.

In total, the major conclusions and contributions of this study were:

(i) interpreting the dose-response and time-resolved relationships on an omics-scale level; combining metabolomics study with traditional toxicology models and endpoints;

(ii) establishing metabolite extrapolation models for untested scenarios predictions; comparing metabolite and metabolic pathways' relative sensitivity; suggesting novel biomarkers;

(iii) revealing BPA's toxicological mode of action with a dose-response and time-resolved featured landscapes; uncovering the dysregulated biofunctions with significant spatial and temporal distinctions.

5.2 Recommendations

Firstly, the reached dose-response and time-resolved omics-dysregulation conclusion needs other supportive evidences (other cell lines, *in vivo* models, metabolic flux analysis, epidemiology study, etc.), to increase the experiment's reproducibility and scalability.

Secondly, the adopted exposure dose and time range in this study is limited, while the intervals can be furtherly modified, to provide a refined and robust dose-response and time-resolved relationship prediction and extrapolation.

Thirdly, more targeted omics study can be implemented to investigate the observed biological dysfunctions in lipids and amino acids regulation, which will lead to a deeper understanding of BPA's toxicological mechanisms with dose-and-time characteristic landscapes.

REFERENCES

Applicable.Acevedo, N., et al. (2013). "Perinatally Administered Bisphenol A Acts as a Mammary Gland Carcinogen in Rats." Environmental health perspectives **121**.

Aghajanpour-Mir, S. M., et al. (2016). "The Genotoxic and Cytotoxic Effects of Bisphenol-A (BPA) in MCF-7 Cell Line and Amniocytes." Int J Mol Cell Med **5**(1): 19-29.

Allman, E., et al. (2016). "Metabolomic Profiling of the Malaria Box Reveals Antimalarial Target Pathways." Antimicrobial Agents and Chemotherapy **60**: AAC.01224-01216.

Alonso-Magdalena, P., et al. (2006). "The estrogenic effect of bisphenol A disrupts pancreatic beta-cell function in vivo and induces insulin resistance." Environ Health Perspect **114**(1): 106-112.

Alonso-Magdalena, P., et al. (2012). "Bisphenol-A acts as a potent estrogen via non-classical estrogen triggered pathways." Molecular and cellular endocrinology **355**(2): 201-207.

Altshuler, B. (1981). "Modeling of dose-response relationships." Environmental health perspectives **42**: 23-27.

Altshuler, B. (1981). "Modeling of dose-response relationships." Environ Health Perspect **42**: 23-27.

Andrzejczyk, N. E., et al. (2020). "Novel Disinfection Byproducts Formed from the Pharmaceutical Gemfibrozil Are Bioaccumulative and Elicit Increased Toxicity Relative to the Parent Compound in Marine Polychaetes (Neanthes arenaceodentata)." Environ Sci Technol **54**(18): 11127-11136.

Antoniewicz, M. R. (2021). "A guide to metabolic flux analysis in metabolic engineering: Methods, tools and applications." Metab Eng **63**: 2-12.

Asimakopoulos, A. G., et al. (2017). "Corrigendum to "Urinary biomarkers of exposure to 57 xenobiotics and its association with oxidative stress in a population in Jeddah, Saudi Arabia" [Environ. Res. 150 (2016) 573-581]." Environ Res **153**: 205.

Atkinson, A. and D. Roy (1995). "In vivo DNA adduct formation by bisphenol A." Environ Mol Mutagen **26**(1): 60-66.

Azevedo, L. F., et al. (2019). "Long-term exposure to bisphenol A or S promotes glucose intolerance and changes hepatic mitochondrial metabolism in male Wistar rats." Food Chem Toxicol **132**: 110694.

Beale, D. J., et al. (2018). "Review of recent developments in GC-MS approaches to metabolomics-based research." Metabolomics **14**(11): 152.

Bernhard, A., et al. (2019). "Tolerance and dose-response assessment of subchronic dietary ethoxyquin exposure in Atlantic salmon (Salmo salar L.)." PLoS One **14**(1): e0211128-e0211128.

Beyer, B. A., et al. (2018). "Metabolomics-based discovery of a metabolite that

enhances oligodendrocyte maturation." Nature chemical biology **14**(1): 22.
Beyer, B. A., et al. (2018). "Metabolomics-based discovery of a metabolite that enhances oligodendrocyte maturation." Nature chemical biology **14**(1): 22-28.
Blom, A., et al. (1998). "Effects of xenoestrogenic environmental pollutants on the proliferation of a human breast cancer cell line (MCF-7)." Arch Environ Contam Toxicol **34**(3): 306-310.
Bordbar, A., et al. (2017). "Elucidating dynamic metabolic physiology through network integration of quantitative time-course metabolomics." Scientific reports **7**(1): 46249.
Brand, K. A. and U. Hermfisse (1997). "Aerobic glycolysis by proliferating cells: a protective strategy against reactive oxygen species." FASEB J **11**(5): 388-395.
Brodsky, A. N., et al. (2019). "High extracellular lactate causes reductive carboxylation in breast tissue cell lines grown under normoxic conditions." PLoS One **14**(6): e0213419.
Buchweitz, L. F., et al. (2020). "Visualizing metabolic network dynamics through time-series metabolomic data." BMC Bioinformatics **21**(1): 130.
Cabaton, N. J., et al. (2013). "Effects of low doses of bisphenol A on the metabolome of perinatally exposed CD-1 mice." Environ Health Perspect **121**(5): 586-593.
Cabaton, N. J., et al. (2018). "An Untargeted Metabolomics Approach to Investigate the Metabolic Modulations of HepG2 Cells Exposed to Low Doses of Bisphenol A and 17β-Estradiol." Frontiers in Endocrinology **9**: 571.
Calabrese, E. J. and L. A. Baldwin (2003). "The Hormetic Dose-Response Model Is More Common than the Threshold Model in Toxicology." Toxicological Sciences **71**(2): 246-250.
Carlborg, F. W. (1981). "Dose-response functions in carcinogenesis and the Weibull model." Food Cosmet Toxicol **19**(2): 255-263.
Carpenter, J. R. (1986). "A method for presenting and comparing dose-response curves." J Pharmacol Methods **15**(4): 283-303.
Castro, B., et al. (2015). "Bisphenol A, bisphenol F and bisphenol S affect differently 5alpha-reductase expression and dopamine-serotonin systems in the prefrontal cortex of juvenile female rats." Environ Res **142**: 281-287.
Chen, D., et al. (2016). "Bisphenol Analogues Other Than BPA: Environmental Occurrence, Human Exposure, and Toxicity—A Review." Environmental Science & Technology **50**(11): 5438-5453.
Chen, M., et al. (2014). "Metabolomic analysis reveals metabolic changes caused by bisphenol A in rats." Toxicol Sci **138**(2): 256-267.
Chen, R., et al. (2012). "Personal omics profiling reveals dynamic molecular and medical phenotypes." Cell **148**(6): 1293-1307.
Chou, K. J., et al. (2021). Electrons and Protons | Renewable Hydrogen From

Biomass Fermentation☆. Encyclopedia of Biological Chemistry III (Third Edition). J. Jez. Oxford, Elsevier**:** 551-559.
Clement, J., et al. (2019). "The Plasma NAD+ Metabolome is Dysregulated in 'normal' Ageing." Rejuvenation Research **22**: 121-130.
Cobbold, S. and M. McConville (2019). Determining the Mode of Action of Antimalarial Drugs Using Time-Resolved LC-MS-Based Metabolite Profiling: Methods and Protocols. **1859:** 225-239.
Cobbold, S. A., et al. (2016). "Metabolic Dysregulation Induced in Plasmodium falciparum by Dihydroartemisinin and Other Front-Line Antimalarial Drugs." J Infect Dis **213**(2): 276-286.
Cobellis, L., et al. (2009). "Measurement of bisphenol A and bisphenol B levels in human blood sera from healthy and endometriotic women." Biomed Chromatogr **23**(11): 1186-1190.
Costello, Z. and H. G. Martin (2018). "A machine learning approach to predict metabolic pathway dynamics from time-series multiomics data." NPJ Syst Biol Appl **4**: 19.
Cowley, G. S., et al. (2014). "Parallel genome-scale loss of function screens in 216 cancer cell lines for the identification of context-specific genetic dependencies." Sci Data **1**: 140035.
Crisp, T. M., et al. (1998). "Environmental endocrine disruption: an effects assessment and analysis." Environ Health Perspect **106 Suppl 1**: 11-56.
Crizer, D. M., et al. (2021). "Benchmark Concentrations for Untargeted Metabolomics Versus Transcriptomics for Liver Injury Compounds in In Vitro Liver Models." Toxicol Sci **181**(2): 175-186.
Dai, D., et al. (2016). "Time-resolved metabolomics analysis of individual differences during the early stage of lipopolysaccharide-treated rats." Sci Rep **6**: 34136.
Desquilbet, L. and F. Mariotti (2010). "Dose-response analyses using restricted cubic spline functions in public health research." Statistics in medicine **29**: 1037-1057.
Dobrzyńska, M. M. and J. Radzikowska (2013). "Genotoxicity and reproductive toxicity of bisphenol A and X-ray/bisphenol A combination in male mice." Drug and Chemical Toxicology **36**(1): 19-26.
Doherty, L. F., et al. (2010). "In utero exposure to diethylstilbestrol (DES) or bisphenol-A (BPA) increases EZH2 expression in the mammary gland: an epigenetic mechanism linking endocrine disruptors to breast cancer." Horm Cancer **1**(3): 146-155.
Duan, Y., et al. (2016). "The role of leucine and its metabolites in protein and energy metabolism." Amino Acids **48**(1): 41-51.
Eckstrum, K., et al. (2016). "Icam5 Expression Exhibits Sex Differences in the Neonatal Pituitary and Is Regulated by Estradiol and Bisphenol A." Endocrinology

157: en20151521.
Engin, A. B. and A. Engin (2021). "The effect of environmental Bisphenol A exposure on breast cancer associated with obesity." Environ Toxicol Pharmacol **81**: 103544.
Ewald, J., et al. (2021). "FastBMD: an online tool for rapid benchmark dose-response analysis of transcriptomics data." Bioinformatics **37**(7): 1035-1036.
Faes, C., et al. (2003). "Use of fractional polynomials for dose-response modelling and quantitative risk assessment in developmental toxicity studies." Statistical Modelling **3**(2): 109-125.
Fan, X., et al. (2020). "Discrepant dose responses of bisphenol A on oxidative stress and DNA methylation in grass carp ovary cells." Chemosphere **248**: 126110.
Fang, M., et al. (2015). "Thermal degradation of small molecules: a global metabolomic investigation." Analytical chemistry **87**(21): 10935-10941.
Fang, M., et al. (2015). "Thermal Degradation of Small Molecules: A Global Metabolomic Investigation." Anal Chem **87**(21): 10935-10941.
Fang, W., et al. (2020). "A Tiered Approach for Screening and Assessment of Environmental Mixtures by Omics and In Vitro Assays." Environ Sci Technol **54**(12): 7430-7439.
Fernandez, M. F., et al. (2007). "Bisphenol-A and chlorinated derivatives in adipose tissue of women." Reprod Toxicol **24**(2): 259-264.
Fernandez, S. V., et al. (2012). "Expression and DNA methylation changes in human breast epithelial cells after bisphenol A exposure." Int J Oncol **41**(1): 369-377.
Fic, A., et al. (2015). "Genome-wide gene expression profiling of low-dose, long-term exposure of human osteosarcoma cells to bisphenol A and its analogs bisphenols AF and S." Toxicol In Vitro **29**(5): 1060-1069.
Fic, A., et al. (2013). "Mutagenicity and DNA damage of bisphenol A and its structural analogues in HepG2 cells." Arh Hig Rada Toksikol **64**(2): 189-200.
Flint, S., et al. (2012). "Bisphenol A exposure, effects, and policy: a wildlife perspective." Journal of environmental management **104**: 19-34.
Folz, J. S., et al. (2021). "Metabolomics analysis of time-series human small intestine lumen samples collected in vivo." Food Funct **12**(19): 9405-9415.
Fritsche, E., et al. (2018). "Consensus statement on the need for innovation, transition and implementation of developmental neurotoxicity (DNT) testing for regulatory purposes." Toxicol Appl Pharmacol **354**: 3-6.
Fu, P. and K. Kawamura (2010). "Ubiquity of bisphenol A in the atmosphere." Environ Pollut **158**(10): 3138-3143.
Fu, Q., et al. (2021). "Metabolomic Profiling and Toxicokinetics Modeling to Assess the Effects of the Pharmaceutical Diclofenac in the Aquatic Invertebrate Hyalella azteca." Environ Sci Technol **55**(12): 7920-7929.
Fujiwara, Y., et al. (2018). "The Effects of Low-Dose Bisphenol A and Bisphenol F

on Neural Differentiation of a Fetal Brain-Derived Neural Progenitor Cell Line." Front Endocrinol (Lausanne) **9**: 24.
Gao, C., et al. (2021). "Oxidative Stress, Endocrine Disturbance, and Immune Interference in Humans Showed Relationships to Serum Bisphenol Concentrations in a Dense Industrial Area." Environmental Science & Technology **55**(3): 1953-1963.
Garside, M. (2020). "U.S. bisphenol A production volume Report (1990-2019)."
Geng, S., et al. (2016). "Jasmonate-mediated stomatal closure under elevated CO2 revealed by time-resolved metabolomics." Plant J **88**(6): 947-962.
Goetz, N., et al. (2010). "Bisphenol A: How the Most Relevant Exposure Sources Contribute to Total Consumer Exposure." Risk analysis : an official publication of the Society for Risk Analysis **30**: 473-487.
Golub, M. S., et al. (2010). "Bisphenol A: developmental toxicity from early prenatal exposure." Birth Defects Res B Dev Reprod Toxicol **89**(6): 441-466.
Gould, J. C., et al. (1998). "Bisphenol A interacts with the estrogen receptor alpha in a distinct manner from estradiol." Molecular and cellular endocrinology **142**(1-2): 203-214.
Guijas, C. and G. Siuzdak (2018). "Reply to Comment on METLIN: A Technology Platform for Identifying Knowns and Unknowns." Anal Chem **90**(21): 13128-13129.
Halama, A., et al. (2019). "Metabolomics of Dynamic Changes in Insulin Resistance Before and After Exercise in PCOS." Frontiers in Endocrinology **10**: 116.
Hamilton, M. A., et al. (1977). "Trimmed Spearman-Karber method for estimating median lethal concentrations in toxicity bioassays." Environmental Science & Technology **11**(7): 714-719.
Hartl, J., et al. (2020). "Untargeted metabolomics links glutathione to bacterial cell cycle progression." Nature Metabolism **2**(2): 153-166.
Hashimoto, S., et al. (2005). "Horizontal and vertical distribution of estrogenic activities in sediments and waters from Tokyo Bay, Japan." Arch Environ Contam Toxicol **48**(2): 209-216.
Heinzmann, S. S., et al. (2010). "Metabolic profiling strategy for discovery of nutritional biomarkers: proline betaine as a marker of citrus consumption." The American Journal of Clinical Nutrition **92**(2): 436-443.
Herold, M., et al. (2020). "Integration of time-series meta-omics data reveals how microbial ecosystems respond to disturbance." Nature Communications **11**(1): 5281.
Herwibawa, B. and F. Kusmiyati (2017). "MUTAGENIC EFFECTS OF SODIUM AZIDE ON THE GERMINATION IN RICE (Oryza sativa L. cv. INPAGO UNSOED 1)." JURNAL AGROTEKNOLOGI **7**: 9.
Holmes, E., et al. (1998). "The identification of novel biomarkers of renal toxicity

using automatic data reduction techniques and PCA of proton NMR spectra of urine." Chemometrics and Intelligent Laboratory Systems **44**(1): 245-255.
Howdeshell, K. L., et al. (1999). "Exposure to bisphenol A advances puberty." Nature **401**(6755): 763-764.
Hu, Y., et al. (2019). "Occurrence, fate and risk assessment of BPA and its substituents in wastewater treatment plant: A review." Environ Res **178**: 108732.
Huang, S. S., et al. (2017). "A multi-omic approach to elucidate low-dose effects of xenobiotics in zebrafish (Danio rerio) larvae." Aquatic toxicology **182**: 102-112.
Huang, W., et al. (2020). "Integration of proteomics and metabolomics reveals promotion of proliferation by exposure of bisphenol S in human breast epithelial MCF-10A cells." Sci Total Environ **712**: 136453.
Huff, J. (2001). "Carcinogenicity of bisphenol-A in Fischer rats and B6C3F1 mice." Odontology **89**(1): 12-20.
Hutler Wolkowicz, I., et al. (2016). "Developmental toxicity of bisphenol A diglycidyl ether (epoxide resin badge) during the early life cycle of a native amphibian species." Environ Toxicol Chem **35**(12): 3031-3038.
Igarashi, T. (1995). "The rationale for using logarithmic transformation of concentration data in toxicokinetic studies." The Journal of toxicological sciences **20**(1): 67-72.
Inoue, K., et al. (2020). "Association of Subclinical Hypothyroidism and Cardiovascular Disease With Mortality." JAMA Netw Open **3**(2): e1920745.
Ishido, M., et al. (2004). "Bisphenol A causes hyperactivity in the rat concomitantly with impairment of tyrosine hydroxylase immunoreactivity." J Neurosci Res **76**(3): 423-433.
Jain, M., et al. (2012). "Metabolite profiling identifies a key role for glycine in rapid cancer cell proliferation." Science **336**(6084): 1040-1044.
Jalal, N., et al. (2018). "Bisphenol A (BPA) the mighty and the mutagenic." Toxicology Reports **5**: 76-84.
Johannesen, C. D. L., et al. (2020). "Association between low density lipoprotein and all cause and cause specific mortality in Denmark: prospective cohort study." BMJ **371**: m4266.
Jordan, K. W., et al. (2009). "Metabolomic characterization of human rectal adenocarcinoma with intact tissue magnetic resonance spectroscopy." Dis Colon Rectum **52**(3): 520-525.
Kalkhof, S., et al. (2015). "Pathway and Time-Resolved Benzo[a]pyrene Toxicity on Hepa1c1c7 Cells at Toxic and Subtoxic Exposure." Journal of Proteome Research **14**(1): 164-182.
Karnam, S. S., et al. (2015). "Evaluation of subacute bisphenol - A toxicity on male reproductive system." Vet World **8**(6): 738-744.
Kawai, M., et al. (2020). "Suppression of lactate production by using sucrose as a carbon source in lactic acid bacteria." Journal of Bioscience and Bioengineering

129(1): 47-51.
Kawata, K., et al. (2018). "Trans-omic Analysis Reveals Selective Responses to Induced and Basal Insulin across Signaling, Transcriptional, and Metabolic Networks." iScience **7**: 212-229.
Kazius, J., et al. (2005). "Derivation and validation of toxicophores for mutagenicity prediction." J Med Chem **48**(1): 312-320.
Keerthisinghe, T. P., et al. (2021). "Feeding state greatly modulates the effect of xenobiotics on gut microbiome metabolism: A case study of tetracycline." J Hazard Mater **413**: 125441.
Kerkhofs, M., et al. (2020). "Cross-Omics: Integrating Genomics with Metabolomics in Clinical Diagnostics." Metabolites **10**(5).
Kim, H., et al. (2010). "Structural basis for the reaction mechanism of UDP-glucose pyrophosphorylase." Mol Cells **29**(4): 397-405.
Kim, S., et al. (2021). "PubChem in 2021: new data content and improved web interfaces." Nucleic Acids Res **49**(D1): D1388-D1395.
Kim, T., et al. (2021). "A hierarchical approach to removal of unwanted variation for large-scale metabolomics data." Nat Commun **12**(1): 4992.
Kimber, I. (2017). "Bisphenol A and immunotoxic potential: A commentary." Regulatory toxicology and pharmacology : RTP **90**.
Kovacic, P. (2010). "How safe is bisphenol A? Fundamentals of toxicity: Metabolism, electron transfer and oxidative stress." Medical Hypotheses **75**(1): 1-4.
Kowalski, G. M., et al. (2015). "Application of dynamic metabolomics to examine in vivo skeletal muscle glucose metabolism in the chronically high-fat fed mouse." Biochem Biophys Res Commun **462**(1): 27-32.
Krycer, J. R., et al. (2017). "Dynamic Metabolomics Reveals that Insulin Primes the Adipocyte for Glucose Metabolism." Cell Reports **21**(12): 3536-3547.
Kuiper, G. G., et al. (1998). "Interaction of estrogenic chemicals and phytoestrogens with estrogen receptor beta." Endocrinology **139**(10): 4252-4263.
Kundu, S., et al. (2019). Chapter 9 - Design and Development of Antibiotic Fermentation Using Different Processing Strategies: Challenges and Perspectives. Applied Microbiology and Bioengineering. P. Shukla, Academic Press**:** 163-183.
Kunz, N., et al. (2011). "Developmental and metabolic brain alterations in rats exposed to bisphenol A during gestation and lactation." Int J Dev Neurosci **29**(1): 37-43.
Lai, Y., et al. (2021). "High-coverage metabolomics uncovers microbiota-driven biochemical landscape of interorgan transport and gut-brain communication in mice." Nature Communications **12**(1): 6000.
Larras, F., et al. (2018). "DRomics: A Turnkey Tool to Support the Use of the Dose–Response Framework for Omics Data in Ecological Risk Assessment." Environmental Science & Technology **52**(24): 14461-14468.
Lautenbacher, L., et al. (2022). "ProteomicsDB: toward a FAIR open-source

resource for life-science research." Nucleic Acids Res **50**(D1): D1541-D1552.
Lazarowski, E. (2003). "Release of Cellular UDP-Glucose as a Potential Extracellular Signaling Molecule." Molecular Pharmacology **63**: 1190-1197.
Lee, H.-J., et al. (2017). "Proteomic and Metabolomic Characterization of a Mammalian Cellular Transition from Quiescence to Proliferation." Cell Reports **20**: 721-736.
Lee, J. and K. T. Lim (2010). "Plant-originated glycoprotein (36 kDa) suppresses interleukin-4 and -10 in bisphenol A-stimulated primary cultured mouse lymphocytes." Drug Chem Toxicol **33**(4): 421-429.
Lee, S., et al. (2015). "Emission of bisphenol analogues including bisphenol A and bisphenol F from wastewater treatment plants in Korea." Chemosphere **119**: 1000-1006.
Lee, S., et al. (2013). "Genotoxic potentials and related mechanisms of bisphenol A and other bisphenol compounds: a comparison study employing chicken DT40 cells." Chemosphere **93**(2): 434-440.
Lee, S. Y., et al. (2011). Chapter four - Application of Metabolic Flux Analysis in Metabolic Engineering. Methods in Enzymology. C. Voigt, Academic Press. **498:** 67-93.
Lewis, D., et al. (2012). "An efficient protocol for radiochromic film dosimetry combining calibration and measurement in a single scan." Med Phys **39**(10): 6339-6350.
Li, L., et al. (2021). Exploring Dynamic Metabolomics Data With Multiway Data Analysis: a Simulation Study.
Li, Y., et al. (2021). "Time-series metabolomics insights into the progressive characteristics of 3,5-diethoxycarbonyl-1,4-dihydrocollidine-induced cholestatic liver fibrosis in mice." Journal of Pharmaceutical and Biomedical Analysis **198**: 113986.
Liang, L., et al. (2020). "Metabolic Dynamics and Prediction of Gestational Age and Time to Delivery in Pregnant Women." Cell **181**(7): 1680-1692 e1615.
Liao, C., et al. (2012). "Occurrence of Eight Bisphenol Analogues in Indoor Dust from the United States and Several Asian Countries: Implications for Human Exposure." Environmental Science & Technology **46**(16): 9138-9145.
Liao, C., et al. (2012). "Bisphenol analogues in sediments from industrialized areas in the United States, Japan, and Korea: spatial and temporal distributions." Environ Sci Technol **46**(21): 11558-11565.
Lin, Z., et al. (2017). "A Study on Environmental Bisphenol A Pollution in Plastics Industry Areas." Water, Air, & Soil Pollution **228**(3): 98.
Link, H., et al. (2015). "Real-time metabolome profiling of the metabolic switch between starvation and growth." Nature Methods **12**(11): 1091-1097.
Link, H., et al. (2013). "Systematic identification of allosteric protein-metabolite interactions that control enzyme activity in vivo." Nature biotechnology **31**.

Liu, M., et al. (2019). "The occurrence of bisphenol plasticizers in paired dust and urine samples and its association with oxidative stress." Chemosphere **216**: 472-478.
Liu, M., et al. "Metabolomic and Transcriptomic Analysis of MCF-7 Cells Exposed to 23 Chemicals at Human-Relevant Levels: Estimation of Individual Chemical Contribution to Effects." Environmental health perspectives **128**(12): 127008.
Liu, M., et al. (2020). "Metabolomic and Transcriptomic Analysis of MCF-7 Cells Exposed to 23 Chemicals at Human-Relevant Levels: Estimation of Individual Chemical Contribution to Effects." Environmental health perspectives **128**(12): 127008.
Liu, M., et al. (2021). "RTP: One Effective Platform to Probe Reactive Compound Transformation Products and Its Applications for a Reactive Plasticizer BADGE." Environ Sci Technol **55**(23): 16034-16043.
Liu, X., et al. (2014). "A characteristic back support structure in the bisphenol A-binding pocket in the human nuclear receptor ERRgamma." PLoS One **9**(6): e101252.
Lu, H., et al. (2020). "Time-resolved multi-omics analysis reveals the role of nutrient stress-induced resource reallocation for TAG accumulation in oleaginous fungus Mortierella alpina." Biotechnol Biofuels **13**: 116.
Lu, W., et al. (2008). "Analytical strategies for LC-MS-based targeted metabolomics." J Chromatogr B Analyt Technol Biomed Life Sci **871**(2): 236-242.
Luan, H., et al. (2021). "Machine Learning for Investigation on Endocrine-Disrupting Chemicals with Gestational Age and Delivery Time in a Longitudinal Cohort." Research **2021**: 9873135.
Lv, Y., et al. (2020). "Nucleotide de novo synthesis increases breast cancer stemness and metastasis via cGMP-PKG-MAPK signaling pathway." PLoS Biol **18**(11): e3000872.
M.R, L. H., et al. (2019). "A Review on GC-MS and Method Development and Validation." INTERNATIONAL JOURNAL OF PHARMACEUTICAL QUALITY ASSURANCE **4**(03): 42-51.
Ma, Y., et al. (2019). "The adverse health effects of bisphenol A and related toxicity mechanisms." Environ Res **176**: 108575.
Martinez-Ibarra, A., et al. (2021). "Multisystemic alterations in humans induced by bisphenol A and phthalates: Experimental, epidemiological and clinical studies reveal the need to change health policies." Environ Pollut **271**: 116380.
Martinez-Pena, A. A., et al. (2017). "Perinatal administration of bisphenol A alters the expression of tight junction proteins in the uterus and reduces the implantation rate." Reprod Toxicol **69**: 106-120.
Matsumoto, H., et al. (2005). "Bisphenol A in Ambient Air Particulates Responsible for theProliferation of MCF-7 Human Breast Cancer Cells and Its ConcentrationChanges over 6 Months." Archives of Environmental Contamination

and Toxicology **48**(4): 459-466.
Matuszewski, B. K., et al. (2003). "Strategies for the assessment of matrix effect in quantitative bioanalytical methods based on HPLC-MS/MS." Anal Chem **75**(13): 3019-3030.
May, S. and C. Bigelow (2006). "Modeling nonlinear dose-response relationships in epidemiologic studies: statistical approaches and practical challenges." Dose Response **3**(4): 474-490.
Mazat, J. P. and S. Ransac (2019). "The Fate of Glutamine in Human Metabolism. The Interplay with Glucose in Proliferating Cells." Metabolites **9**(5).
McGlinchey, A. (2009). "The Effects of Bisphenol A on in-vitro Cell Viability of Mammalian Cell Line by Neutral Red Assay." The Plymouth Student Scientist **2**: 25-31.
Meli, R., et al. (2020). "Oxidative Stress and BPA Toxicity: An Antioxidant Approach for Male and Female Reproductive Dysfunction." Antioxidants (Basel) **9**(5).
Meng, Z., et al. (2019). "Effects of perinatal exposure to BPA, BPF and BPAF on liver function in male mouse offspring involving in oxidative damage and metabolic disorder." Environ Pollut **247**: 935-943.
Mesnage, R., et al. (2017). "Editor's Highlight: Transcriptome Profiling Reveals Bisphenol A Alternatives Activate Estrogen Receptor Alpha in Human Breast Cancer Cells." Toxicol Sci **158**(2): 431-443.
Metallo, C. M. and M. G. Vander Heiden (2013). "Understanding metabolic regulation and its influence on cell physiology." Mol Cell **49**(3): 388-398.
Michalowicz, J. (2014). "Bisphenol A--sources, toxicity and biotransformation." Environ Toxicol Pharmacol **37**(2): 738-758.
Moffatt, B. A. and H. Ashihara (2002). "Purine and pyrimidine nucleotide synthesis and metabolism." Arabidopsis Book **1**: e0018.
Mokra, K., et al. (2016). "Evaluation of DNA damaging potential of bisphenol A and its selected analogs in human peripheral blood mononuclear cells (in vitro study)." Food and chemical toxicology **100**.
Moreira, J. D., et al. (2016). "The Redox Status of Cancer Cells Supports Mechanisms behind the Warburg Effect." Metabolites **6**(4).
Moreno-Sanchez, R., et al. (2008). "Metabolic control analysis: a tool for designing strategies to manipulate metabolic pathways." J Biomed Biotechnol **2008**: 597913.
Naderi, M., et al. (2014). "Developmental exposure of zebrafish (Danio rerio) to bisphenol-S impairs subsequent reproduction potential and hormonal balance in adults." Aquat Toxicol **148**: 195-203.
Neri, M., et al. (2015). "In vitro Cytotoxicity of Bisphenol A in Monocytes Cell Line." Blood Purif **40**(2): 180-186.
Nyamundanda, G., et al. (2014). "A dynamic probabilistic principal components model for the analysis of longitudinal metabolomics data." Journal of the Royal

Statistical Society: Series C (Applied Statistics) **63**(5): 763-782.
Ortiz-Villanueva, E., et al. (2017). "Metabolic disruption of zebrafish (Danio rerio) embryos by bisphenol A. An integrated metabolomic and transcriptomic approach." Environmental pollution **231**: 22-36.
Owen, J. B. and D. A. Butterfield (2010). "Measurement of oxidized/reduced glutathione ratio." Methods Mol Biol **648**: 269-277.
Padberg, F., et al. (2019). "Minor structural modifications of bisphenol A strongly affect physiological responses of HepG2 cells." Arch Toxicol **93**(6): 1529-1541.
Pant, J. and S. B. Deshpande (2012). "Acute toxicity of bisphenol A in rats." Indian J Exp Biol **50**(6): 425-429.
Papoutsakis, E. T. and C. L. Meyer (1985). "Equations and calculations of product yields and preferred pathways for butanediol and mixed-acid fermentations." Biotechnol Bioeng **27**(1): 50-66.
Paris, L. P., et al. (2016). "Global metabolomics reveals metabolic dysregulation in ischemic retinopathy." Metabolomics **12**: 15.
Patra, B., et al. (2021). "Time-resolved non-invasive metabolomic monitoring of a single cancer spheroid by microfluidic NMR." Sci Rep **11**(1): 53.
Patti, G., et al. (2012). "Innovation: Metabolomics: The apogee of the omics trilogy." Nature reviews. Molecular cell biology **13**: 263-269.
Peng, B., et al. (2022). "Gut microbial metabolite p-cresol alters biotransformation of bisphenol A: Enzyme competition or gene induction?" J Hazard Mater **426**: 128093.
Pereira Braga, C. and J. Adamec (2019). Metabolome Analysis. Encyclopedia of Bioinformatics and Computational Biology. S. Ranganathan, M. Gribskov, K. Nakai and C. Schönbach. Oxford, Academic Press**:** 463-475.
Petroff, O. A. C. (2007). 6 - Metabolic Biopsy of the Brain. Molecular Neurology. S. G. Waxman. San Diego, Academic Press**:** 77-100.
Peyre, L., et al. (2014). "Comparative study of bisphenol A and its analogue bisphenol S on human hepatic cells: A focus on their potential involvement in nonalcoholic fatty liver disease." Food and chemical toxicology **70**: 9-18.
Phillips, J. R., et al. (2019). "BMDExpress 2: enhanced transcriptomic dose-response analysis workflow." Bioinformatics **35**(10): 1780-1782.
Pitt, J. J. (2009). "Principles and applications of liquid chromatography-mass spectrometry in clinical biochemistry." Clin Biochem Rev **30**(1): 19-34.
Potratz, S., et al. (2017). "Combination of Metabolomics with Cellular Assays Reveals New Biomarkers and Mechanistic Insights on Xenoestrogenic Exposures in MCF-7 Cells." Chem Res Toxicol **30**(4): 883-892.
Quemeneur, L., et al. (2003). "Differential control of cell cycle, proliferation, and survival of primary T lymphocytes by purine and pyrimidine nucleotides." J Immunol **170**(10): 4986-4995.
Ramos, C., et al. (2019). "Cytotoxic and genotoxic effects of environmental relevant

concentrations of bisphenol A and interactions with doxorubicin." Mutat Res Genet Toxicol Environ Mutagen **838**: 28-36.
Richter, C. A., et al. (2007). "In vivo effects of bisphenol A in laboratory rodent studies." Reprod Toxicol **24**(2): 199-224.
Rinschen, M. M., et al. (2019). "Identification of bioactive metabolites using activity metabolomics." Nature Reviews Molecular Cell Biology **20**(6): 353-367.
Ritz, C. (2010). "Toward a unified approach to dose-response modeling in ecotoxicology." Environ Toxicol Chem **29**(1): 220-229.
Ritz, C., et al. (2016). "Dose-Response Analysis Using R." PLoS One **10**(12): e0146021.
Rubin, B. S. (2011). "Bisphenol A: an endocrine disruptor with widespread exposure and multiple effects." J Steroid Biochem Mol Biol **127**(1-2): 27-34.
Rykowska, I. and W. Wasiak (2006). "Properties, Threats, and Methods of Analysis of Bisphenol A and Its Derivatives." Acta Chromatographica **16**.
Sakazaki, H., et al. (2002). "Estrogen receptor alpha in mouse splenic lymphocytes: possible involvement in immunity." Toxicol Lett **133**(2-3): 221-229.
Samuelsen, M., et al. (2001). "Estrogen-like properties of brominated analogs of bisphenol A in the MCF-7 human breast cancer cell line." Cell Biol Toxicol **17**(3): 139-151.
Sano, T., et al. (2016). "Selective control of up-regulated and down-regulated genes by temporal patterns and doses of insulin." Sci Signal **9**(455): ra112.
Sass, N. (2000). "Humane endpoints and acute toxicity testing." ILAR J **41**(2): 114-123.
Schmidt, P. J., et al. (2013). "Harnessing the Theoretical Foundations of the Exponential and Beta-Poisson Dose-Response Models to Quantify Parameter Uncertainty Using Markov Chain Monte Carlo." Risk Analysis: An International Journal **33**(9): 1677-1693.
Schmidt, T., et al. (2018). "ProteomicsDB." Nucleic Acids Res **46**(D1): D1271-D1281.
Schrimpe-Rutledge, A. C., et al. (2016). "Untargeted Metabolomics Strategies-Challenges and Emerging Directions." J Am Soc Mass Spectrom **27**(12): 1897-1905.
Schymanski, E. L., et al. (2014). "Identifying small molecules via high resolution mass spectrometry: communicating confidence." Environ Sci Technol **48**(4): 2097-2098.
Scopel, C. F. V., et al. (2021). "BPA toxicity during development of zebrafish embryo." Braz J Biol **81**(2): 437-447.
Seong, K. M., et al. (2016). "Is the Linear No-Threshold Dose-Response Paradigm Still Necessary for the Assessment of Health Effects of Low Dose Radiation?" Journal of Korean Medical Science **31**: S10.
Shimizu, K. (2013). 4 - Conventional flux balance analysis and its applications.

Bacterial Cellular Metabolic Systems. K. Shimizu, Woodhead Publishing**:** 215-262.
Shimizu, K. (2013). 5 - 13C-metabolic flux analysis and its applications. Bacterial Cellular Metabolic Systems. K. Shimizu, Woodhead Publishing**:** 263-358.
Singleton, D. W., et al. (2004). "Bisphenol-A and estradiol exert novel gene regulation in human MCF-7 derived breast cancer cells." Molecular and cellular endocrinology **221**(1-2): 47-55.
Slominski, A., et al. (2012). "L-tyrosine and L-dihydroxyphenylalanine as hormone-like regulators of melanocyte functions." Pigment Cell & Melanoma Research.
Smetanova, S., et al. (2015). "High-throughput concentration-response analysis for omics datasets." Environ Toxicol Chem **34**(9): 2167-2180.
Smilde, A. K., et al. (2010). "Dynamic metabolomic data analysis: a tutorial review." Metabolomics **6**(1): 3-17.
Smith, C. A., et al. (2005). "METLIN: A Metabolite Mass Spectral Database." Therapeutic Drug Monitoring **27**(6).
Smith, C. A., et al. (2006). "XCMS: Processing Mass Spectrometry Data for Metabolite Profiling Using Nonlinear Peak Alignment, Matching, and Identification." Analytical Chemistry **78**(3): 779-787.
Son, S., et al. (2018). "Cytotoxicity measurement of Bisphenol A (BPA) and its substitutes using human keratinocytes." Environmental research **164**: 655-659.
Song, H., et al. (2017). "Bisphenol A induces COX-2 through the mitogen-activated protein kinase pathway and is associated with levels of inflammation-related markers in elderly populations." Environmental research **158**: 490-498.
Song, J. W., et al. (2020). "Omics-Driven Systems Interrogation of Metabolic Dysregulation in COVID-19 Pathogenesis." Cell Metab **32**(2): 188-202 e185.
Song, S., et al. (2014). "Occurrence and profiles of bisphenol analogues in municipal sewage sludge in China." Environ Pollut **186**: 14-19.
Spegel, P., et al. (2013). "Time-resolved metabolomics analysis of beta-cells implicates the pentose phosphate pathway in the control of insulin release." Biochem J **450**(3): 595-605.
Stewart, D., et al. (2015). Chapter 4 - Omics Technologies Used in Systems Biology. Systems Biology in Toxicology and Environmental Health. R. C. Fry. Boston, Academic Press**:** 57-83.
Sun, Y., et al. (2004). "Determination of bisphenol A in human breast milk by HPLC with column-switching and fluorescence detection." Biomedical Chromatography **18**(8): 501-507.
Sun, Y., et al. (2021). "Protective effect of metformin on BPA-induced liver toxicity in rats through upregulation of cystathionine β synthase and cystathionine γ lyase expression." Science of the Total Environment **750**: 141685.
Sunde, K., et al. (2007). "Performance characteristics of a cystatin C immunoassay with avian antibodies." Ups J Med Sci **112**(1): 21-37.
Sweeney, K., et al. (1998). "Lack of relationship between CDK activity and G(1)

cyclin expression in breast cancer cells." Oncogene **16**: 2865-2878.
Tandon, D., et al. (2019). "A prospective randomized, double-blind, placebo-controlled, dose-response relationship study to investigate efficacy of fructo-oligosaccharides (FOS) on human gut microflora." Sci Rep **9**(1): 5473.
Teunis, P. and A. Havelaar (2000). "The Beta Poisson Dose-Response Model is Not a Single-Hit Model." Risk analysis : an official publication of the Society for Risk Analysis **20**: 513-520.
Tugizimana, F., et al. (2019). "Time-resolved decoding of metabolic signatures of in vitro growth of the hemibiotrophic pathogen Colletotrichum sublineolum." Sci Rep **9**(1): 3290.
Vahdati Hassani, F., et al. (2018). "Proteomics and phosphoproteomics analysis of liver in male rats exposed to bisphenol A: Mechanism of hepatotoxicity and biomarker discovery." Food Chem Toxicol **112**: 26-38.
Vandenberg, L. N., et al. (2012). "Hormones and endocrine-disrupting chemicals: low-dose effects and nonmonotonic dose responses." Endocr Rev **33**(3): 378-455.
Vandenberg, L. N., et al. (2007). "Human exposure to bisphenol A (BPA)." Reprod Toxicol **24**(2): 139-177.
Vander Heiden, M. G., et al. (2009). "Understanding the Warburg effect: the metabolic requirements of cell proliferation." science **324**(5930): 1029-1033.
Vavricka, C. J., et al. (2020). "Dynamic Metabolomics for Engineering Biology: Accelerating Learning Cycles for Bioproduction." Trends Biotechnol **38**(1): 68-82.
Vemuri, G., et al. (2007). "Increasing NADH oxidation reduces overflow metabolism in Saccharomyces cerevisiae." Proceedings of the National Academy of Sciences **104**(7): 2402-2407.
Wang, D., et al. (2021). "A comprehensive review on the analytical method, occurrence, transformation and toxicity of a reactive pollutant: BADGE." Environ Int **155**: 106701.
Wang, H., et al. (2021). "Simultaneous determination of 9 environmental pollutants including bisphenol A in vegetable oil by solid phase extraction-liquid chromatography-tandem mass spectrometry." Analytical Methods.
Wang, W., et al. (2015). "A comparative assessment of human exposure to tetrabromobisphenol A and eight bisphenols including bisphenol A via indoor dust ingestion in twelve countries." Environ Int **83**: 183-191.
Wang, Z., et al. (2018). "Development of a Correlative Strategy To Discover Colorectal Tumor Tissue Derived Metabolite Biomarkers in Plasma Using Untargeted Metabolomics." Analytical chemistry **91**(3): 2401-2408.
Wang, Z. and C. Dong (2019). "Gluconeogenesis in Cancer: Function and Regulation of PEPCK, FBPase, and G6Pase." Trends Cancer **5**(1): 30-45.
West, P. R., et al. (2010). "Predicting human developmental toxicity of pharmaceuticals using human embryonic stem cells and metabolomics." Toxicology and applied pharmacology **247**(1): 18-27.

Wetherill, Y. B., et al. (2007). "In vitro molecular mechanisms of bisphenol A action." Reprod Toxicol **24**(2): 178-198.
Wishart, D. S., et al. (2018). "HMDB 4.0: the human metabolome database for 2018." Nucleic Acids Res **46**(D1): D608-D617.
Wu, G., et al. (2004). "Glutathione metabolism and its implications for health." J Nutr **134**(3): 489-492.
Wu, J., et al. (2016). "Sources and implications of NADH/NAD(+) redox imbalance in diabetes and its complications." Diabetes Metab Syndr Obes **9**: 145-153.
Wu, N. C. and F. Seebacher (2020). "Effect of the plastic pollutant bisphenol A on the biology of aquatic organisms: A meta-analysis." Glob Chang Biol **26**(7): 3821-3833.
Xiao, C., et al. (2021). "Inherited disorders of complex lipid metabolism: A clinical review." J Inherit Metab Dis.
Xu, T., et al. (2021). "System Biology-Guided Chemical Proteomics to Discover Protein Targets of Monoethylhexyl Phthalate in Regulating Cell Cycle." Environ Sci Technol **55**(3): 1842-1851.
Xu, T., et al. (2020). "A Novel Mechanism of Monoethylhexyl Phthalate in Lipid Accumulation via Inhibiting Fatty Acid Beta-Oxidation on Hepatic Cells." Environ Sci Technol **54**(24): 15925-15934.
Xu, T., et al. (2021). "Metabolomics and In Silico Docking-Directed Discovery of Small-Molecule Enzyme Targets." Analytical Chemistry **93**(6): 3072-3081.
Xu, T., et al. (2021). "Metabolomics and In Silico Docking-Directed Discovery of Small-Molecule Enzyme Targets." Anal Chem **93**(6): 3072-3081.
Xu, X., et al. (2021). "Rewiring of purine metabolism in response to acidosis stress in glioma stem cells." Cell Death Dis **12**(3): 277.
Xue, J., et al. (2015). "Urinary levels of endocrine-disrupting chemicals, including bisphenols, bisphenol A diglycidyl ethers, benzophenones, parabens, and triclosan in obese and non-obese Indian children." Environ Res **137**: 120-128.
Yamazaki, E., et al. (2015). "Bisphenol A and other bisphenol analogues including BPS and BPF in surface water samples from Japan, China, Korea and India." Ecotoxicol Environ Saf **122**: 565-572.
Yanes, O., et al. (2010). "Metabolic oxidation regulates embryonic stem cell differentiation." Nat Chem Biol **6**(6): 411-417.
Yang, L., et al. (2007). "BMDExpress: a software tool for the benchmark dose analyses of genomic data." BMC Genomics **8**: 387.
Yang, S.-T., et al. (2007). Chapter 4 - Metabolic Engineering – Applications, Methods, and Challenges. Bioprocessing for Value-Added Products from Renewable Resources. S.-T. Yang. Amsterdam, Elsevier**:** 73-118.
Yang, Y., et al. (2014). "Urinary levels of bisphenol analogues in residents living near a manufacturing plant in south China." Chemosphere **112**: 481-486.
Yang, Y., et al. (2014). "Simultaneous determination of seven bisphenols in

environmental water and solid samples by liquid chromatography-electrospray tandem mass spectrometry." J Chromatogr A **1328**: 26-34.
Yao, C. H., et al. (2020). "Dose-Response Metabolomics To Understand Biochemical Mechanisms and Off-Target Drug Effects with the TOXcms Software." Anal Chem **92**(2): 1856-1864.
Yin, J., et al. (2018). "Potential Mechanisms Connecting Purine Metabolism and Cancer Therapy." Front Immunol **9**: 1697.
Yu, X., et al. (2015). "Occurrence and estrogenic potency of eight bisphenol analogs in sewage sludge from the U.S. EPA targeted national sewage sludge survey." J Hazard Mater **299**: 733-739.
Yuan, C., et al. (2016). "Enhanced GSH synthesis by Bisphenol A exposure promoted DNA methylation process in the testes of adult rare minnow Gobiocypris rarus." Aquat Toxicol **178**: 99-105.
Yue, S., et al. (2019). "Metabolomic modulations of HepG2 cells exposed to bisphenol analogues." Environ Int **129**: 59-67.
Zaborowska, M., et al. (2021). "Role of Chlorella sp. and rhamnolipid 90 in maintaining homeostasis in soil contaminated with bisphenol A." Journal of Soils and Sediments **21**(1): 27-41.
Zamboni, N., et al. (2009). "(13)C-based metabolic flux analysis." Nat Protoc **4**(6): 878-892.
Zampieri, M., et al. (2017). "Frontiers of high-throughput metabolomics." Curr Opin Chem Biol **36**: 15-23.
Zetzsche, C. and U. Nuding (2005). "Nonlinear and higher-order approaches to the encoding of natural scenes." Network: Computation in Neural Systems **16**(2-3): 191-221.
Zhan, J., et al. (2021). "Dose-dependent responses of metabolism and tissue injuries in clam Ruditapes philippinarum after subchronic exposure to cadmium." Sci Total Environ **779**: 146479.
Zhang, W., et al. (2012). "Effect of bisphenol A on the EGFR-STAT3 pathway in MCF-7 breast cancer cells." Mol Med Rep **5**(1): 41-47.
Zhang, W., et al. (2015). "A weighted relative difference accumulation algorithm for dynamic metabolomics data: long-term elevated bile acids are risk factors for hepatocellular carcinoma." Scientific reports **5**(1): 8984.
Zhang, Y., et al. (2018). "“Cocktail” of Xenobiotics at Human Relevant Levels Reshapes the Gut Bacterial Metabolome in a Species-Specific Manner." Environmental Science & Technology **52**(19): 11402-11410.
Zhang, Y., et al. (2020). "Impact of Mixture Effects between Emerging Organic Contaminants on Cytotoxicity: A Systems Biological Understanding of Synergism between Tris(1,3-dichloro-2-propyl)phosphate and Triphenyl Phosphate." Environmental Science & Technology **54**(17): 10722-10734.
Zhang, Z., et al. (2011). "Urinary Bisphenol A Concentrations and Their

Implications for Human Exposure in Several Asian Countries." Environmental Science & Technology **45**(16): 7044-7050.
Zhao, C., et al. (2019). "Metabolic perturbation, proliferation and reactive oxygen species jointly contribute to cytotoxicity of human breast cancer cell induced by tetrabromo and tetrachloro bisphenol A." Ecotoxicol Environ Saf **170**: 495-501.
Zhao, H., et al. (2021). "Dose-response metabolomics and pathway sensitivity to map molecular cartography of bisphenol A exposure." Environ Int **158**: 106893.
Zimmer, B. M., et al. (2021). "Integration of Sugar Metabolism and Proteoglycan Synthesis by UDP-glucose Dehydrogenase." J Histochem Cytochem **69**(1): 13-23.

APPENDICES

Appendix A

Fig A1. Joint network analysis performed by metabolome (20 μM) and transcriptome data mapping with Cytoscape database.

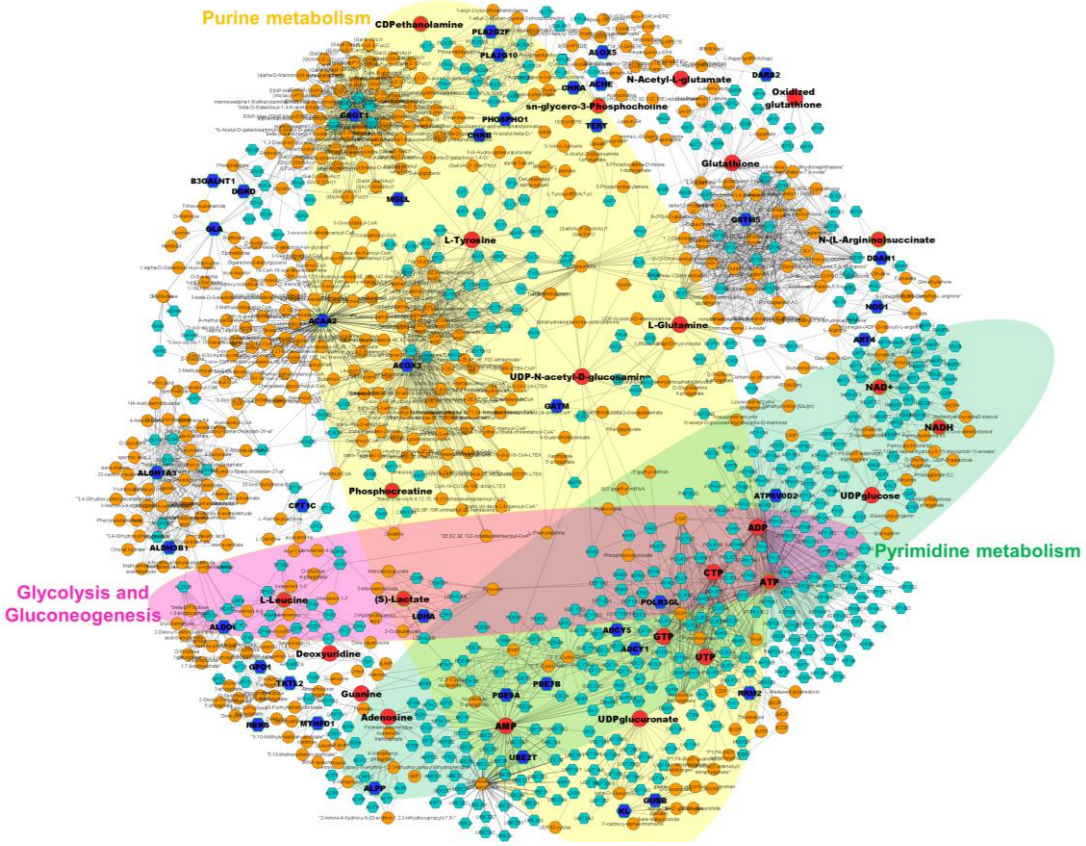

* Dots in red represent the detected metabolites. Dots in orange represent mapped metabolites. Dots in dark blue represent detected genes. Dots in vivid blue represent mapped genes. The node size represents the log transferred fold change value (the larger the size, the higher the log fold change value). Three enriched pathways are emphasized by ellipse in light yellow, magenta and jasmine, respectively (p <0.05).

Table A1. Identified metabolites with MSI information. (m/z stands for mass-to-charge ratio; RT stands for retention time)

Compound name	KEGG	m/z	RT (min)
Adenosine	C00212	302.0714 $[M+Cl]^-$	2.63
ADP	C00008	426.0274 $[M-H]^-$	7.45
AMP	C00020	346.0615 $[M-H]^-$	6.95
Argininosuccinic acid	C03406	289.1218 $[M-H]^-$	7.68
ATP	C00002	505.9939 $[M-H]^-$	8.28
CDP-ethanolamine	C00570	445.0587 $[M-H]^-$	7.26
CTP	C00063	481.9827 $[M-H]^-$	8.42
Deoxyuridine	C00526	227.0818 $[M-H]^-$	4.39
Glutamine	C00064	145.0654 $[M-H]^-$	6.19
Glutathione	C00051	306.0821 $[M-H]^-$	6.67
Glutathione disulfide	C00127	611.1496 $[M-H]^-$	8.08
Glycerophosphocholine	C00670	256.0975 $[M-H]^-$	6.26
GTP	C00044	521.9940 $[M-H]^-$	4.84
Guanine	C00242	150.0414 $[M-H]^-$	4.98
Lactate	C00186	89.0250 $[M-H]^-$	3.86
Leucine	C00123	130.0898 $[M-H]^-$	4.62
N-acetylaspartyl-glutamic acid	C12270	303.0899 $[M-H]^-$	7.14
N-Acetylglutamic acid	C00624	188.0583 $[M-H]^-$	6.25
NAD	C00003	662.1052 $[M-H]^-$	7.11
NADH	C00004	664.1095 $[M-H]^-$	7.10
O-Succinyl-L-homoserine	C01118	218.0714 $[M-H]^-$	6.12
Pantothenic acid	C00864	218.1065 $[M-H]^-$	4.46
Phosphocreatine	C02305	210.0354 $[M-H]^-$	7.14
Proline	C00148	114.0572 $[M-H]^-$	5.21
Tyrosine	C00082	180.0670 $[M-H]^-$	5.12
UDPGA	C00167	579.0313 $[M-H]^-$	7.74
UDP-glucose	C00029	565.0520 $[M-H]^-$	7.20
UDP-N-acetyl-glucosamine	C00043	606.0793 $[M-H]^-$	6.99
UTP	C00075	482.9671 $[M-H]^-$	8.35

Table A2. Identified metabolites with fold change and *p*-value upon BPA exposure at 20 μM, 50 μM and 100 μM. (FC stands for fold change; *p* stands for *FDR-adjusted p-value*)

Compound name	20 μM			50 μM			100 μM		
	FC	***p***	**FDR**	**FC**	***p***	**FDR**	**FC**	***p***	**FDR**
Adenosine	0.89	0.41	0.62	0.90	0.63	0.62	1.69	0.36	0.11
ADP	0.53	<0.01	<0.01	0.63	<0.01	<0.01	1.02	0.82	0.88
AMP	0.59	<0.01	<0.01	0.67	0.01	0.03	1.12	0.88	0.29
Argininosuccinic acid	1.51	0.01	0.02	1.98	<0.01	0.01	2.71	<0.01	<0.01
ATP	0.79	0.04	0.09	0.85	0.12	0.18	1.36	0.03	0.08
CDP-ethanolamine	1.01	0.28	0.95	1.18	0.87	0.11	1.70	<0.01	<0.01
CTP	0.49	0.01	0.03	0.81	0.16	0.23	1.51	0.10	0.16
Deoxyuridine	0.48	<0.01	0.01	0.59	0.08	0.09	0.96	0.53	0.88
Glutamine	0.85	0.26	0.03	0.83	0.43	0.11	1.01	0.34	0.88
Glutathione	0.83	0.17	0.43	0.75	0.06	0.20	0.80	0.14	0.20
Glutathione disulfide	0.85	0.05	0.10	0.87	0.02	0.04	0.94	0.30	0.39
Glycerophosphocholine	0.80	0.03	0.07	0.59	<0.01	<0.01	0.45	<0.01	<0.01
GTP	0.01	0.02	0.06	0.10	0.03	0.08	1.51	0.48	0.58
Guanine	0.82	0.18	0.25	0.99	0.94	0.95	1.36	0.05	0.11
Lactate	1.13	0.08	0.14	1.73	<0.01	0.01	3.11	<0.01	<0.01
Leucine	0.86	0.19	0.26	0.98	0.85	0.89	1.39	0.01	0.02

N-acetylaspartyl-glutamic acid	1.05	0.46	0.56	1.03	0.82	0.88	0.91	0.51	0.60
N-Acetylglutamic acid	1.12	0.53	0.39	1.35	0.95	0.19	1.44	0.87	0.01
NAD	0.82	0.09	0.15	0.89	0.22	0.29	1.33	<0.01	0.02
NADH	0.77	0.08	0.13	0.89	0.26	0.35	1.38	0.01	0.02
O-Succinyl-L-homoserine	1.79	0.01	<0.01	2.28	<0.01	0.01	3.38	<0.01	<0.01
Pantothenic acid	0.55	<0.01	<0.01	0.60	<0.01	<0.01	0.96	0.61	0.68
Phosphocreatine	0.75	0.01	0.02	0.55	<0.01	0.01	0.39	<0.01	<0.01
Proline	0.96	0.61	0.68	1.00	0.98	0.98	1.30	<0.01	0.02
Tyrosine	0.51	0.01	0.02	0.62	0.02	0.05	1.33	0.08	0.14
UDPGA	0.61	0.01	0.03	0.79	0.09	0.15	1.34	0.09	0.14
UDP-glucose	0.78	0.01	0.02	0.81	<0.01	0.02	0.96	0.46	0.56
UDP-N-acetyl-glucosamine	0.83	0.06	0.11	0.85	0.05	0.10	1.11	0.09	0.15
UTP	0.91	0.32	0.40	0.80	0.04	0.08	1.01	0.94	0.95

Table A3. Predicted effective concentration for metabolites dysregulation pattern demonstration.

Compound name	KEGG	EC_{-30}	EC_{-20}	EC_{-10}	EC_{+10}	EC_{+20}	EC_{+30}
Adenosine	C00212	N/A	N/A	16.5	69.5	75.5	80.3
ADP	C00008	9.7	5.9	2.7	N/A	N/A	N/A
AMP	C00020	11.6	6.8	3.2	89.1	N/A	N/A
Argininosuccinic acid	C03406	N/A	N/A	N/A	3.4	7.9	11.9
ATP	C00002	N/A	16.7	6.8	75.4	84.7	93.4
CDP-ethanolamine	C00570	N/A	N/A	N/A	39.0	52.4	63.1
CTP	C00063	7.8	4.6	2.3	61.7	65.6	70.1
Deoxyuridine	C00526	27.4	5.6	2.7	N/A	N/A	N/A
Glutamine	C00064	N/A	N/A	10.3	N/A	N/A	N/A
Glutathione	C00051	99.6	27.4	8.6	N/A	N/A	N/A
Glutathione disulfide	C00127	N/A	21.3	7.1	N/A	N/A	N/A
Glycerophosphocholine	C00670	32.1	18.6	8.3	N/A	N/A	N/A
GTP	C00044	4.9	3.4	2.2	74.1	76.2	77.9
Guanine	C00242	N/A	N/A	7.2	60.5	69.7	82.9
Lactate	C00186	N/A	N/A	N/A	17.3	25.7	31.1
Leucine	C00123	N/A	N/A	10.2	63.1	73.9	85.9
N-acetylaspartyl-glutamic acid	C12270	N/A	N/A	N/A	22.7	N/A	N/A
N-Acetylglutamic acid	C00624	N/A	N/A	N/A	18.0	28.4	41.9
NAD	C00003	N/A	29.9	8.0	74.2	85.4	97.3
NADH	C00004	N/A	N/A	10.6	76.2	85.4	93.9
O-Succinyl-L-homoserine	C01118	N/A	N/A	N/A	0.8	4.3	7.8
Pantothenic acid	C00864	10.2	6.1	2.9	N/A	N/A	N/A
Phosphocreatine	C02305	28.6	16.1	7.1	N/A	N/A	N/A
Proline	C00148	N/A	N/A	19.6	64.9	79.1	99.6
Tyrosine	C00082	9.1	5.4	2.7	79.1	86.3	95.7
UDPGA	C00167	11.7	6.7	3.2	69.5	76.6	86.6
UDP-glucose	C00029	N/A	12.4	5.2	N/A	N/A	N/A
UDP-N-acetyl-glucosamine	C00043	N/A	48.9	16.9	96.9	N/A	N/A
UTP	C00075	N/A	48.6	29.7	97.6	N/A	N/A

* Metabolite 10% downregulation effective concentration (EC_{-10}). EC_{+10}, EC_{+20}, EC_{+30}, EC_{-10}, EC_{-20}, EC_{-30} are reported, respectively. N/A stands for Not Applicable.

Appendix B

Table B1. Identified time-resolved dysregulated metabolites with MS1 information. (m/z stands for mass-to-charge ratio; RT stands for retention time; FDR-adjusted *p*-value is calculated by one-way ANOVA.

Compound name	KEGG	m/z $[M-H]^-$	RT (min)	*P*
Adenosine monophosphate	C00020	346.0553	7.757	0.045
Adenosine triphosphate	C00002	505.9879	8.237	0.035
Adenylsuccinic acid	C03794	462.0662	0.559	<0.01
ADP	C00008	426.0216	8.055	0.026
CDP-Ethanolamine	C00570	445.0587	8.003	<0.01
Cholesterol sulfate	C18043	465.3027	0.609	<0.01
Citraconic acid	C02226	129.0186	6.632	0.050
Citric acid	C00158	191.0192	8.171	<0.01
Cytidine	C00475	242.0777	7.955	<0.01
Cytidine triphosphate	C00063	481.9827	8.402	<0.01
Deoxyuridine	C00526	227.0665	6.731	<0.01
D-Fructose	C02336	179.0556	6.086	<0.01
D-Glucose	C00221	179.0556	7.045	<0.01
Glutathione	C00051	306.0765	7.426	0.05
Guanosine	C00387	282.0839	0.625	<0.01
Guanosine triphosphate	C00044	521.994	8.416	0.038
L-Glutamic acid	C00025	146.0454	7.426	<0.01
L-Glutamine	C00064	145.0613	6.748	0.039
L-Lactic acid	C00186	89.025	5.488	<0.01
L-Leucine	C00123	130.0868	5.06	<0.01
L-Lysine	C00047	145.0977	7.591	0.012
L-Proline	C00148	180.0661	5.573	0.05
L-Tyrosine	C00082	116.0712	5.639	0.034
L-Valine	C00183	188.0583	7.36	<0.01

N-Acetylglutamic acid	C00624	308.0982	0.592	0.011
NAD	C00003	662.1013	7.79	0.034
NADH	C00004	664.1095	7.409	<0.01
Oxidized glutathione	C00127	611.1442	8.468	0.048
Palmitic acid	C00249	255.2331	0.94	0.031
Pantothenic acid	C00864	218.1028	5.589	0.020
Phosphocreatine	C02305	210.0354	8.003	<0.01
Pyroglutamic acid	C01879	128.0348	7.426	<0.01
Taurine	C00245	124.0069	5.871	0.028
Uridine diphosphate glucose	C00029	565.0472	8.086	<0.01
Uridine diphosphate glucuronic acid	C00167	579.0313	8.334	<0.01
Uridine diphosphate-N-acetylglucosamine	C00043	606.0793	7.989	<0.01
Uridine triphosphate	C00075	482.9671	8.35	0.024

Fig B1. Time-resolved cell counting to assess dynamic biomass change. (T=0 hr, cell counts approximately 9.5×10^5 for a 35 mm petri dish)

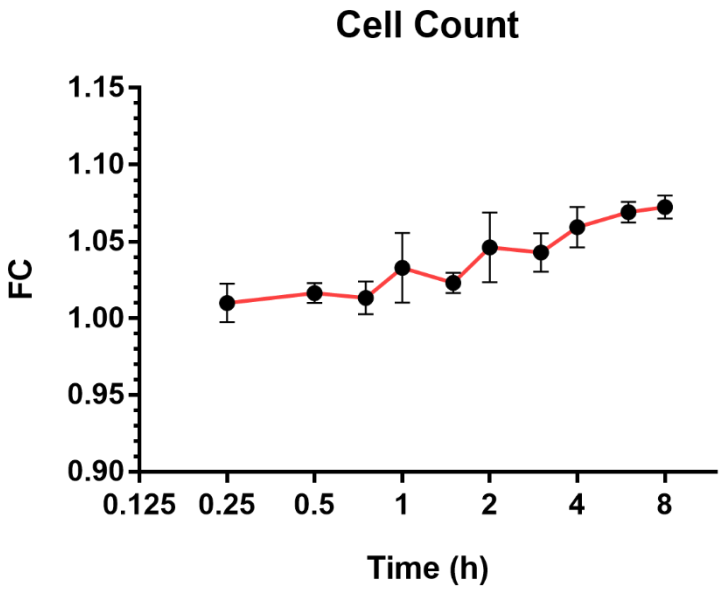

Fig B2. Scatterplots of fold changes at the adjacent time steps for 37 significant metabolites.